ELUCIDATING THE CENTRAL CARBON METABOLISM OF *BACILLUS MEGATERIUM* QM B1551

A Thesis

Presented to the Faculty of the Graduate School

of Cornell University

In Partial Fulfillment of the Requirements for the Degree of

Master of Engineering

by

Julie Anna Wushensky

May 2017

ABSTRACT

We investigated the central carbon metabolism of *Bacillus megaterium* QM B1551 cells using various carbon substrates, long-term isotopic enrichment experiments with ^{13}C-labeled carbons, metabolic flux analysis (MFA), and kinetic incorporation of ^{13}C-labeled carbons. We determined that gluconate can be incorporated into the metabolic network structure of *B. megaterium* QM B1551, particularly when gluconate was present in the environment. It was shown in the same experiment that *B. megaterium* QM B1551 did not use the Entner-Doudoroff (ED) pathway for glucose (Gluc) metabolism, and instead relied primarily on the Embden-Mayerhof-Parnas (EMP) and oxidative pentose phosphate (PP) pathways. The TCA cycle of this bacterium was incompletely bifurcated, although this bifurcation did not impede the ability of the bacterium to grow. There were bottlenecks in the fluxes from metabolite nodes alpha-ketoglutarate (αKG) to succinate, from succinate to fumarate, and from oxaloacetate (OAA) to fumarate. This bifurcation was overcome with a direct input of substrate into the TCA cycle. The stereochemistry of citrate formation and cleavage was different compared to other bacterial flux studies. It was hypothesized that the carboxylation reaction which combines CO_2 and pyruvate (PYR) added CO_2 behind the third carbon position of PYR to form OAA. It was further hypothesized that OAA was flipped such that the fourth carbon position of OAA became the fourth carbon position of citrate. Finally, it was observed that *B. megaterium* QM B1551 had an early preference for glutamate catabolism in the TCA cycle, followed by a preference for Gluc catabolism across the metabolic network. These findings provide clarification regarding contradictions in the literature, and thus contribute towards finding new platforms for optimized industrial use of this bacterium.

BIOGRAPHICAL SKETCH

Julie Wushensky earned her Bachelor of Science degree from Cornell University's Biological and Environmental Engineering department in 2016. During her undergraduate years, she was involved with plant breeding research in the Mazourek Lab, the Gore Lab, and the Nelson Lab. Julie remained at Cornell the following year to join the lab of her advisor, Dr. Ludmilla Aristilde, to pursue her Master of Engineering degree.

ACKNOWLEDGEMENTS

I would like to deeply thank my advisor, Professor Ludmilla Aristilde, for the opportunity to work in her lab and for all of her guidance, patience, encouragement and support over the past year of MEng and the final two years of my undergraduate program. I'd also like to thank the other members of the Aristilde Lab for giving me such great support and great company over the many long experiments. I would especially like to thank Tracy Youngster for showing me the ropes and keeping me going, as well as Rebecca Wilkes and Caroll Mendonca for their continuous collaborations and all the laughs.

Thanks to Professors John March, Michael Mazourek, Rebecca Nelson, Douglas Haith, and Michael Gore for all the opportunities and support they gave me during my studies.

Thanks to Ivan Keresztes, who tolerated my monopoly of his NMR facility for several weeks.

A profound thank you to Nicholle Aston, Marek Kwasnica, my brothers, and my parents for their never-ending love and support. This effort would not have been possible without them.

TABLE OF CONTENTS

LIST OF FIGURES

[U-^{13}C]-Gluc was abbreviated as Gluc
[1,2-^{13}C]-Gluc was abbreviated as 1,2-Gluc
[U-^{13}C]-Gluc and unlabeled gluconate was abbreviated as Gluc:Glucn
[U-^{13}C]-Gluc and unlabeled gluconate was abbreviated as Gluc:Glu
[1,2,3-^{13}C]-Gluc, [1,6-^{13}C]-Fruc, and unlabeled Xyl was abbreviated as GFX

LIST OF ABBREVIATIONS

LB	Lysogeny Broth
Gluc	Glucose
Fruc	Fructose
Xyl	Xylose
OD, OD_{600}	Optical Density
DSS	Dimethyl-2-silapentane-5-sulfonate
NMR	Nuclear magnetic resonance
LC-MS	Liquid chromatography mass spectrometry
G6P	Glucose-6-phosphate
F6P	Fructose-6-phosphate
6PG, 6-PG	6-phospho-gluconate
FBP	Fructose-bis-phosphate
R5P	Ribose-5-phosphate
Xu5P	Xyulose-5-phosphate
S7P	Sedoheptulose-7-phosphate
DHAP	Dihydroxy-acetone-phosphate
PEP	Phosphoenolpyruvate
GAP	Glyceraldehyde 3-phosphate
3PG	3-phosphoglycate
PYR	Pyruvate
αKG, α-KG	α-ketoglucterate
OAA	Oxaloacetate
Ac-CoA	Acetyl coenzyme A
PP	Pentose phosphate (pathway)
TCA	Tricarboxylic acid
EMP	Embden-Meyerhof-Parnas
KEGG	Kyoto Encyclopedia of Genes and Genomes
ED	Enter-Doudoroff

INTRODUCTION

Bacillus megaterium is an aerobic sporulating bacterium that is ubiquitous in a diverse range of environments, including soils, salt water, honey, and dried food (Vary, 1994; Vary et al., 2007). This bacterium is known to be endophytic, as it has been found to enter plants via junctions between root cells and slowly migrate into the intercellular spaces throughout the plant tissue (Liu et al., 2006). The metabolic products it excretes in the rhizosphere, such as antibiotics and siderophores, are thought to promote plant health (Eppinger et al., 2011; Santos et al., 2014). Several strains of *B. megaterium* have proven to be industrial staples in the large-scale production of biological products, due to their ready exportation of proteins without the accompanying secretion of endotoxins (Vary, 1994; Vary et al., 2007). Other applications of *B. megaterium* include bioremediation and the production of pharmaceutical compounds, recombinant proteins, vitamin B12, and fungicidal chemicals (Quinn, 1989; Vary, 1994; Vary et al., 2007). Numerous types of organic substrates including sugars and amino acids can be used as carbon sources to grow *B. megaterium* (Vary et al., 2007), and the types of substrates used have been shown to influence the biosynthetic pathways employed for product generation (Furch et al., 2007b; Vary et al., 2007; Santos et al., 2014; Aristilde et al., 2015; Kukurugya, 2017). Therefore, a comprehensive understanding of the cellular metabolism in *B. megaterium* is of particular interest. However, despite extensive genetic characterization of *B. megaterium*, detailed elucidation of its metabolic network structure and the cellular carbon fluxes is lacking.

Here we seek to provide detailed insights into the sugar metabolism of *B. megaterium* QM B1551. Specifically, we explored the central carbon metabolism of *B. megaterium* when grown on glucose alone, or in a mixture with fructose and xylose. Since *B. megaterium* is both an

endophyte and a key player in the rhizosphere environment, it is critical to understand how this bacterium processes sugars common to the rhizosphere (Liu et al., 2006). Glucose is the sugar monomer of the polymers cellulose and starch, both of which are found in plant matter (KoÈgel-Knabner, 2002). Quantifying how *B. megaterium* QM B1551 metabolizes glucose will provide a basis of comparison for other studies, because glucose has been established in literature as a principle substrate for characterizing the growth and functionality of a given bacterium. Similarly, fructose is a hexose sugar monomer common in plant tissue, and is usually found bound to glucose as sucrose. Xylose, a pentose sugar, is found in hemicellulose, an abundant component of plant cell walls (KoÈgel-Knabner, 2002). Understanding how *B. megaterium* QM B1551 utilizes these sugars when they are all present in a mixture will allow for better predictions of the bacterium's metabolic ability to process these sugars simultaneously in the rhizosphere. It has been reported that adding supplementations of casamino acids to sugar media increases growth and protein production in *B. megaterium* cultures (Korneli, 2012; Marchland, 2016). For completeness, bacterial growth was also characterized for a mixture of glucose and glutamate.

A model of the metabolic network was hypothesized based on the fully sequenced genome of *B. megaterium* QM B1551 (Eppinger et al., 2011; Kanehisa and Goto, 2000; Kanehisa et al., 2017). To date, this metabolic network has not been validated explicitly using carbon mapping techniques (Furch et al, 2007a; Furch et al., 2007b; Biedendieck et al., 2010). Most of what is known about carbon metabolism in *Bacillus* species is derived from studies on *B. subtilis*, a popular model organism for Gram-positive bacteria (Sauer et al., 1997; Dauner et al., 2001a; Dauner et al., 2001b). Thus, many of the metabolic network assumptions used to construct *B. megaterium* models are based on *B. subtilis* models and *B. subtilis* data. A few

strains of *B. megaterium* have been studied in the context of metabolic flux analysis, including MS941, WH323, and WH320, but all of these strains were mutants lacking specific functions within the metabolic network (Furch et al., 2007a). Therefore, while inferences about the metabolic network of *B. megaterium* QM B1551 were drawn from these other *B. megaterium* strains, the assumptions needed to be experimentally verified.

It has been well established that *B. megaterium* undergoes glycolysis via the Embden-Meyerhof-Parnas (EMP) pathway, which then feeds into the tricarboxylic acid (TCA) cycle (Vary, 2007; Furch et al., 2007; Sauer et al., 2008; Eppinger et al., 2011) (Fig. 1, 2). In the EMP pathway, glucose is first converted to glucose-6-phosphate (G6P), then its isomer fructose-6-phosphate (F6P); it is next phosphorylated to fructose-bis-phosphate (FBP), and finally cleaved into dihydroxyacetone phosphate (DHAP) and glyceraldehyde-3-phosphate (GAP) (Fig. 1). The EMP pathway metabolites can also contribute to the pentose phosphate (PP) pathway. The oxidative phase of the PP pathway involves first the conversion of G6P to 6-phosphogluconate (6-PG) (Fig. 1). The carbon in the first position of 6-PG is then cleaved, resulting in ribulose 5-phosphate (Ru5P). In the nonoxidative phase of the PP pathway, Ru5P can interconvert to form ribose 5-phosphate (R5P) and xylulose 5-phosphate (Xu5P) (Fig. 1). A transketolase reaction then adds the carbons in the first and second position of Xu5P onto R5P, forming sedoheptulose 7-phosphate (S7P) and GAP (Fig. 1). A second transketolase reaction can add the carbons in the first and second position of Xu5P before the first carbon position of erythrose 4-phosphate (E4P) to form F6P, while the last three carbons of Xu5P become GAP. A transaldolase reaction adds the carbons in the first three positions of F6P before the first carbon position of E4P to form S7P, and the last three carbons of F6P become GAP. The output of both the EMP and PP pathways, GAP, eventually generates pyruvate (PYR) to feed into the TCA cycle (Fig. 1, 2). Through

decarboxylation and carboxylation, PYR can form acetyl-co-enzyme A (Ac-CoA) and oxaloacetate (OAA), respectively (Fig. 2). In the former case, the third carbon of PYR is cleaved and lost as CO_2, resulting in Ac-CoA (Sasnow et al., 2016). In the latter case, a CO_2 is added to first carbon of PYR, resulting in OAA (Sasnow et al., 2016). In the first step of the TCA cycle, Ac-CoA is added to the third carbon of OAA to form citrate (Sasnow et al., 2016) (Fig. 2). Citrate undergoes a decarboxylation, in which the first carbon is lost as CO_2 and alpha-ketogluterate (αKG) is generated (Sasnow et al., 2016). In turn, the first carbon of αKG is decarboxylated to form succinate and CO_2 (Sasnow et al., 2016) (Fig. 2). These reactions are considered irreversible (Sasnow et al., 2016). Succinate can be interconverted with fumarate, which in turn can be interconverted with malate (Fig. 2). Rounding out the TCA cycle, malate can either lose the carbon in its first position to form PYR, or can interconvert with OAA (Fig. 2). Canonically, the TCA cycle is thought to proceed in this clockwise fashion from OAA to succinate to malate and back to OAA.

There are conflicting results regarding the relative distribution of fluxes from G6P going towards either the EMP pathway or the PP pathway (Sauer et al., 1997, Dauner et al., 2001a; Tannlet et al., 2008; Furch et al., 2007a; Furch et al., 2007b). Some previous studies suggest that *B. subtilis* exhibits a higher degree of activity in the PP pathway than the EMP pathway (Sauer et al., 1997), while others have found the converse to be true (Dauner et al., 2001a; Tannlet et al., 2008). Metabolic flux studies on *B. megaterium* have found that carbon-starved *B. megaterium* tends to utilize both the EMP pathway and PP pathway equally, while recombinant strains of *B. megaterium* encoding *Thermobidfida fusca* hydrolase (TFH) exhibit higher degrees of activity in the PP pathway only when the TFH-production genes are induced (Furch et al., 2007a; Furch et al., 2007b). These same studies have not provided a high resolution of fluxes through the TCA

cycle, and so the flux distribution between the TCA cycle nodes are relatively unexplored in *Bacillus* species (Furch et al., 2007a; Furch et al., 2007b) Specifically, the only TCA metabolites included in the previous model were malate, OAA, and a lumped grouping of organic acids (Furch et al., 2007a; Furch et al., 2007b).

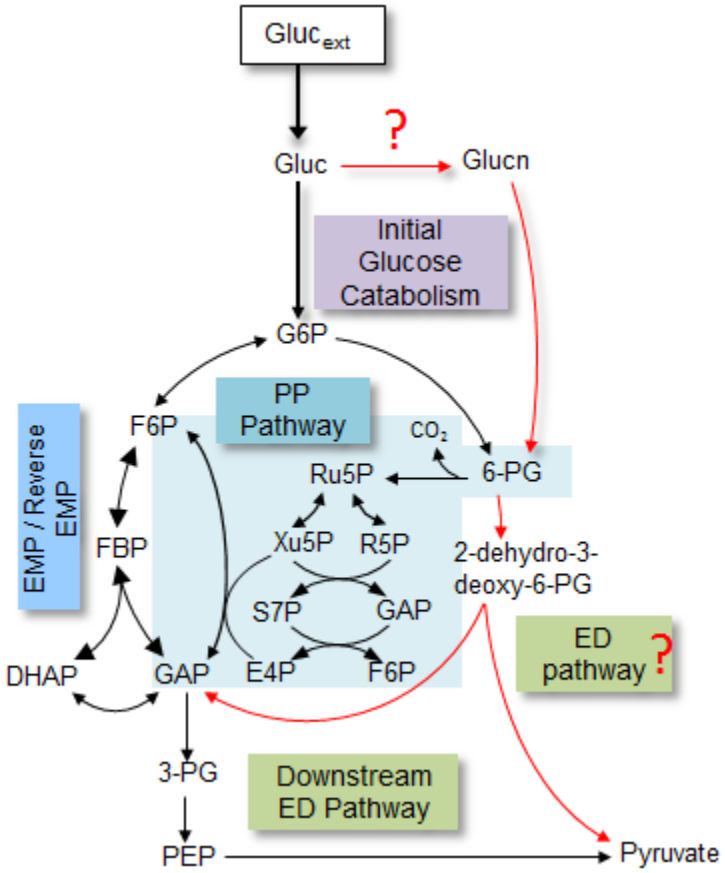

Figure 1. A simplified model network of the EMP, Reverse EMP, ED, Downstream ED (or lower glycolytic), and PP pathways during the uptake of glucose by *B. megaterium*. Reactions which are reported to occur but have not been experimentally verified are shown in red.

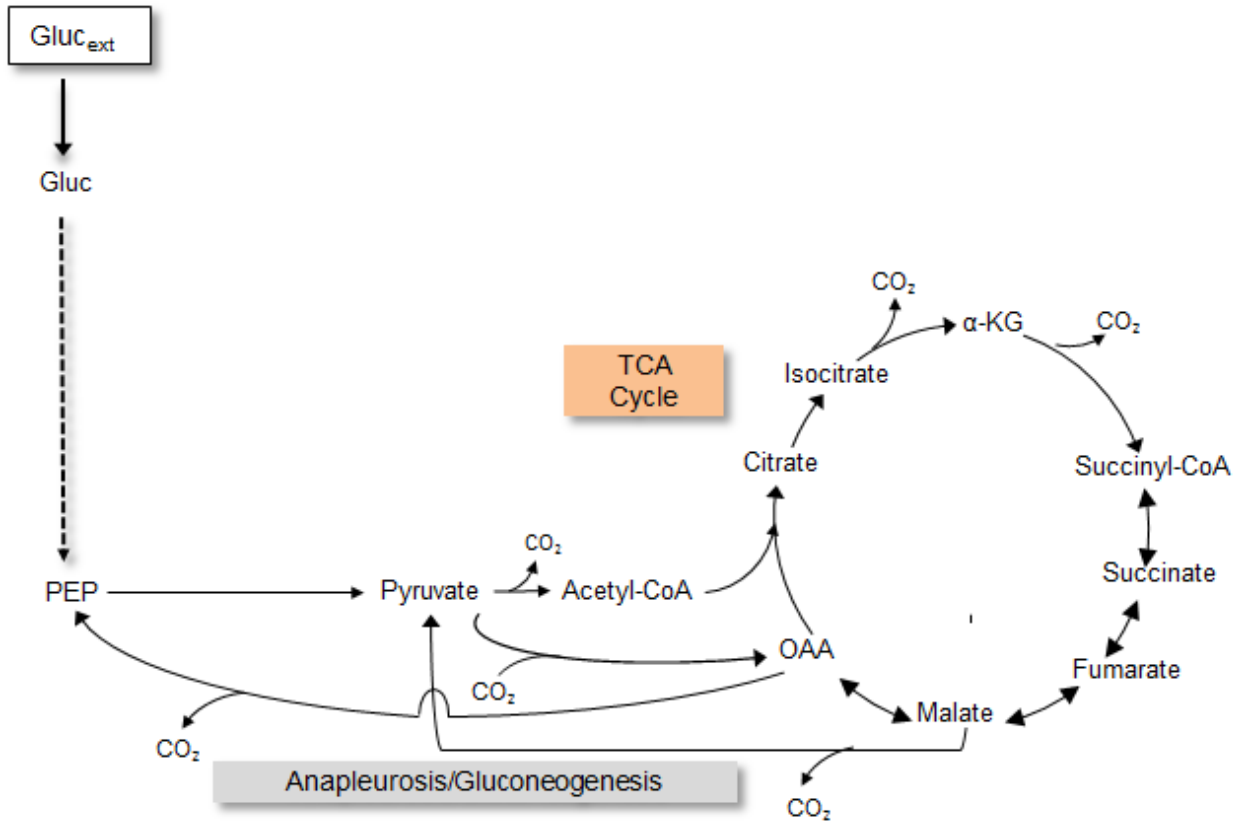

Figure 2. A simplified model network of the TCA cycle and gluconeogenic pathway in *B. megaterium*.

Another possible metabolic pathway for initial glucose catabolism is the Entner-Doudoroff (ED) pathway, which has not been considered in previous metabolic studies of *Bacillus* species (Tannlet er al., 2008; Furch et al., 2007a; Furch et al., 2007b). The ED pathway involves first the conversion of G6P to 6-PG, followed by the cleavage of 6-PG to form GAP and PYR (Sasnow et al., 2016) (Fig. 1). Tannler et al. (2008) reported that several strains of related *Bacillus* species, including *B. subtilis, B. licheniformis, B. pumilus,* and *B. amyloliquefaciens*, lack the genes encoding the ED pathway. However, *B. megaterium* QM B1551 is reported to possess the genes that encode ED pathway-associated enzymes (Kanehisa and Goto, 2000; Kanehisa et al., 2017). Metabolic flux networks constructed for *Bacillus* species, including *B. megaterium*, only show a uni-directional flow through the glycolysis pathway (Sauer et a., 1997; Dauner et al., 2001a; Furch et al., 2007a; Furch et al., 2007b; Tannler et al., 2008). However, *B.*

megaterium QM B1551 has been reported to have the enzymes necessary to perform gluconeogenesis and the reverse EMP pathway (Kanehisa and Goto, 2000; Kanehisa et al., 2017), which have been previously unexplored for *Bacillus* species (Sauer et a., 1997; Dauner et al., 2001a; Furch et al., 2007a; Furch et al., 2007b; Tannler et al., 2008). Since *B. megaterium* is heavily integrated in the economy of industrial bioproducts, it is of great importance to understand how efficiently certain pathways are operating within the bacterium under certain growth conditions.

Before glucose has the chance to be catabolized through the EMP or ED pathways, it can be converted to gluconate (Fig. 1). Overwhelmingly, gluconate has not been considered as a viable node in metabolic networks of *Bacillus* species (Sauer et al., 1997; Dauner et al., 2001a; Furch et al., 2007a; Furch et al., 2007b; Tannler et al., 2008; Korneli et al., 2012) (Fig. 1). Other species of bacteria will have a flux towards gluconate as an overflow mechanism when the cell encounters more carbon than it can use under certain conditions (Sasnow et al., 2016). Gluconate is a common product secreted by other bacterial species in the rhizosphere (Werra et al., 2009), and thus a ubiquitous soil bacterium like *B. megaterium* QM B1551 would be likely to encounter it in its native environment. It is therefore of interest to examine if *B. megaterium* QM B1551 can process gluconate from the environment.

There are several shortcomings to the previous MFA studies on *Bacillus* species (Sauer et al., 1997; Dauner et al., 2001a; Furch et al., 2007a; Furch et al., 2007b; Tannler et al., 2008; Korneli et a., 2012). These studies primarily considered glucose alone as the sole sugar carbon-source for their models, and have not investigated mixed carbon substrates. Their models thus cannot predict what would happen when a *B. megaterium* cell in the rhizosphere encountered a mixture of sugars, or even simply a pentose sugar. Metabolic considerations regarding the

variety of carbon-sources that *B. megaterium* encounters in its nutritional environment, either in soil environments or in large-scale reactors, are essential for the generation and optimization of more realistic and predictive metabolic flux networks. In addition, all of these studies have used fractionally ^{13}C-labeled amino acid quantification to constrain the flux network (Sauer et al., 1997; Dauner et al., 2001a; Furch et al., 2007a; Furch et al., 2007b; Tannler et al., 2008; Korneli et a., 2012). This method relies on the bacterium producing free amino acids from specific metabolic nodes while the cell is growing on partially or fully isotopically-labeled substrates, typically ^{13}C (Furch et al., 2007a; Furch et al., 2007b). The fraction of ^{13}C-labeled amino acids is detected via gas chromatography coupled with mass-spectrometry (MS), and can then be used to calculate the fraction of ^{13}C-labeled metabolites from which the acids were immediately derived (Furch et al., 2007a; Furch et al., 2007b). This method is insensitive to those amino acids which are hydrolytically unstable and relies on indirect observations to quantify intracellular metabolites. By contrast, the methodology employed by Aristilde et al. (2015) uses a metabolomics approach, which uses LC-MS technology to directly detect and quantify individual intracellular metabolites. This improves the overall resolution of both the metabolic network structure and the flux analysis, and is utilized in the present study.

The *Bacillus megaterium* strain QM B1551 is one of the best-studied Gram-positive bacteria; the whole genome is sequenced and reports have indicated its potential for genetic recombination (Vary et al., 2007; Eppinger et al., 2011; Marchland et al, 2016). To address the lack of investigative research on the industrial workhorse and ubiquitous soil bacterium *B. megaterium* QM B1551, this study characterized the bacterium's growth phenotype in the presence of glucose alone, fructose alone, xylose alone, and several mixtures of sugars and metabolite substrates. The implementation of isotopic labeling schemes allowed for individual

carbon atoms to be tracked through the metabolic network, and thus allowed for the verification and reassessment of the metabolic pathways available in *B. megaterium* QM B1551. In addition, the experimental labeling data provided constraints for the MFA analysis. A system of fluxes was generated through the MFA for growth on glucose, which was compared to the flux values reported in literature (Furch et al., 2007a). This will provide important information regarding the optimization of growth of this bacterium both in its natural habitat and in industrial applications.

METHODS

I. Culturing conditions

Bacillus megaterium QM B1551 cells were obtained from the Bacillus Genetic Stock Center (Columbus, OH) on solid medium. Single colonies were re-suspended in 7 mL of Lysogeny Broth (LB) media, grown until late exponential phase, and plated on solid agar LB media. All plates were stored at 4°C until use. For carbon source-specific growth, liquid cultures were maintained in 20-mL glass test tubes or in 125-mL glass baffled flasks; these cultures were kept in an incubator shaker (New Brunswick Scientific, Edison, NJ) at 30°C and shaken at 220 rpm (Sasnow et al., 2016). Tubes and flasks were covered with sponge caps to protect the cultures from contamination while allowing gas exchange. The bacterial cells were grown at pH 7.0, in filter-sterilized (0.22 µm nylon; Waters Corporation, MA) minimal media, which contained the following in Milli-Q water: 18.7 mM NH_4Cl, 0.81 mM $MgSO_4$, 0.034 mM $CaCl_2 \bullet 2H_2O$, 89.4 mM K_2HPO_4, 56.4 mM $NaH_2PO_4 \bullet H_2O$, 8.6 mM NaCl, and trace metals. The trace metal concentrations were as follows: 30 µM $FeSO_4 \bullet 7H_2O$, 1.9 µM H_3BO_3, 0.86 µM $CuSO_4 \bullet 5H_2O$, 7.7 µM $ZnSO_4 \bullet 7H_2O$, 0.75 µM $MnSO_4 \bullet H_2O$, 0.26 µM $NiCl_2 \bullet 6H_2O$, 0.31 µM $Na_2MoO_4 \bullet 2H_2O$. The carbon-source for each experiment (330 mM C) was added to the minimal media as follows: only glucose (Gluc), only fructose (Fruc), only xylose (Xyl), 1:1:1 Gluc:Fruc:Xyl, 1:1 Gluc:Glutamate, or 1:1 Gluc:Gluconate.

II. Monitoring growth

Cell growth was monitored via optical density (OD_{600}) using an Agilent Cary UV-visible spectrophotometer (Santa Clara, CA). Single colonies of *B. megaterium* were first grown to late exponential phase in test tubes of LB media before being transferred to test tubes containing

minimal media. Once the cells had again reached late exponential phase, an aliquot from these test tubes was transferred to fresh minimal media in baffled flasks. The OD_{600} of a culture immediately following transfer was between 0.05 and 0.07. Two transfers as described above were performed for all experiments to ensure that the cells were well acclimated to their growing conditions prior to experimental sampling. To determine the cell dry weight in grams (g_{CDW}), 1.5 mL of culture was sampled after each OD_{600} reading and spun down at 9,391 g for 5 minutes at 4°C (Centrifuge 5424 R, Eppendorf, Hauppauge, NY). The retentate was then stored at -20°C until it could be dried using a Labconco freeze-dryer (Kansas City, MO). The g_{CDW} conversion factors for each carbon-source condition were found to be (in $g_{CDW}\ L^{-1}\ OD_{600}^{-1}$): 0.61 ± 0.08 for Gluc; 0.69 ± 0.09 for Fruc; 0.42 ± 0.07 for Xyl; 0.43 ± 0.10 for Gluc:Fruc:Xyl.

III. Measurement of sugar uptake

To quantify the rate of consumption of carbon from the media in the Gluc, Fruc, Xyl, and Gluc:Fruc:Xyl conditions, 0.7 mL samples were harvested from three biological replicates throughout cell growth. These samples were centrifuged for 30 minutes at 15,871 g and 4°C in filter microcentrifuge tubes (0.22 µm pore size nylon). The filtered supernatants were frozen at -20°C until further processing. In preparation for analysis via nuclear magnetic resonance (NMR), 200 µL of filtered sample were mixed with 60 µL of 100% D_2O, 50 µL of 6 mM 2,2-dimethyl-2-silapentane-5-sulfonate (DSS) as an internal standard, 240 µL of 100 mM sodium bicarbonate as a pH control, and 50 µL of 10 mM sodium-azide as an antimicrobial agent. Samples were stored at 4°C until analysis (Kukurugya, 2017). The NMR samples were analyzed by proton NMR using a Varian Unity INOVA 600-MHz NMR spectrometer at 25°C, with a relaxation delay of 5 seconds, recording of 16 scans per sample, and receiver gain of 32 dB

(Aristilde et al., 2015; Kukurugya, 2017). As done previously, the depletion of sugars in the extracellular medium was taken to approximate sugar uptake (Aristilde et al., 2015). Carbon consumption rates of exponentially-growing cells (in mmol g_{CDW}^{-1} h^{-1}) were determined via regression analysis. For the sugar substrate mixture, the consumption rates of the individual sugars were calculated by normalizing the NMR signal intensity of the stock solution to the NMR signal intensity of several concentration standards of the mixture of sugars.

IV. LC-MS analysis

As described in introduction, isotopic-labeling samples and metabolic excretion samples were generated to create constraining parameters for MFA. Metabolite standards of 1000 nM, 500 nM, 250 nM, 100 nM, 50 nM, and 10 nM concentrations were run in parallel with the excretion sample. These samples and standards were analyzed by reversed-phase ion-pairing LC via ultra-high performance LC (Thermo Scientific DionexUltiMate 3000) coupled to high-resolution/accurate-mass mass spectrometer (Thermo Scientific Q Exactive quadrupole-Orbitrap hybrid MS) with electrospray ionization (ESI), run in full scan negative mode (Kukurugya, 2017; Sasnow, 2016). Mobile phases for the LC-MS consisted of solvents A and B; Solvent A was composed of 97:3 (v/v) LC-MS grade H_2O: methanol with 15 mM acetic acid and 10 mM tributylamine; Solvent B was pure methanol (Kukurugya, 2017). The flow rate was 180 µL min^{-1} for the duration of a given sample's analysis, with a solvent A gradient of 0 min, 100%; 2.5 min, 100%; 5 min, 80%; 7.5 min, 80%; 10 min, 45%; 12 min, 45%; 14 min, 5%; 17 min, 5%; 18 min, 0%; 25 min, 0% (Kukurugya, 2017; Sasnow, 2016). Injection volume for each sample was 10 µL, with a consistent column temperature of 25°C. An Acquity UPLC Waters 1.7 µm particle size column was used for all samples and experiments (Milford, MA). The following metabolites

were tracked for the MFA: gluconate, 6-phospho-gluconate (6-PG), G6P, F6P, FBP, PYR, xylulose-5-phosphate (Xu5P), ribose-5-phosphate (R5P), DHAP, phosphoenolpyruvate (PEP), citrate, α-ketogluterate, succinate, fumarate, malate, aspartate, and sedoheptulose-1/7-bisphosphate (S7P). Aspartate was taken as a proxy for oxaloacetate (OAA), as was done previously (Amador-Noguez et al., 2010; Kukurugya, 2017; Sasnow et al., 2016).

V. Metabolite excretion

To determine the rate of excretion of metabolites, 50 µL of filtered supernatant was taken from the Gluc and Gluc:Fruc:Xyl consumption samples during growth. These samples were then diluted 1:20 with LC-MS grade water (Fisher Scientific, Pittsburgh, PA) during early exponential phase, or 1:200 during late exponential and stationary phases. Higher dilutions were used at higher OD_{600} readings due to very high concentrations of metabolites in the extracellular media. The samples were stored at 4°C for no more than 5 hours prior to processing in the LC-MS. Excretion rates (µmol g_{CDW}^{-1} h^{-1}) were calculated via regression analysis.

VI. Long-term isotopic labeling

The intracellular metabolite pool levels at pseudo-steady state were observed for cells in exponential growth (Sasnow, 2016). Long-term isotopic enrichment of the metabolites was achieved with [U-$^{13}C_6$]-Gluc, [1,2-$^{13}C_6$]-Gluc, 1:1 [U-$^{13}C_6$]-Gluc: unlabeled glutamate, 1:1:1 [1,2,3-$^{13}C_6$]-Gluc: [1,6-$^{13}C_6$]-Fruc: unlabeled Xyl, and 1:1 [U-$^{13}C_6$]-Gluc: unlabeled gluconate. All labeled sugars were purchased from Cambridge Isotopes (Tewskbury, MA) or Omicron Biochemicals (South Bend, IN). Batch cultures (two biological replicates) were grown twice in labeled minimal media until the OD_{600} reached 1 and 2. At each OD_{600}, aliquots (3 mL) of

culture were filtered through 0.22 µm pore nylon filter disks in the presence of both a vacuum and a flame from a Bunsen burner to prevent contamination. The cells remaining on the filter disk were immediately quenched in 2 mL of 4°C 2:2:1 methanol:acetonitrile:water. The lysed cells were scraped from the filter disk into the quenching solution, which was then centrifuged for 5 minutes at 4°C and 9,391 g. Two 100 µL aliquots of the resulting supernatant were dried down under N_2 gas (50 minutes). The dried metabolites were then re-suspended in 100 µL LC-MS water, and processed via LC-MS as described in section IV. The isotopic labeling patterns were analyzed with the MAVEN (Metabolomic Analysis and Visualization Engine) software suite (Melamud et al., 2010; Clasquin et al., 2012). Natural abundance of ^{13}C was corrected for using a correctional MATLAB code developed at Princeton University. The relative abundances of individual metabolites were normalized and compared across carbon-source conditions.

The MAVEN software determined the relative proportions of the isotopes of each metabolite according to the signal intensity of the metabolite in the sample (Clasquin et al., 2012); to ascertain that the signals detected by MAVEN were legitimate representations of the metabolite concentrations, a series of metabolite calibrations were run using carbon source standards at fixed concentrations, and the total size of several metabolite pools were calculated in tractable units of uM/g_{CDW}.

The isotopic labeling of the environmental CO_2 was monitored by tracking the long-term isotopic enrichment profiles of ornithine and citrulline. Citrulline, a six-carbon metabolite, was formed when CO_2 was captured as a carbamoyl phosphate and incorporated with ornithine, a five-carbon metabolite (Legrain et al, 1977). Other *Bacillus* species have been reported to express ornithine carbamoyltransferase, the enzyme responsible for catalyzing this reaction, and thus it was assumed that *B. megaterium* QM B1551 also possessed a copy of the gene encoding

this enzyme (Issaly et. al., 1974). Since fully ^{13}C-labeled citrulline could only be derived from fully ^{13}C-labeled ornithine combining with ^{13}C-labeled CO2, the fraction of ^{13}C-labeled CO_2 was calculated by dividing the fraction of sextuply ^{13}C-labeled citrulline by the fraction of quintuply ^{13}C-labeled ornithine.

VII. Kinetic isotopic labeling

In vivo incorporation of carbon into *B. megaterium* was determined via kinetic flux experiments. Batch cultures (three biological replicates) were grown twice in unlabeled minimal media with either Gluc or Gluc:Glutamate until early exponential phase, corresponding to OD_{600} 0.4 to 0.6. Aliquots (3 mL) of the cultures were then filtered through 0.22 µm pore nylon filter disks in the presence of both a vacuum and a flame from a Bunsen burner. A total of 18 cell-laden filter disks were generated. Each disk was then placed cell-side up on a small agar plate containing unlabeled carbon in minimal media and allowed to grow to exponential phase, corresponding to OD_{600} 0.5 (Sasnow, 2016). The cells experienced multiple doubling times to become fully acclimated to the new growing conditions prior to the kinetic incorporation of isotopes. The disks were transferred to agar plates containing labeled carbon in minimal media and allowed to grow on the labeled media for fixed time intervals. The labeled carbon used was either [U-$^{13}C_6$]-Gluc or 1:1 [U-$^{13}C_6$]-Gluc:unlabeled glutamate. After a set period of time following the isotopic switch (0 sec, 20 sec, 1 min, 4 min, 12 min, 30 min), the filter disk was removed from the labeled plate and metabolism was immediately quenched by flipping the disk cell-side down into 2 mL of 4°C 2:2:1 methanol:acetonitrile:water. The lysed cells were scraped from the filter disk into the quenching solution, which was then centrifuged for 5 minutes at 4°C and 9,391 g. Two 100 µL aliquots of the supernatant were dried down under N_2 gas (50

minutes). The dried metabolites were then re-suspended in 100 µL of LC-MS water and processed as described in section IV. The isotopic labeling patterns were analyzed with the MAVEN software suite, as described in section VI, and corrected for the natural abundance of ^{13}C (Melamud et al., 2010; Clasquin et al., 2012).

VIII. Metabolic Flux Analysis

To predict the relative flux of carbon through a *B. megaterium* QM B1551 cell, a model was constructed using metabolomics flux analysis (MFA). This analysis estimated the relative flux of metabolites, normalized to the uptake of carbon substrate, between different nodes in a metabolic network. Determining which reaction pathways were utilized by *B. megaterium* QM B1551 required *a priori* knowledge of the metabolic network within the strain. Metabolites of interest were considered as nodes in the network. The reactions between them were used to construct ordinary differential equations to solve for the fluxes, provided some constraining parameters and initial conditions. The consumption rates, excretion rates, LC-MS isotopic labeling data, and biomass composition of *B. megaterium* for the Gluc alone condition were used as system constraints on the MFA model.

The stoichiometric biomass composition of *B. megaterium* was not available, so the composition of *B. subtilis* was used instead (Dauner et al., 2001b). Briefly, the metabolic requirements for cell growth were calculated for each substrate condition, and used as effluxes in the metabolic network. Any reaction which involved a carboxylation or decarboxylation was treated as irreversible. All reversible reactions within the network were reported as a net flux between the nodes. The network was limited to a set number of nodes in the glycolytic pathway, PP pathway, and TCA cycle (Fig. 37). The model was initialized using a number of free fluxes,

which were chosen to 1) force the system to have a 100% influx of Gluc and 2) ensure that the resulting fluxes were physically realistic. The latter point was accomplished by setting the free fluxes to values that were similar or identical to previously determined fluxes in *B. megaterium* (Furch et al., 2007a).

The software suite 13CFLUX2 was run to generate metabolic reaction rates between a supplied set of metabolite network nodes (Weitzel et al., 2012). The model assumed that only succinate, gluconate, fumarate, aspartate, citrate, αKG, glutamate, and PYR would be secreted, and included biomass effluxes from the G6P, R5P, E4P, 3PG, PEP, PYR, Ac-CoA, OAA, αKG, and DHAP nodes. The program generated an initial set of flux values which were then optimized according to the supplied constraints. The program used each iteration of generated flux values to compute the likely labeling patterns for each metabolite node of interest in the network; the program then calculated the error (residuals) between the experimental LC-MS long-term isotope labeling data and the generated patterns to ascertain the quality of the fit. The user determined the duration of the optimization process (Sasnow, 2016).

RESULTS AND DISCUSSION

I. Growth phenotype and sugar consumption

To begin assembling the necessary constraints for the MFA in *Bacillus megaterium* QM B1551, the growth rates and substrate consumption rates during growth on the various carbon sources were investigated. The growth rate on each carbon-source was found to be (in h^{-1}): 0.71 ± 0.04 for Gluc, 0.62 ± 0.04 for Fruc, 0.38 ± 0.02 for Xyl, 0.57 ± 0.07 for Gluc:Fruc:Xyl, 0.73 ± 0.04 for Gluc:Glutamate, and 0.75 ± 0.05 for Gluc:Gluconate (Fig. 3). The growth curves for all carbon-conditions are shown in Figure S1 in the Appendix.

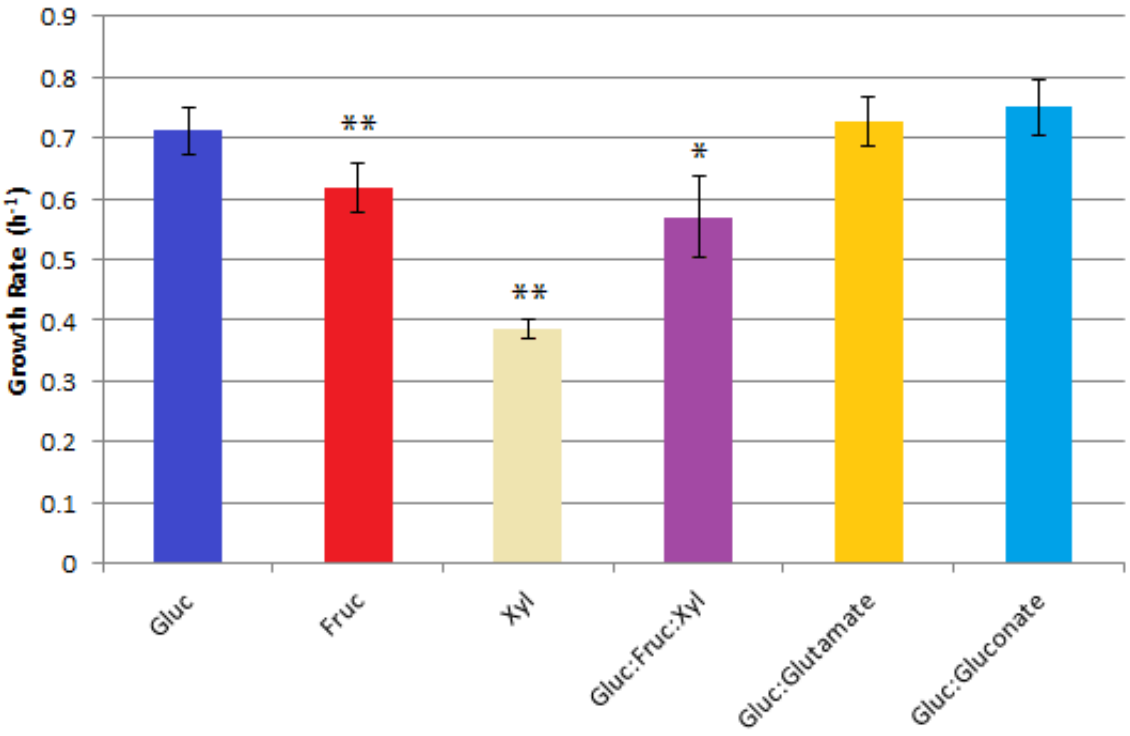

Figure 3. The specific growth rate (h^{-1}) of *B. megaterium* QM B1551 grown on glucose (dark blue), fructose (red), xylose (tan), Gluc:Fruc:Xyl (purple), Gluc:Glutamate (yellow), or Gluc:Gluconate (light blue). The growth rates were determined using just the exponential growth. Two-tailed unpaired *t*-test analysis was conducted to compare the growth rates relative to the Gluc condition with n=3. * indicates $P < 0.05$, and ** indicates $P < 0.01$

The sugar consumption rates of Gluc, Fruc, and Xyl as the sole substrates (mmol sugar $g_{CDW}^{-1}\, h^{-1}$) were found to be 5.30 ± 1.61, 2.88 ± 2.30, and 0.41 ± 0.06 respectively. The sugar

consumption rates of Gluc, Fruc, and Xyl in the Gluc:Fruc:Xyl mixture (mmol sugar g_{CDW}^{-1} h^{-1}) were found to be 2.8 ± 0.06, 1.3 ± 0.05, and negligible, respectively.

II. Metabolic Network Structure

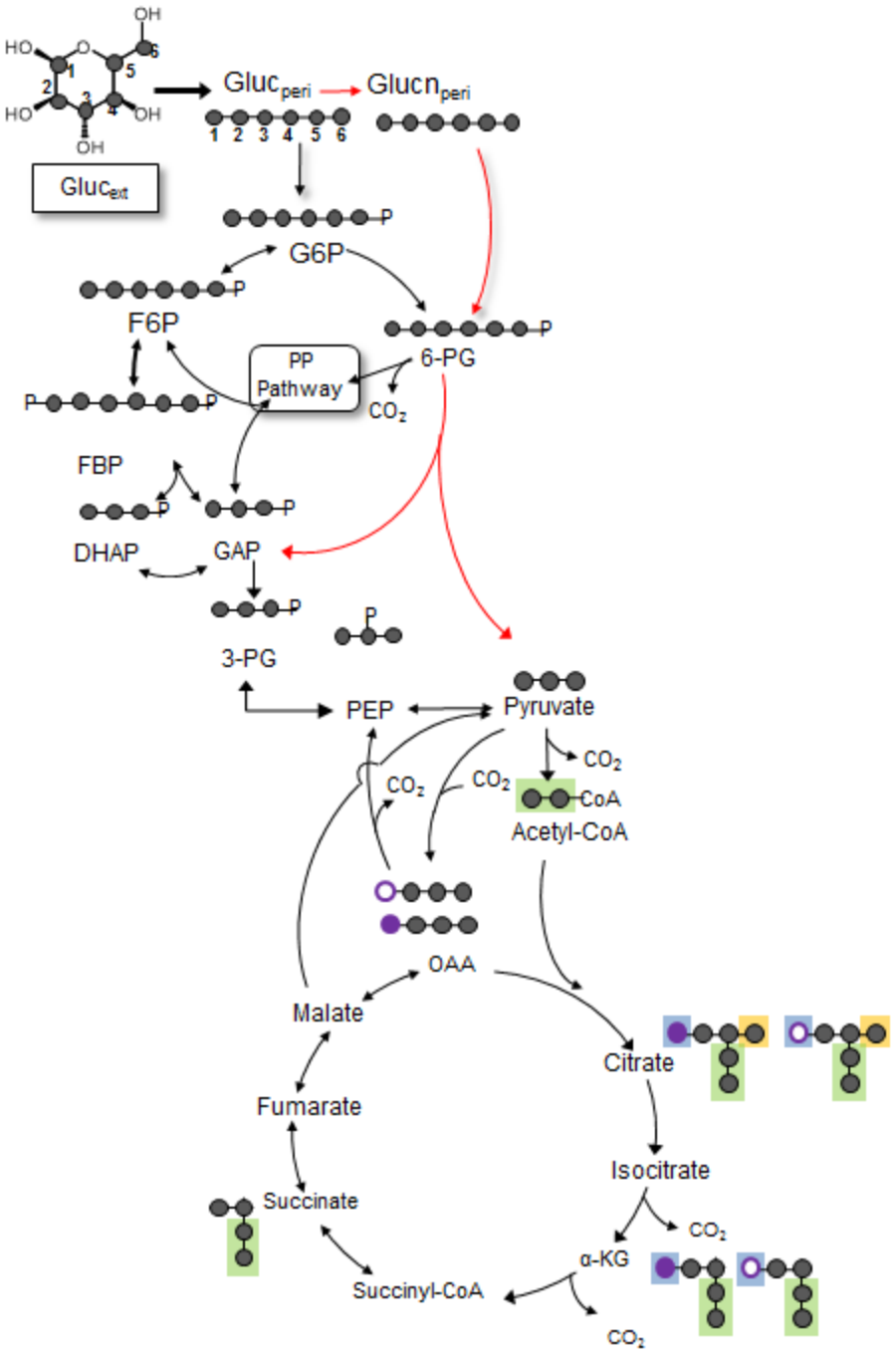

Figure 4. The theoretical isotopic distribution of the metabolic network of *B. megaterium* growing on [U-^{13}C]-Gluc. The pathways shown in red (gluconate incorporation and ED pathway) have been proposed, but are not verified in this experiment. The purple carbons are incorporated CO_2. The green background shows the fate of the Ac-CoA atoms in the TCA cycle. The yellow background shows the carbons that are canonically cleaved in the citrate decarboxylation reaction; the blue background shows the carbons that are canonically cleaved in the αKG decarboxylation reaction.

To determine that *Bacillus megaterium* QM B1551 had reached metabolic pseudo-steady state, we obtained long-term isotopic enrichment of its intracellular metabolites using [U-^{13}C]-Gluc at two sampling points during the exponential growth phase (OD_{600} 1 and 2). In a pseudo-steady state condition, complete isotopic enrichment across all metabolites at both sampling times would indicate that the cells had fully incorporated the ^{13}C-labeled Gluc, and that a flux-balance was achieved at each metabolic network node (Fig. 4). Indeed, we found that enrichment with [U-^{13}C]-Gluc resulted in fully ^{13}C-labeled metabolites in the EMP and PP pathways at both sampling times (Fig. 5, 6). The complete ^{13}C labeling of metabolites continued through pyruvate (PYR), the three-carbon metabolite downstream of glycolysis and directly upstream of the TCA cycle (Fig. 6). These data were thus consistent with pseudo-steady state metabolic conditions.

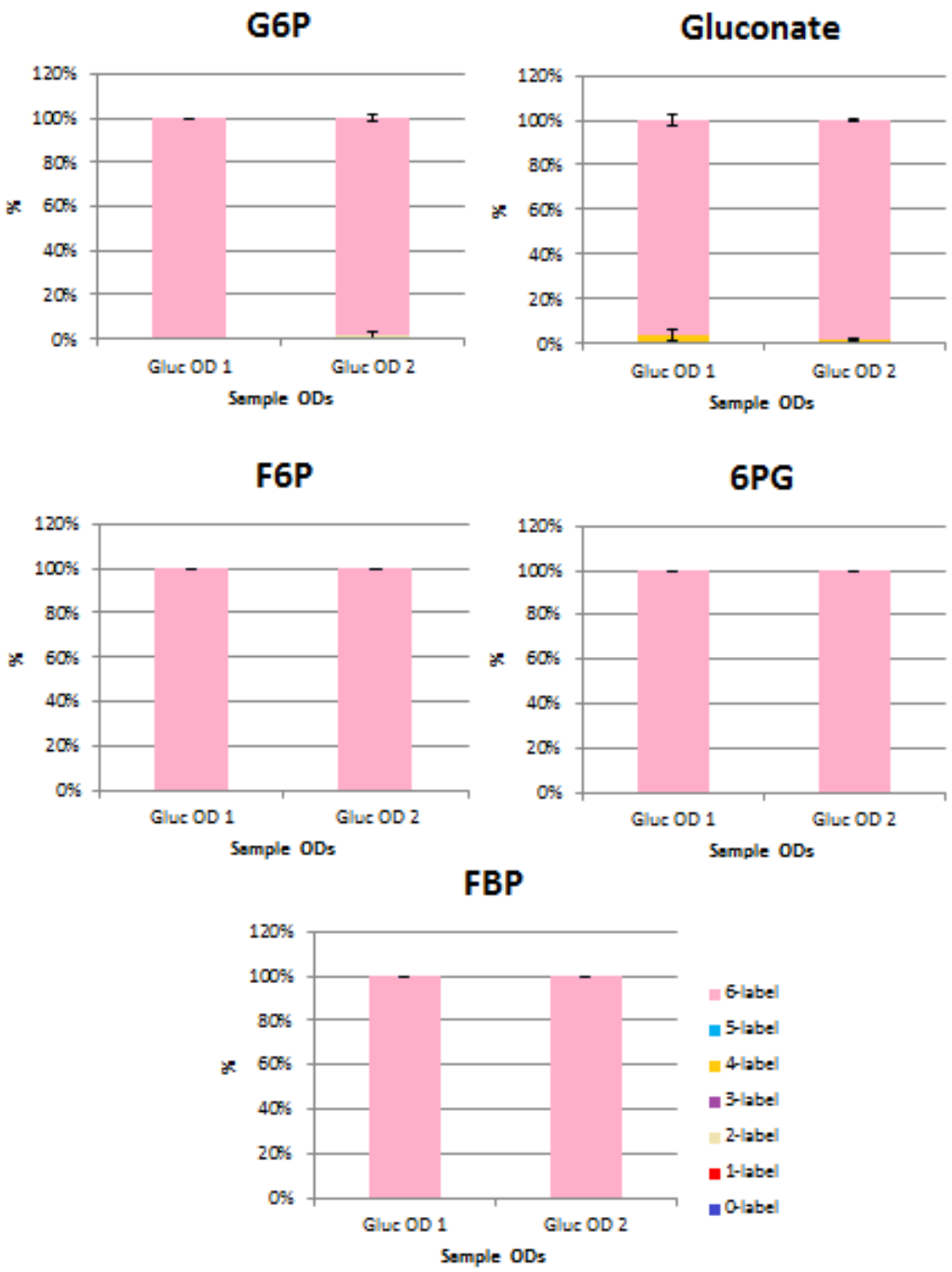

Figure 5. The isotopic labeling fractions, with standard deviations, for five metabolites in the glycolytic EMP pathway when grown on [U-^{13}C]-Gluc. The two columns for each metabolite represent the average isotopic labeling distribution at OD 1 (left) and OD 2 (right). Abbreviations used: G6P, glucose-6-phosphate; F6P, fructose-6-phosphate; 6PG, 6-phospho-gluconate; FBP, fructose-bis-phosphate

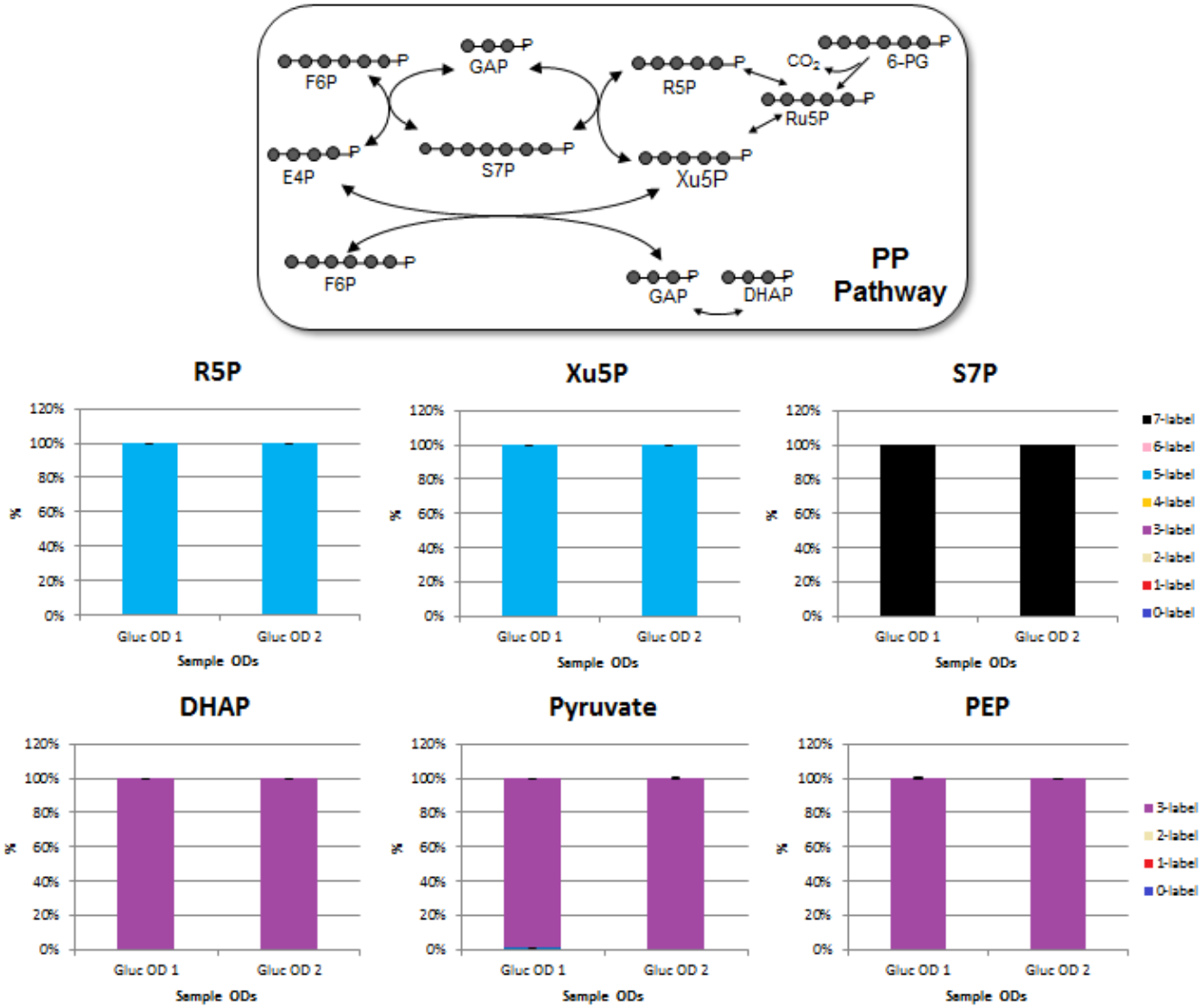

Figure 6. The isotopic labeling fractions, with standard deviations, for three PP pathway metabolites and three lower glycolytic 3C metabolites when grown on [U-^{13}C]-Gluc. The two columns for each metabolite represent the average isotopic labeling distribution at OD 1 (left) and OD 2 (right). The theoretical isotopic distribution of the PP pathway of *B. megaterium* growing on [U-^{13}C]-Gluc is shown. Abbreviations used: R5P, ribose-5-phosphate; Xu5P, xyulose-5-phosphate; S7P, sedoheptulose-7-phosphate; DHAP, dihydroxy-acetone-phosphate; PEP, phosphoenolpyruvate

The TCA cycle metabolites did not reflect fully ^{13}C-labeled fractions due to the incorporation of unlabeled CO_2 from the environment (Fig. 7, 8). Citrate, a six-carbon metabolite, was approximately 80% sextuply ^{13}C-labeled and 20% quintuply ^{13}C-labeled (Fig. 8). It follows that the average fraction of nonlabeled CO_2 should be about 20% (Fig. 8). However,

the fraction of non^{13}C-labeled CO_2 was only 8%, which was too low to account for all of the ^{13}C-labeled citrate (Fig. 7, 8). One possible explanation for this discrepancy was that the flux into the TCA cycle may have be limited, and that the TCA cycle metabolites had not yet reached pseudo-steady state by OD_{600} 1 or 2. This hypothesis was supported by the observation that the other metabolites in the TCA cycle also displayed differences in their isotopic profiles at both OD_{600} readings (Fig. 8).

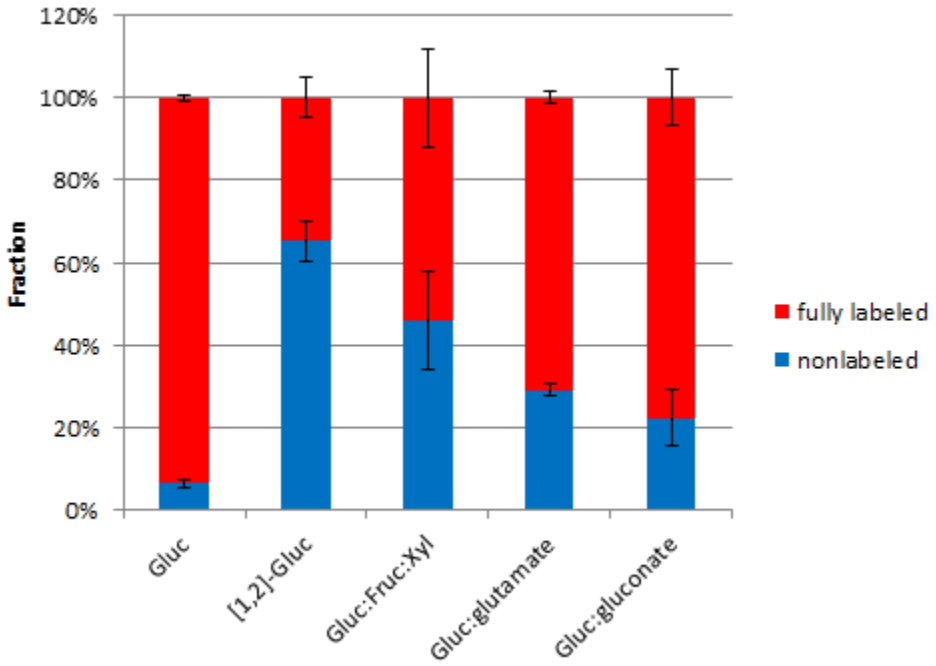

Figure 7. The fraction of unlabeled CO_2 (blue) and fully ^{13}C-labeled CO_2 (red) dissolved in the growth medium for each of the experimental conditions tested. These values represent an average of CO_2 measurements from OD_{600} 2.

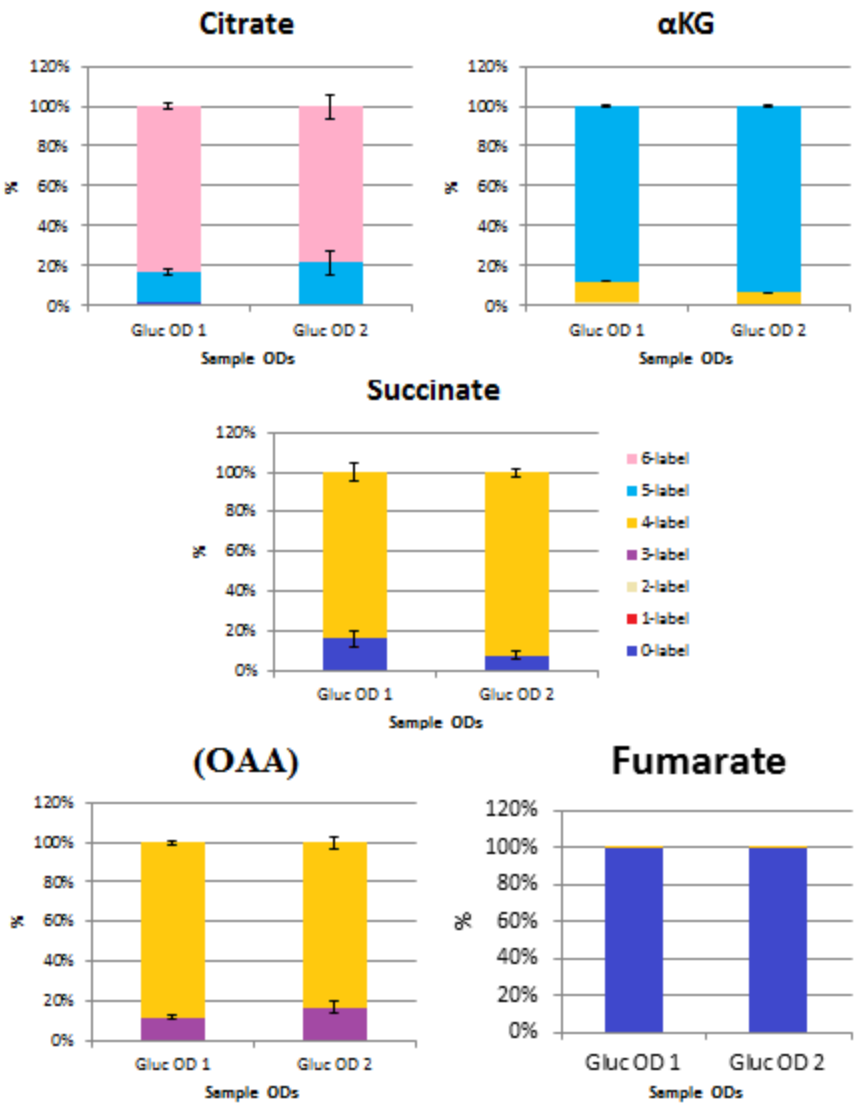

Figure 8. The isotopic labeling fractions, with standard deviations, for five metabolites in the TCA cycle when grown on [U-^{13}C]-Gluc. The two columns for each metabolite represent the average isotopic labeling distribution at OD 1 (left) and OD 2 (right). The abbreviation αKG stands for α-ketoglutarate.

Moving through the TCA cycle, citrate lost its first carbon position to become αKG, a five-carbon metabolite which was 90-95% quintuply ^{13}C-labeled and 10-5% quadruply ^{13}C-labeled (Fig. 8). Compared to the citrate labeling, which was 80% sextuply ^{13}C-labeled and 20% quintuply ^{13}C-labeled, the αKG labeling implied that the carbon lost as CO_2 from citrate was primarily nonlabeled (Fig. 8). This hypothesis holds interesting implications for the stereochemistry of citrate, as the canonical cleavage of citrate to αKG involves the loss of the

first carbon of citrate, which is ^{13}C-labeled in this scheme (Fig. 4). This implies that a different carbon position of citrate may have been cleaved during the decarboxylation reaction to αKG. In this ^{13}C-labeling scheme, the only nonlabeled carbon in citrate was derived from the addition of unlabeled CO_2 to PYR to form OAA, which became the fourth carbon position of citrate (Fig. 4). For this carbon to be cleaved in the decarboxylation to αKG, either *B. megaterium* possessed a unique enzyme which cleaved citrate at the fourth carbon position, or the orientation of the OAA molecule was flipped prior to its incorporation into citrate such that the nonlabeled carbon occupied the first carbon position of citrate.

Subsequent decarboxylation of αKG resulted in CO_2 and succinate, a four-carbon metabolite (Fig. 1). At pseudo-steady state, succinate was between 84-92% quadruply ^{13}C-labeled, which closely matched quintuply ^{13}C-labeled αKG (Fig. 8). If succinate was derived entirely from αKG, it would be expected that the remaining 8-16% of the metabolite pool would be triply ^{13}C-labeled; however, the remaining succinate isotope was nonlabeled (Fig. 8). This means that even when grown twice on [U-^{13}C]-Gluc, *B. megaterium* QM B1551 was somehow able to retain unlabeled carbon atoms in its succinate metabolite pool, or was deriving them from some other carbon source than the sugar substrate. Since the growth medium contained no other carbon source besides fully ^{13}C-labeled Gluc, this latter theory is unlikely. Fumarate was almost entirely nonlabeled at both OD_{600} readings, indicating that the ^{13}C-labeled carbon derived from the Gluc substrate was not reaching the fumarate metabolite pool (Fig. 8).

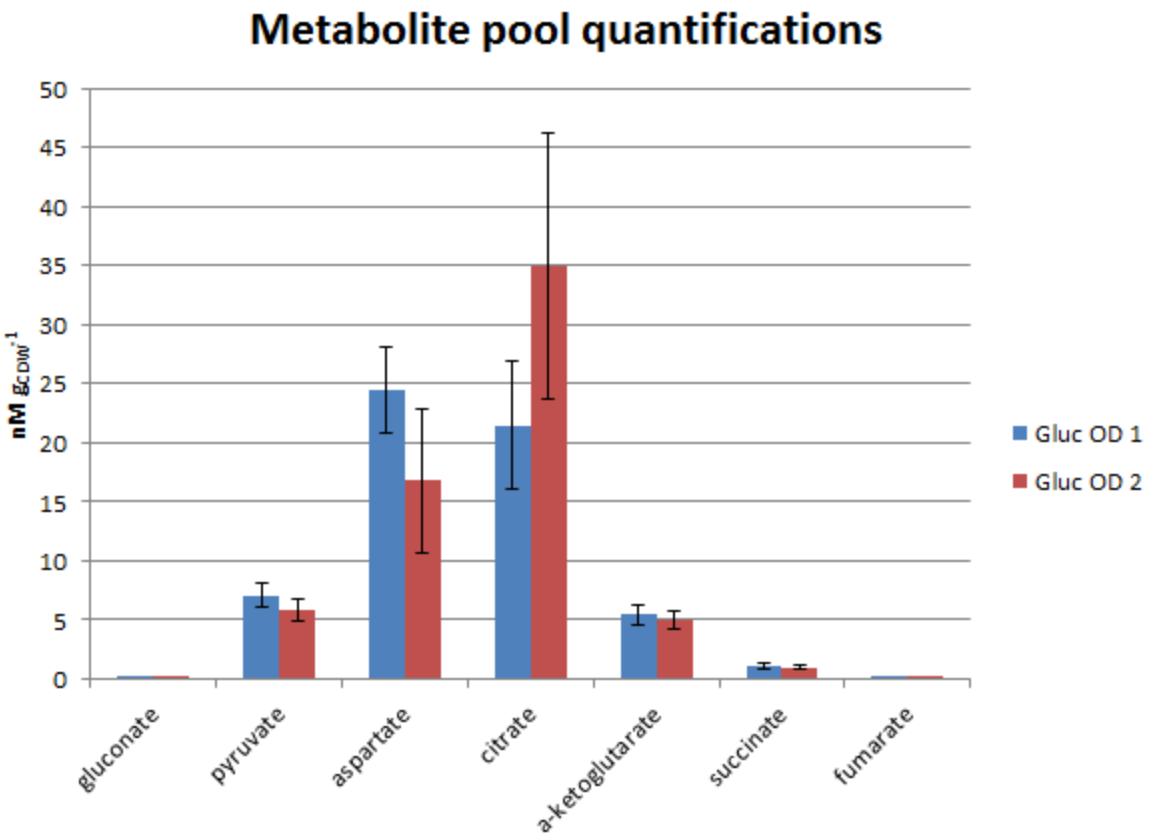

Figure 9. The total size of several metabolite pools, summed over all isotopic fractions for a given metabolite, for OD_{600} 1 and 2.

Fumarate could have been primarily nonlabeled for two reasons; either fumarate was not synthesized, or there was an error in the MAVEN isotopic fractionation. The low level of fumarate in the samples, in addition to the low quality of the fumarate peaks in MAVEN (data not shown), support the theory that there was an error in the MAVEN isotopic algorithm (Fig. 9). However, succinate had a reasonable quantifiable level of expression, and therefore should not have experienced errors in MAVEN. This implies that the increase in non ^{13}C-labeling in succinate is legitimate. This in turn implies that the flux through the TCA cycle is severely constricted, and that pseudo-steady state was likely not achieved for these metabolites by OD_{600} 1 and 2 (Fig. 9).

As mentioned previously, PYR is carboxylated to form OAA. In this experiment, the isotopic labeling of OAA, as determined from aspartate, closely resembled that of PYR, with the addition of some unlabeled CO_2 (Fig. 6, 8). Specifically, OAA was approximately 85% quadruply ^{13}C-labeled and 15% triply ^{13}C-labeled (Fig. 8). These isotopic proportions were very similar to those of citrate, which supports the generally accepted model of the TCA cycle, wherein OAA combines with Ac-CoA to form citrate in a non-reversible reaction. Provided that Ac-CoA is derived from the triply ^{13}C-labeled PYR, adding doubly ^{13}C-labeled carbon to the isotopic fractions of OAA could yield the measured isotopic fractions of citrate (Fig. 8). It should be noted that unlike succinate, OAA does not have a significant fraction of nonlabeled moieties (Fig. 8). This observation again leads us to suspect that *B. megaterium* QM B1551 is not producing fumarate in significant quantities. Since all bacterial cultures grew to OD_{600} readings of 10 or higher, the metabolite quantification implied that a complete TCA cycle is not necessary for sufficient cell growth (Fig 9, S1).

We verified the proposed metabolic network structure of *B. megaterium* QM B1551 using [1,2-^{13}C]-Gluc. This isotope of Gluc was chosen because of the unique ^{13}C-labeling patterns that would be generated throughout the metabolic network. Upon entering the cell, doubly ^{13}C-labeled Gluc is converted to doubly ^{13}C-labeled G6P, which in turn becomes doubly ^{13}C-labeled 6-PG (Fig. 10). The first position of 6-PG is cleaved through the oxidative PP pathway to yield singly ^{13}C-labeled pentose-phosphate metabolites, R5P and Xu5P (Fig. 10). Alternatively, G6P can follow the EMP pathway, eventually producing nonlabeled and doubly ^{13}C-labeled triose-phosphates (Fig. 10). These triose-phosphates combined with doubly ^{13}C-labeled F6P generate primarily doubly ^{13}C-labeled pentose-phosphates (Fig. 10). Thus, we

expected to use the pentose metabolites to determine the bacterium's preference for oxidative vs non-oxidative PP pathway.

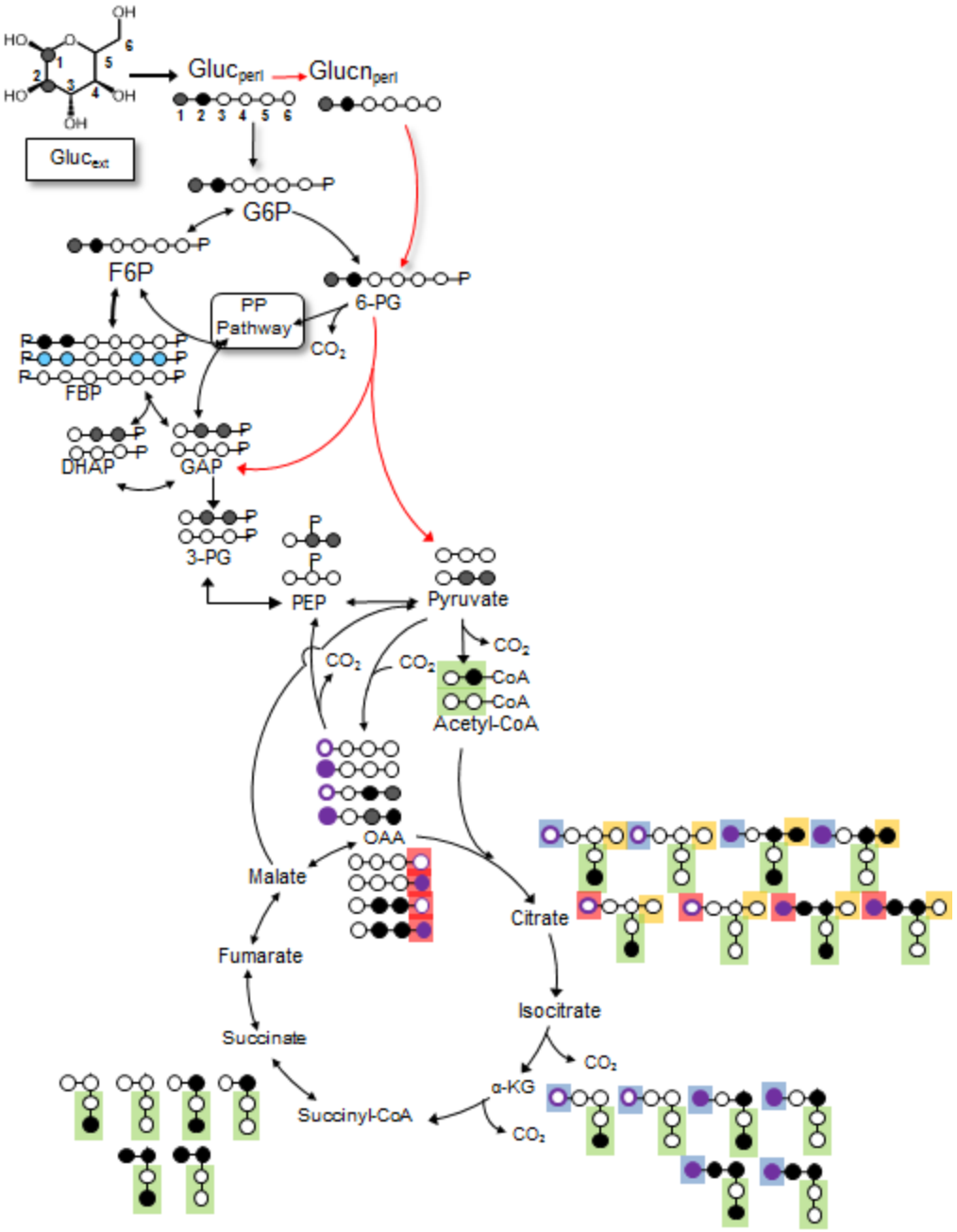

Figure 10. The theoretical isotopic distribution of the metabolic network of *B. megaterium* growing on [1,2-^{13}C]-Gluc. The pathways shown in red (gluconate incorporation and ED pathway) have been proposed, but are not verified in this experiment. The blue filled carbons in FBP indicate isotopes derived from gluconeogenesis. The purple carbons are incorporated CO_2. The purple carbons show two different CO_2 incorporation schemes, either addition to the front of PYR or addition to the end of PYR. The green background shows the fate of the Ac-CoA atoms in the TCA cycle. The yellow background shows the carbons that are canonically cleaved in decarboxylation of citrate to αKG. The blue background shows the carbons that are canonically cleaved in decarboxylation of αKG to succinate. The red background reiterates the position of the added CO_2 when OAA is flipped prior to its acetylation.

In the upper glycolytic pathway, G6P, gluconate, F6P, and 6-PG were all primarily doubly ^{13}C-labeled, as would be expected from growing on doubly ^{13}C-labeled Gluc (Fig. 10, 11). FBP was largely doubly ^{13}C-labeled, but also had 15% quadruply ^{13}C-labeled, 10% nonlabeled, and fractions of singly ^{13}C-labeled and triply ^{13}C-labeled moieties (Fig. 11). Downstream from FBP, PYR was 50% nonlabeled and slightly over 40% doubly ^{13}C-labeled (Fig. 12); this would be an expected labeling pattern if [1,2-^{13}C]-6-PG or [1,2-^{13}C]-FBP split to make nonlabeled or doubly ^{13}C-labeled DHAP and PYR (Fig. 10). It is possible, then, that the quadruply ^{13}C-labeled and nonlabeled FBP moieties were derived from gluconeogenesis, which has not yet been reported for this strain (Fig. 1, 10, 11, 12).

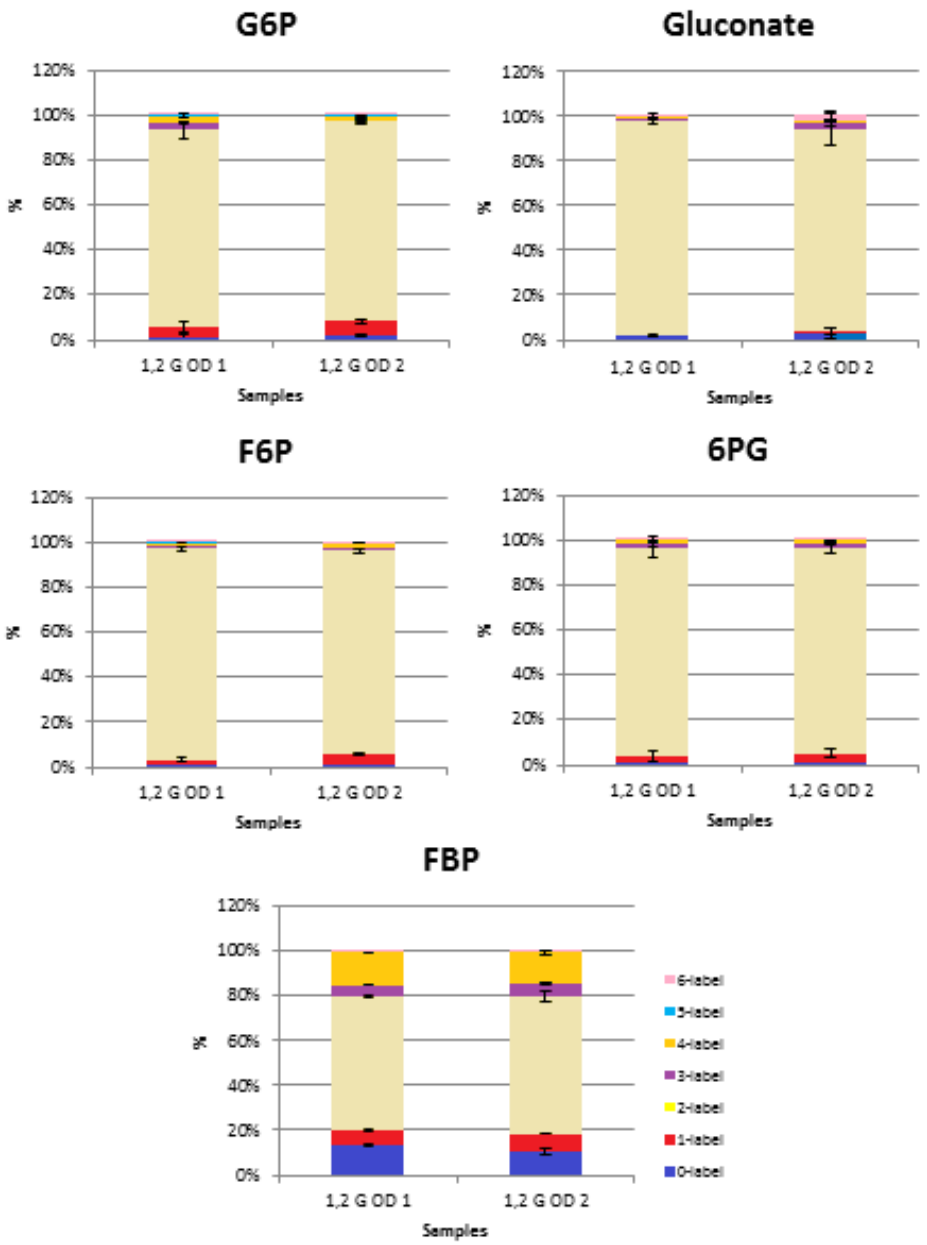

Figure 11. The isotopic labeling fractions, with standard deviations, for five metabolites in the glycolytic EMP pathway when grown on [1,2-^{13}C]-Gluc. The two columns for each metabolite represent the average isotopic labeling distribution at OD 1 (left) and OD 2 (right). Abbreviations used: G6P, glucose-6-phosphate; F6P, fructose-6-phosphate; 6PG, 6-phospho-gluconate; FBP, fructose-bis-phosphate

The roughly 5% of PYR, DHAP, and PEP that were singly ^{13}C-labeled were most likely derived from the PP pathway (Fig. 10, 12, 13). The pentose-phosphate metabolites R5P and Xu5P were both approximately 75% singly ^{13}C-labeled, indicating that these metabolites were

derived primarily through the oxidative PP pathway (Fig. 10, 13). In this scheme, the oxidative PP pathway involved doubly ^{13}C-labeled 6-PG losing the ^{13}C-labeled carbon in its first position to become a singly ^{13}C-labeled pentose sugar (Fig. 10). If the ribose sugars were populated via the nonoxidative PP pathway, one would expect to see a much higher isotopic fraction of doubly ^{13}C-labeled pentose sugars; the non-oxidative PP pathway would use a transketolase reaction to transfer the two labeled carbons in the first and second positions of doubly ^{13}C-labeled F6P onto nonlabeled GAP to form doubly ^{13}C-labeled Xu5P (Fig. 10, 11, 13). As described in the Introduction, the previously reported fluxes for the oxidative PP pathway in *B. megaterium* strains were inconsistent, and therefore this finding was significant (Sauer et al., 1997; Dauner et al., 2001; Furch et al., 2007a; Furch et al., 2007b; Tannlet et al., 2008).

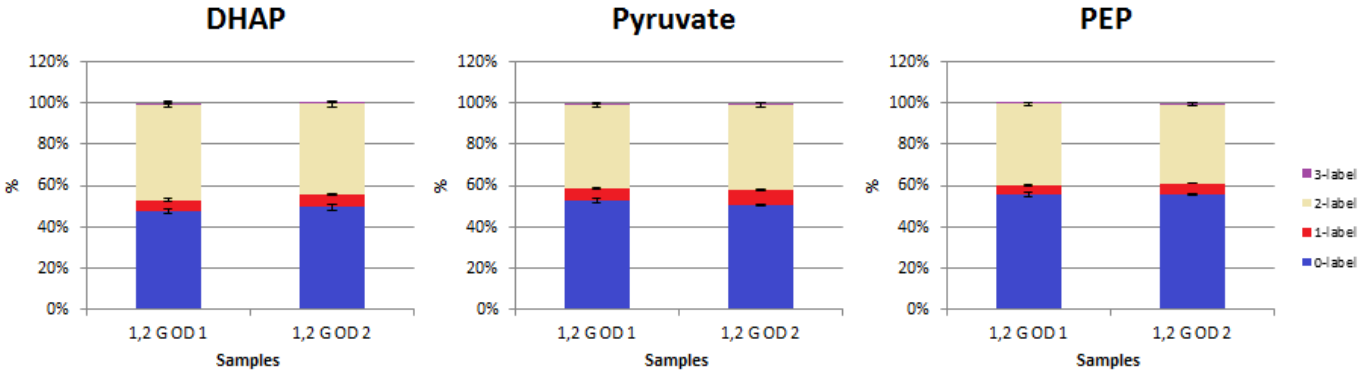

Figure 12. The isotopic labeling fractions, with standard deviations, for three lower glycolytic 3C metabolites when grown on [1,2-^{13}C]-Gluc. The two columns for each metabolite represent the average isotopic labeling distribution at OD 1 (left) and OD 2 (right). Abbreviations used: DHAP, dihydroxy-acetone-phosphate; PEP, phosphoenolpyruvate

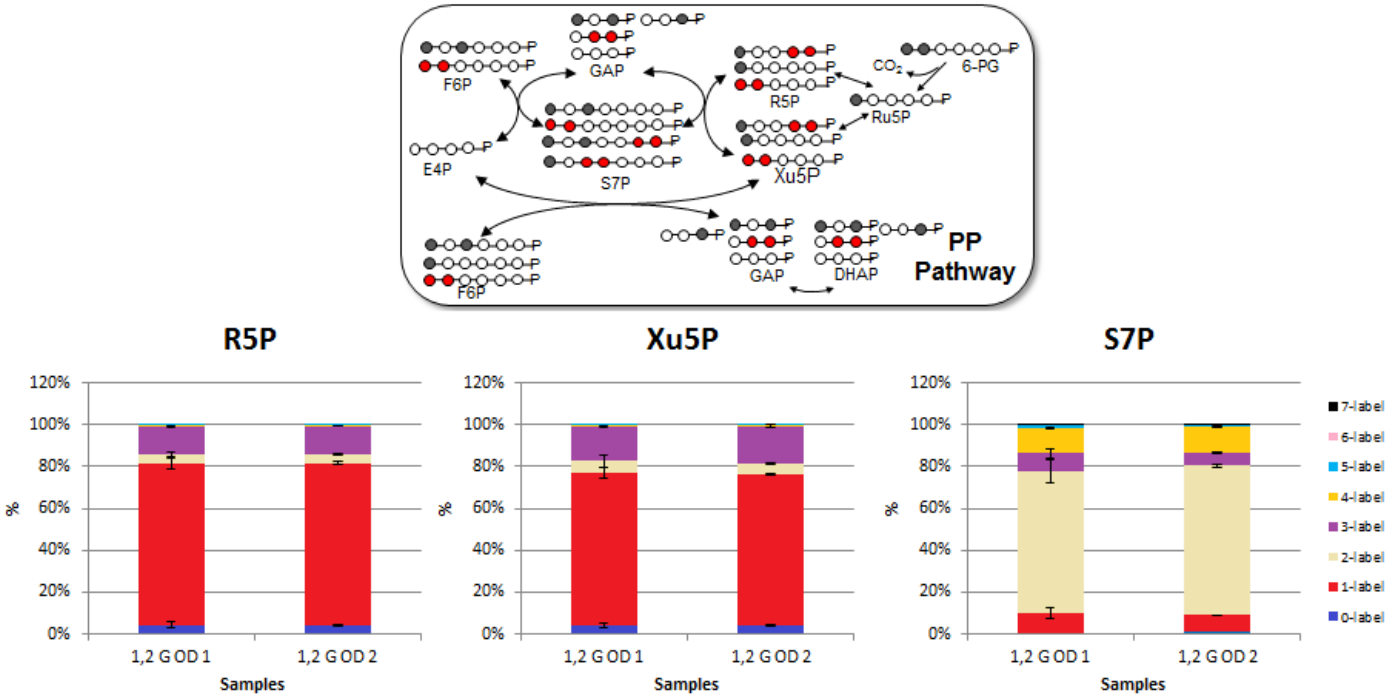

Figure 13. The isotopic labeling fractions, with standard deviations, for three PP pathway metabolites when grown on [1,2-^{13}C]-Gluc. The two columns for each metabolite represent the average isotopic labeling distribution at OD 1 (left) and OD 2 (right). The theoretical isotopic distribution of the PP pathway of *B. megaterium* growing on [1,2-^{13}C]-Gluc is shown. The red carbons were derived from the nonoxidative PP pathway, and the black carbons refer to those derived from the oxidative PP pathway. Abbreviations used: R5P, ribose-5-phosphate; Xu5P, xyulose-5-phosphate; S7P, sedoheptulose-7-phosphate

Moving into the TCA cycle, PYR generated primarily nonlabeled and doubly ^{13}C-labeled Ac-CoA, which combined with OAA to form citrate (Fig. 10, 14). Citrate had a fairly broad distribution of isotopic fractions, including 23% nonlabeled, 13% singly ^{13}C-labeled, 33% doubly ^{13}C-labeled, 14% triply ^{13}C-labeled, 13% quadruply ^{13}C-labeled, and 3% quintuply ^{13}C-labeled moieties (Fig. 14). The isotopic proportions of αKG were nearly identical to those of citrate (Fig. 14). These findings directly contrasted those of Sasnow (2016), who found that in the metabolic network of *Pseudomonas putida* grown on [1,2-^{13}C]-Gluc, the isotopic fractions of αKG matched those of citrate, implying that a labeled carbon was lost in the decarboxylation. The results for *B. megaterium* QM B1551 suggested that the carbon lost in this reaction was nonlabeled, which could indicate a unique stereochemistry for citrate synthesis and cleavage in

this organism (Fig. 14). This finding also supported the observation from the [U-^{13}C]-Gluc condition, in which an unlabeled carbon was suspected to be lost during the decarboxylation reaction from citrate to αKG (Fig. 4).

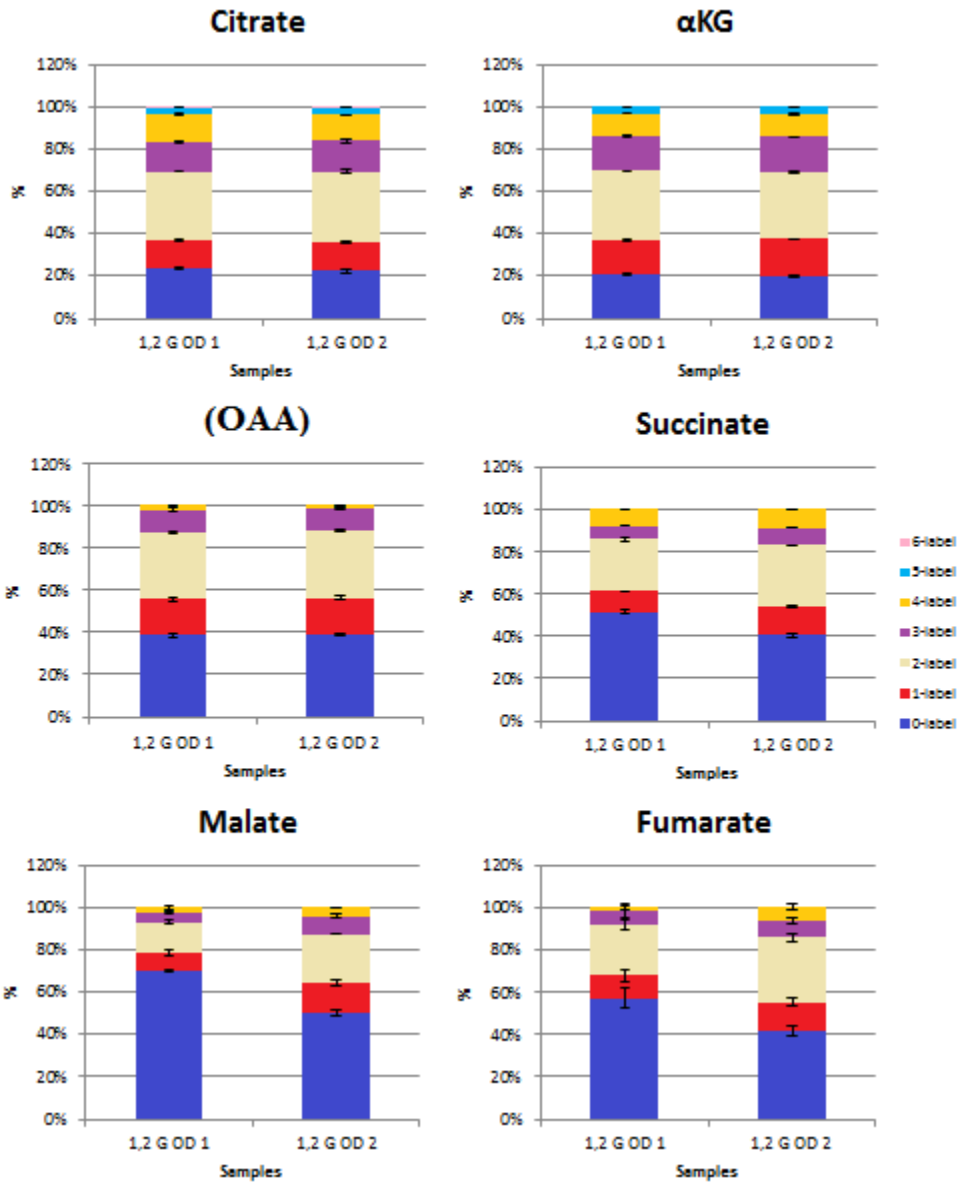

Figure 14. The isotopic labeling fractions, with standard deviations, for six metabolites in the TCA cycle when grown on [1,2-^{13}C]-Gluc. The two columns for each metabolite represent the average isotopic labeling distribution at OD 1 (left) and OD 2 (right). The abbreviation αKG stands for α-ketoglutarate.

There are a number of alternative chemical reactions which could explain the identical isotopic profiles in citrate and αKG (Fig. 14). For the labeling profiles to remain the same from

citrate to αKG after decarboxylation, the carbon cleaved from citrate must be a nonlabeled terminal carbon in the citrate structure accessible to an enzyme. One hypothesis was that there was an alternate addition of CO_2 to PYR to form a stereoisomer of OAA (Fig. 10). It was previously reported that in the carboxylation reaction which combines CO_2 and PYR to form OAA, the carbon from CO_2 is added in front of the first carbon position in the PYR molecule (Sasnow et al., 2016) (Fig. 2). Once OAA combines with Ac-CoA, what had been the fourth carbon of OAA is cleaved in the decarboxylation from citrate to αKG (Fig. 2). If, however, the carbon from CO_2 were added to the end of PYR to take the final position of OAA, that would leave a consistently nonlabeled carbon at the first position of OAA (Fig. 10). This would subsequently become the fourth carbon of citrate. If, however, OAA was flipped prior to its incorporation into citrate, the consistently nonlabeled carbon would occupy the first position of citrate, which could be cleaved to maintain an identical isotopic profile in αKG (Fig. 10). Other possibilities for alternative reactions include a different cleavage of PYR to form Ac-CoA, or an altered addition of Ac-CoA to OAA to form citrate. These hypotheses and others not listed here will require additional isotopic experiments to verify their validity

Continuing on in the TCA cycle, succinate had a higher fraction of nonlabeled moieties (40-50%) than could have been derived solely from αKG (21% nonlabeled) (Fig. 14). This mirrored the increased proportion of nonlabeled succinate observed in the [U-^{13}C]-Gluc condition (Fig. 8). Also as before, fumarate had a significant fraction of nonlabeled moieties, between 40 and 60% (Fig. 14). A similar metabolic quantification was employed for this condition and compared to the metabolite quantifications from the [U-^{13}C]-Gluc condition (Fig. 15). Based on the metabolite quantifications, the observed increased nonlabeled moieties in

fumarate were assumed to be either software error or indicative of a low flux through the TCA cycle (Fig. 14, 15).

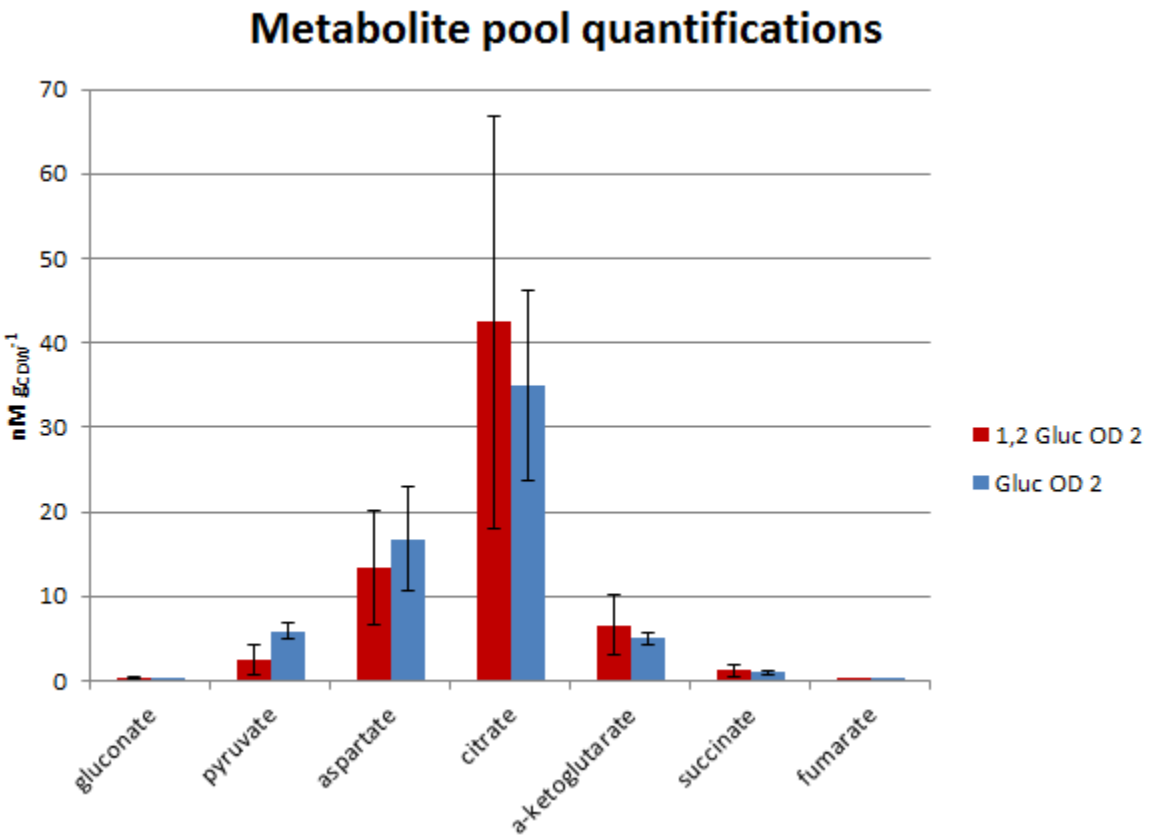

Figure 15. The quantifications of several metabolites averaged over two bioreplicates at OD_{600} 2 for both the [U-^{13}C]-Gluc condition (Gluc) and the [1,2-^{13}C]-Gluc condition (1,2 Gluc).

OAA had an isotopic distribution of 39% nonlabeled, 17% singly ^{13}C-labeled, 32% doubly ^{13}C-labeled, 10% triply ^{13}C-labeled, and 2% quadruply ^{13}C-labeled moieties (Fig. 14). The isotopic distribution of aspartate was reminiscent of that of PYR, likely because the CO_2 was largely nonlabeled (Fig. 7, 12, 14). This means that any OAA derived from the carboxylation of PYR and CO_2 would have similar proportions of isotopes as PYR (Fig. 12, 14). The 10% of aspartate that was triply ^{13}C-labeled was derived from a carboxylation combining ^{13}C-labeled CO_2 and doubly ^{13}C-labeled PYR (Fig. 7, 12, 14).

Once again, these findings are suggestive of a bifurcated TCA cycle. Both the metabolic labeling and the metabolite pools implied a bottleneck of fluxes from citrate to αKG, from αKG to succinate, and from OAA to fumarate (Fig. 14, 15).

In the above experiments, we obtained a small pool of fully ^{13}C-labeled gluconate during growth on [U-^{13}C]-Gluc and a small pool of doubly ^{13}C-labeled gluconate during growth on [1,2-^{13}C]-Gluc (Fig. 5, 9, 11, 15). Since these labeling patterns of gluconate could only be derived from the provided Gluc sources, these results indicate that gluconate could be involved in the initial Gluc metabolism. However, in previous MFA models of *Bacillus* species, the gluconate node was frequently omitted from the glycolytic pathway (Sauer et al., 1997; Dauner et al., 2001a; Furch et al., 2007a; Furch et al., 2007b; Tannler et al., 2008; Korneli et al., 2012. To prove if *B. megaterium* QM B1551 could incorporate and utilize gluconate, cell cultures were fed a 50:50 mixture of [U-^{13}C]-Gluc and unlabeled gluconate (Fig. 16). If gluconate could be incorporated into the metabolic network, nonlabeled moieties should be present in metabolites downstream from gluconate, such as 6-PG (Fig. 16). Metabolites that were not synthesized from gluconate should have full ^{13}C-labeling patterns, derived from glucose (Fig. 16).

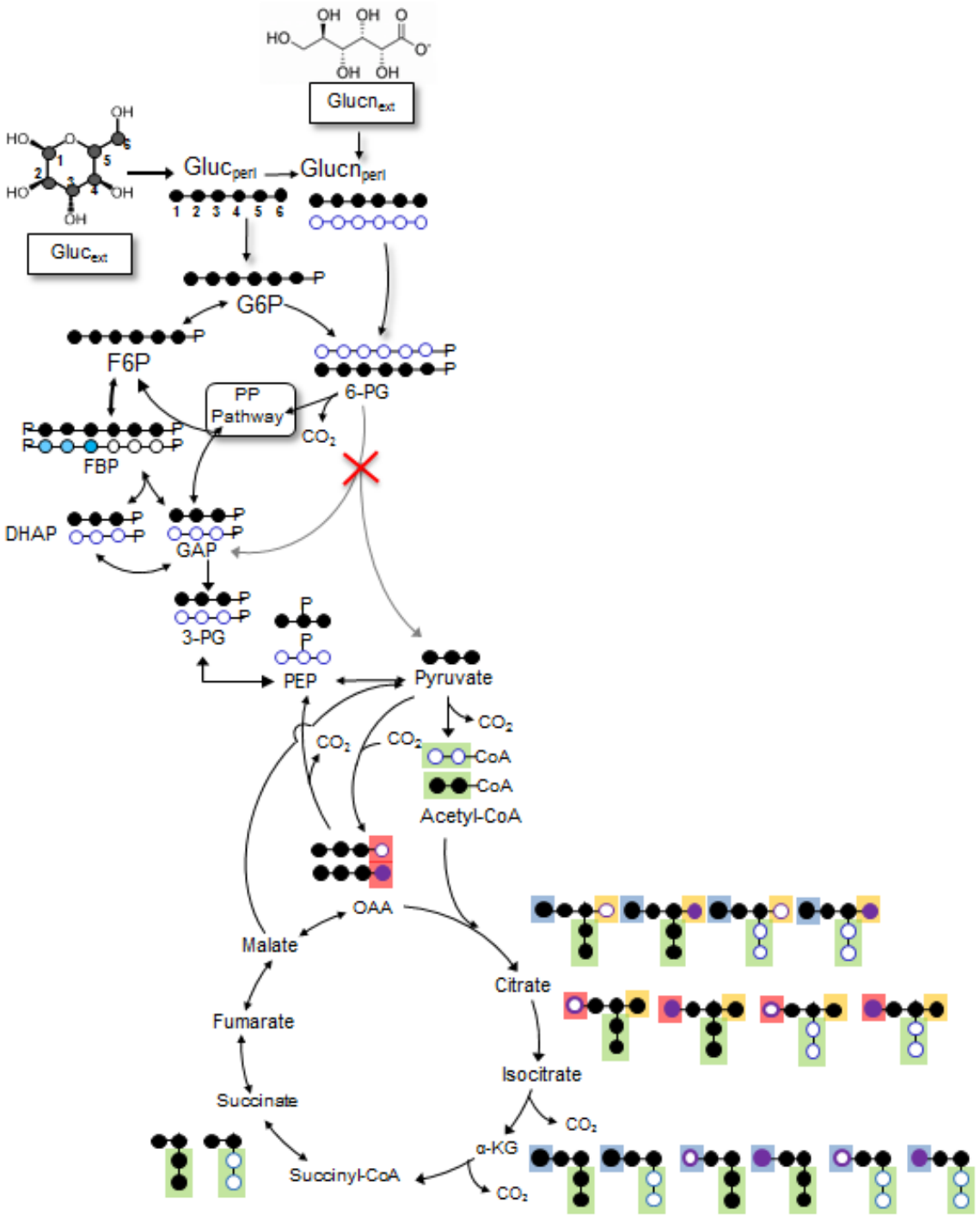

Figure 16. The theoretical isotopic distribution of the metabolic network of *B. megaterium* growing on [U-^{13}C]-Gluc and unlabeled gluconate. The ED pathway was shown not to be present in this bacterium. The blue carbons in FBP indicate isotopes derived from gluconeogenesis. The purple carbons are incorporated CO_2. The green background shows the fate of the Ac-CoA atoms in the TCA cycle. The yellow background shows the carbons that are canonically cleaved in decarboxylation from citrate to αKG. The blue background shows the carbons that are canonically cleaved in decarboxylation from αKG to succinate. The red background reiterates the position of the added CO_2 when OAA is flipped prior to its acetylation.

Figure 17. The isotopic labeling fractions, with standard deviations, for five intracellular metabolites in the glycolytic EMP pathway when grown on [U-^{13}C]-Gluc and nonlabeled gluconate. The two columns for each metabolite represent the average isotopic labeling distribution at OD 1 (left) and OD 2 (right). Abbreviations used: G6P, glucose-6-phosphate; F6P, fructose-6-phosphate; 6PG, 6-phospho-gluconate; FBP, fructose-bis-phosphate

As expected, G6P was almost entirely sextuply ^{13}C-labeled, indicating that it was derived from glucose (Fig. 16, 17). The isotopic profile of gluconate, which was almost entirely nonlabeled, could not be distinguished between the extracellular and intracellular pools of

gluconate (Fig. 17). Thus, a more reliable indication of gluconate incorporation necessitated the monitoring of downstream metabolites such as 6-PG. We found that 6-PG was 18% and 36% nonlabeled at OD_{600} 1 and 2, respectively (Fig. 17). This indicated that both G6P and gluconate contributed to the 6-PG metabolite pool, and that the flux from G6P to 6-PG was preferred to the flux from gluconate to 6-PG at earlier OD_{600} readings than at later OD_{600} readings (Fig. 17). The isotopic profiles of the metabolites of the PP pathway were also in agreement with gluconate assimilation downstream in the metabolic network (Fig. 16, 17, 18).

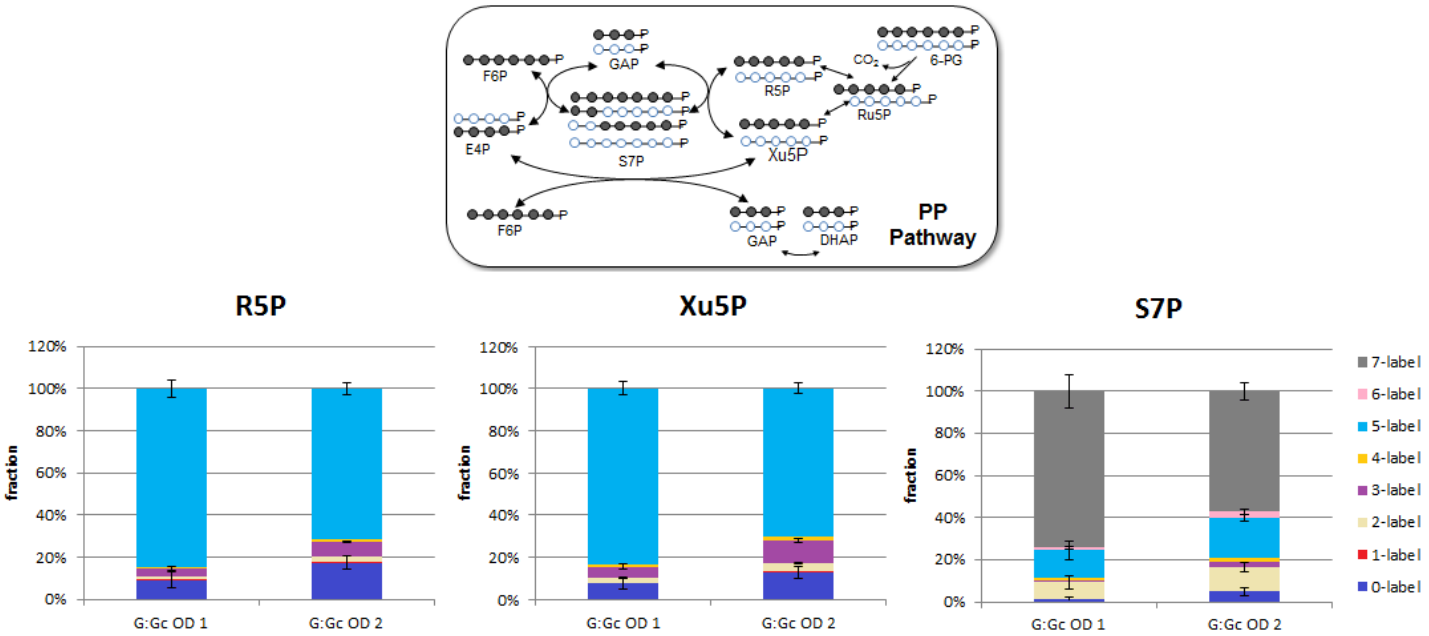

Figure 18. The isotopic labeling fractions, with standard deviations, for three intracellular PP pathway metabolites when grown on [U-^{13}C]-Gluc and nonlabeled gluconate. The two columns for each metabolite represent the average isotopic labeling distribution at OD 1 (left) and OD 2 (right). The theoretical isotopic distribution of the PP pathway of *B. megaterium* growing on Gluc:gluconate is shown. The blue carbon outline indicates carbons derived from gluconate. Abbreviations used: R5P, ribose-5-phosphate; Xu5P, xyulose-5-phosphate; S7P, sedoheptulose-7-phosphate

Nonlabeled carbons in the oxidative PP pathway also generated nonlabeled and triply ^{13}C-labeled 3-phosphoglycerate (3PG) (Fig. 16, 19). As a downstream metabolite of DHAP and GAP, 3PG was used as a proxy for GAP isotopic labeling. Specifically, 3PG was ~90% triply

^{13}C-labeled, and ~6% nonlabeled (Fig. 19). The triply ^{13}C-labeled 3PG moieties were derived from Gluc, and the slight decrease in triply ^{13}C-labeled 3PG moieties with increasing OD_{600} supported the aforementioned hypothesis that Gluc was the preferred substrate at early stages of exponential growth (Fig. 19). The low proportion of nonlabeled 3PG moieties indicated that carbons derived from gluconate were incorporated as far downstream as the lower glycolytic pathway, but to a lesser extent than they were incorporated in the oxidative PP pathway (Fig. 16, 19).

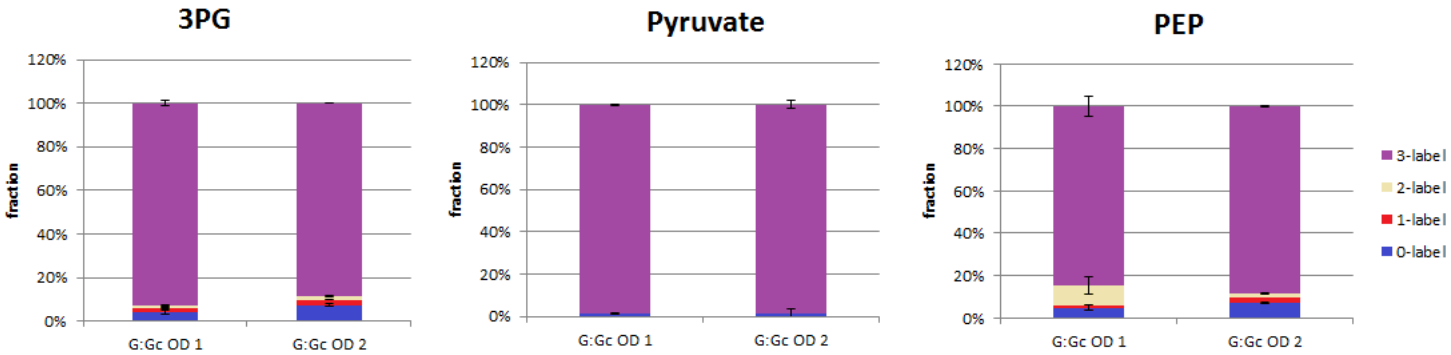

Figure 19. The isotopic labeling fractions, with standard deviations, for three intracellular lower glycolytic 3C metabolites when grown on [U-^{13}C]-Gluc and nonlabeled gluconate. The two columns for each metabolite represent the average isotopic labeling distribution at OD 1 (left) and OD 2 (right). Abbreviations used: 3PG, 3-phosphglycerate; PEP, phosphoenolpyruvate

A series of reactions convert GAP to PEP to PYR, and while GAP and PEP both contained nonlabeled moieties, PYR was 99% triply ^{13}C-labeled (Fig. 16, 19). This could suggest that Gluc is consumed sooner than gluconate and that the flux through the three-carbon metabolites is relatively low, that PYR was synthesized through an alternative pathway, or that the PYR metabolite was relatively low in concentration and could not be adequately isotopically fractionated.

The MAVEN signal intensity of PYR was investigated to determine if the unexpected labeling pattern in PYR followed a similar error as the labeling patterns previously seen in fumarate. As before, the metabolite pools for this condition were quantified (Fig. 20). The

MAVEN signal for PYR was low in the Gluc:gluconate mixture samples, and so the resulting isotopic profile could easily be software error (Fig. 20). As a confirmation of the isotopic patterns in the lower glycolytic metabolites, several amino acids were examined (Fig. 21). Alanine is derived from PYR, glycine is derived from alanine, valine is derived from the combination of two PYR molecules, and serine is derived from GAP; we therefore expected that the alanine, glycine, and valine isotopic ratios would support the profiles observed in PYR, while serine would support the isotopic profile of DHAP. Acetyl-L-serine was used instead of serine because acetyl-L-serine is very stable, and had a strong peak in the samples.

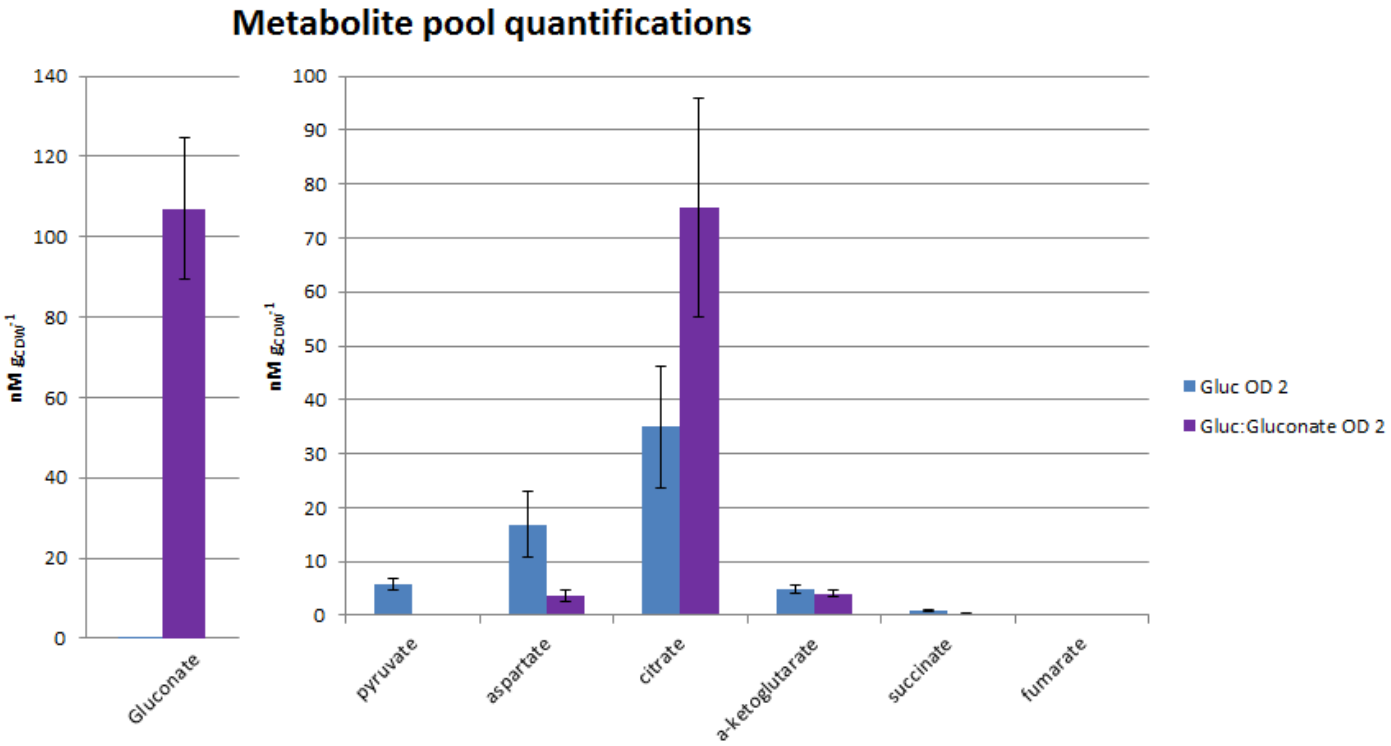

Figure 20. The quantification of several metabolites for the [U-^{13}C]-Gluc condition (blue) and the equimolar [U-^{13}C]-Gluc and unlabeled gluconate (purple) conditions. The quantifications shown were averages of the quantifications of two bioreplicates at OD_{600} 2. Gluconate was shown on a separate scale due to its overwhelming concentration per g_{CDW} relative to the other metabolites.

To confirm the isotopic distribution of PYR, the immediate downstream amino acids alanine and glycine were examined. The MAVEN signals for alanine and glycine were weak and

choppy, indicating that these amino acids were not very prevalent in the samples. While the isotopic profile of alanine and glycine imply that PYR was completely triply ^{13}C-labeled, none of these isotopic signatures are reliable (Fig. 19, 21). We next considered another immediate downstream metabolite from PYR, Ac-CoA. The isotopic profile of Ac-CoA was calculated using the isotopic profiles of citrate and aspartate (Fig. 21, 22). Since PYR undergoes a decarboxylation to form Ac-CoA, we expected the isotopic profile of Ac-CoA to reflect that of PYR minus one isotopic label. Ac-CoA was calculated to be 84% doubly ^{13}C-labeled, 7% singly ^{13}C-labeled, and 9% nonlabeled (Fig. 21). This distribution indicated a PYR metabolite pool that was primarily triply 13C-labeled, but with a significant proportion of other isotopic moieties. Since the Ac-CoA distribution was based on two reliable sets of data, it is therefore likely that the original PYR isotopic profile overestimated the fraction of triply ^{13}C-labeled PYR in this condition (Fig. 19, 21).

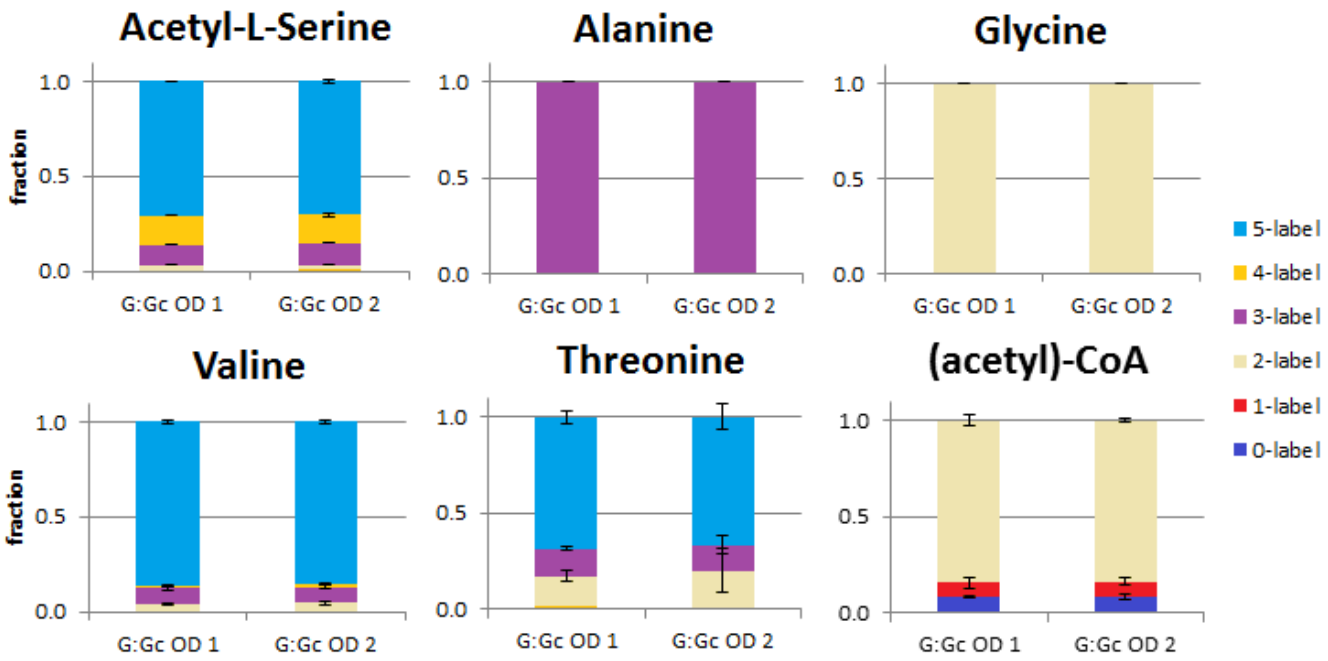

Figure 21. The isotopic labeling fractions, with standard deviations, of select amino acids and Ac-CoA when grown on [U-^{13}C]-Gluc and nonlabeled gluconate. The two columns for each metabolite represent the average isotopic labeling distribution at OD 1 (left) and OD 2 (right). Abbreviations used: (acetyl)-CoA, acetyl-coenzyme A

As mentioned previously, it was important to discern if the PYR pool contained fractions of nonlabeled PYR, which could be evidence for the ED pathway. To obtain a clear, experimental picture of the PYR isotopes, valine was investigated, as it is a downstream metabolite from PYR. Valine is a five carbon metabolite and is synthesized by the combination of two PYR molecules, one of which undergoes a decarboxylation. Valine was 86% quintuply ^{13}C-labeled, which was likely predominantly derived from two triply ^{13}C-labeled PYR (Fig. 21). This ratio supports the previously calculated 84% doubly ^{13}C-labeled Ac-CoA, lending further evidence that PYR is likely ~85% triply ^{13}C-labeled (Fig. 21). While not visibly discernable, valine was ~0.05% nonlabeled, which is too low of a value to be distinguishable from error in the software algorithm (Fig. 21). Since nonlabeled valine can only be produced from nonlabeled PYR (or a nonlabeled PYR and a specific singly ^{13}C-labeled PYR), it was concluded that PYR

lacked any nonlabeled moieties. The ED pathway splits a molecule of 6-PG in half to form a molecule of PYR and a molecule of GAP (Fig. 16). If the ED pathway were active, PYR would have an even greater fraction of nonlabeled moieties (derived from the 18-36% of nonlabeled 6-PG) than it would have if it were derived from PEP (5-7% nonlabeled) (Fig. 16, 17, 19). Thus we can conclude that the ED pathway is not used in *B. megaterium* QM B1551 when fed a mixture of Gluc and gluconate.

Phosphorylated metabolites tend to be unstable over time, and thus we sought confirmation of the isotopic profile of 3PG. In contrast with the 3PG data, acetyl-L-serine had a clean, strong peak in MAVEN. Acetyl-L-serine is synthesized from combining 3PG, a downstream metabolite of DHAP, and Ac-CoA. The isotopic profile of acetyl-L-serine consisted of ~70% quintuply ^{13}C-labeled, 15% quadruply ^{13}C-labeled, and 11% triply ^{13}C-labeled isotopes (Fig. 21). Given that Ac-CoA was predominantly doubly ^{13}C-labeled with some smaller fractions of singly ^{13}C-labeled and nonlabeled moieties, the high fraction of quintuply, quadruply, and triply ^{13}C-labeling in acetyl-L-serine corresponded to the primarily triply ^{13}C-labeled and nonlabeled isotopes of 3PG combined with Ac-CoA (Fig. 19, 21). This result indicated that serine was derived from 3PG (Fig. 19, 21).

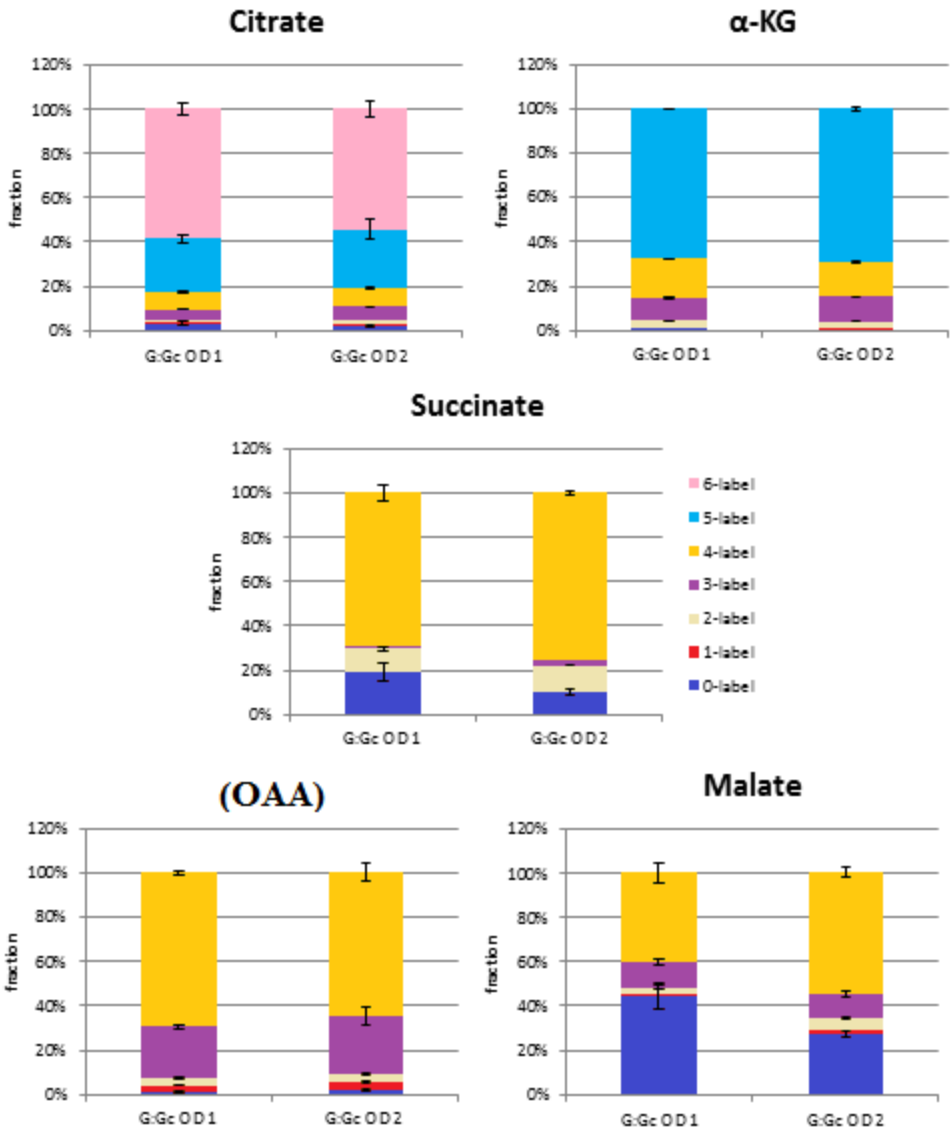

Figure 22. The isotopic labeling fractions, with standard deviations, for five intracellular metabolites in the TCA cycle when grown on [U-^{13}C]-Gluc and nonlabeled gluconate. The two columns for each metabolite represent the average isotopic labeling distribution at OD 1 (left) and OD 2 (right). The abbreviation α-KG stands for α-ketoglutarate

The triply ^{13}C-labeled PYR becomes incorporated into the TCA cycle either through a carboxylation reaction to become OAA, or through a decarboxylation reaction to form Ac-CoA (Fig. 16). The OAA isotopic labeling pattern was derived from the addition of nonlabeled or singly ^{13}C-labeled CO_2 with triply ^{13}C-labeled pyruvate (Fig. 7, 16, 22). Indeed, the OAA labeling was determined via aspartate to be about 67% quadruply ^{13}C-labeled and 24% triply

^{13}C-labeled (Fig. 22). Subsequent combination of OAA with doubly ^{13}C-labeled acetyl moiety from Ac-CoA led to citrate labeling with 56% sextuply ^{13}C-labeled and 25% quintuply ^{13}C-labeled (Fig. 21, 22). These proportions confirm that primarily labeled CO_2 was incorporated. As before, malate and succinate showed an increased proportion of nonlabeled moieties (Fig. 22). Since the succinate and fumarate pools were comparable to those from the [U-^{13}C]-Gluc condition, it was again hypothesized that there was a bottleneck in the flux from αKG to succinate, and from OAA to malate. Since there was an unlabeled substrate in this condition, additional experiments are needed to confirm that the increase in nonlabeled malate was not a result of gluconate incorporation into the TCA cycle.

Comparing the Gluc and gluconate mixture condition to the Gluc alone condition, we noted that citrate was accumulated while both PYR and Ac-CoA were depleted (Fig. 20). Following previous reasoning, we suspect that PYR is rapidly depleted in this condition. This depletion could be due to a strong flux from pyruvate to the TCA cycle, or pyruvate to amino acid synthesis. The accumulation of citrate in the Gluc and gluconate condition supported the former theory, although further experiments will be needed to fully address this question (Fig. 20).

While the previous long-term isotopic enrichment experiments have suggested that *B. megaterium* QM B1551 could have a bifurcated TCA cycle, none of the experiments directly probed the TCA cycle. Thus, the bacterium was fed an equimolar carbon mixture of [U-^{13}C]-Gluc and unlabeled glutamate to ascertain how preferentially the amino acid would be used, if it would be incorporated as α-KG as predicted by the KEGG pathway, and if the TCA cycle was always bifurcated in this strain (Fig. 23). Any nonlabeled metabolite moieties would be derived from glutamate, while all fully ^{13}C-labeled moieties would be derived from Gluc (Fig. 23). If

glutamate entered the metabolic network via α-KG, then α-KG should have a higher proportion of nonlabeled isotopes than any upstream metabolites like citrate or aconitate. Feeding a substrate directly into the TCA cycle should reveal if the TCA cycle is bifurcated under all conditions.

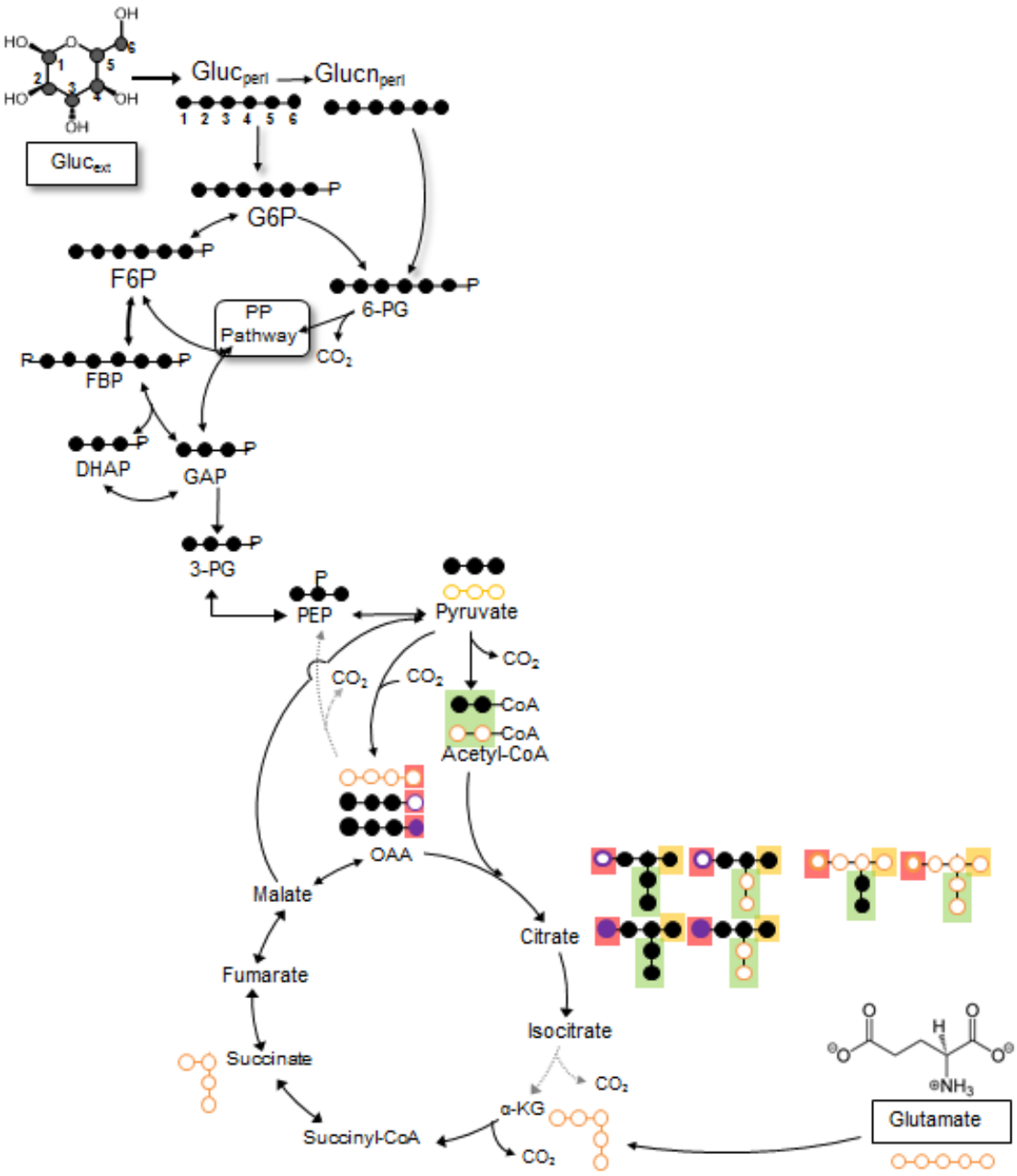

Figure 23. The theoretical isotopic distribution of the metabolic network of *B. megaterium* growing on [U-^{13}C]-Gluc and unlabeled glutamate. The purple carbons are incorporated CO_2. The green background shows the fate of the Ac-CoA atoms in the TCA cycle. The red background reiterates the position of the added CO_2 when OAA is flipped prior to its acetylation. The faded reaction from isocitrate and αKG indicates that this flux was limited in this condition.

Figure 24. The isotopic labeling fractions, with standard deviations, for five intracellular metabolites in the glycolytic EMP pathway when grown on [U-^{13}C]-Gluc and nonlabeled glutamate. The two columns for each metabolite represent the average isotopic labeling distribution at OD 1 (left) and OD 2 (right). Abbreviations used: G6P, glucose-6-phosphate; F6P, fructose-6-phosphate; 6PG, 6-phospho-gluconate; FBP, fructose-bis-phosphate

Every metabolite in the EMP pathway was fully ^{13}C-labeled, indicating that glutamate was not incorporated in this pathway and that all glycolytic metabolites were derived from glucose (Fig. 24). The same could be said for the PP pathway metabolites, excluding some error

in the first OD_{600} reading of S7P (Fig. 25). Interestingly, neither DHAP nor PEP had any nonlabeled moieties, yet PYR was approximately 7% nonlabeled (Fig. 26). This seems to indicate a partial backwards flux from OAA or malate to PYR, and a lack of further gluconeogenic flux (Fig. 23, 26, 27).

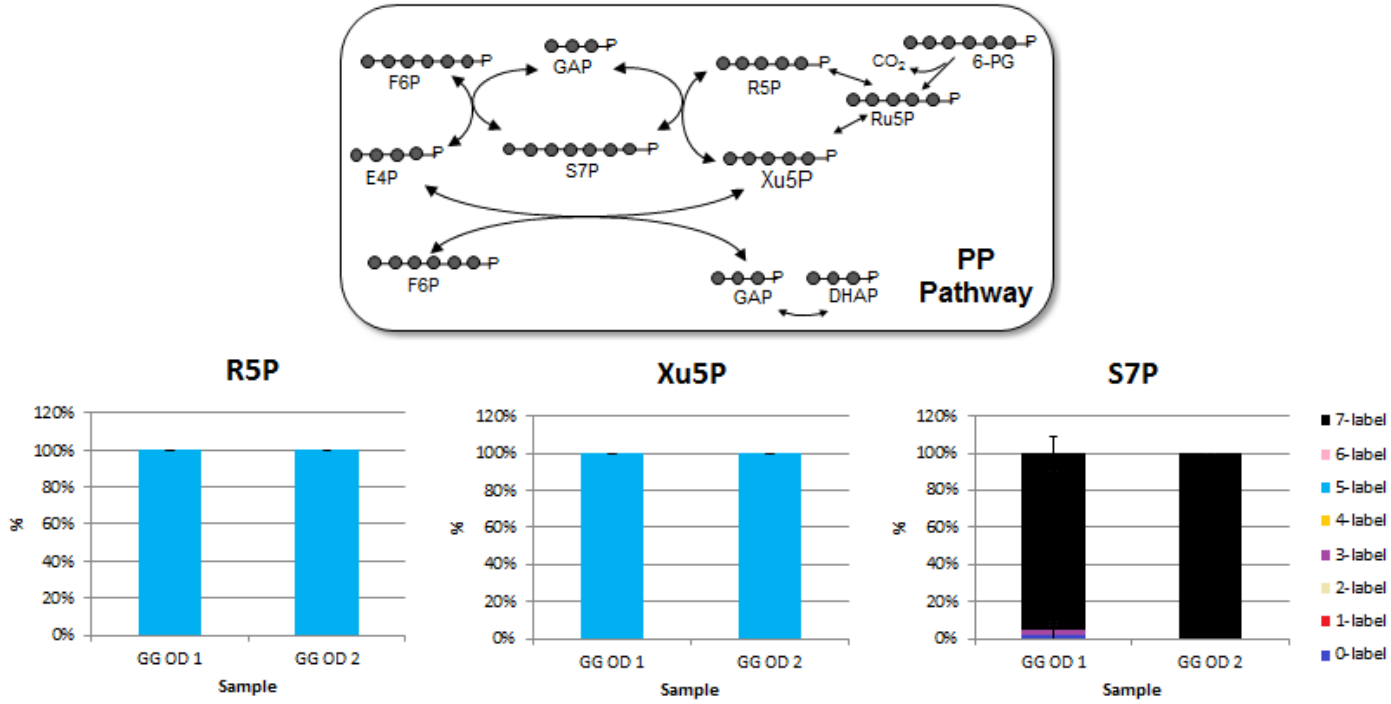

Figure 25. The isotopic labeling fractions, with standard deviations, for three intracellular PP pathway metabolites when grown on [U-^{13}C]-Gluc and nonlabeled glutamate. The two columns for each metabolite represent the average isotopic labeling distribution at OD 1 (left) and OD 2 (right). The theoretical isotopic distribution of the PP pathway of *B. megaterium* growing on Gluc:glutamate is shown. Abbreviations used: R5P, ribose-5-phosphate; Xu5P, xyulose-5-phosphate; S7P, sedoheptulose-7-phosphate

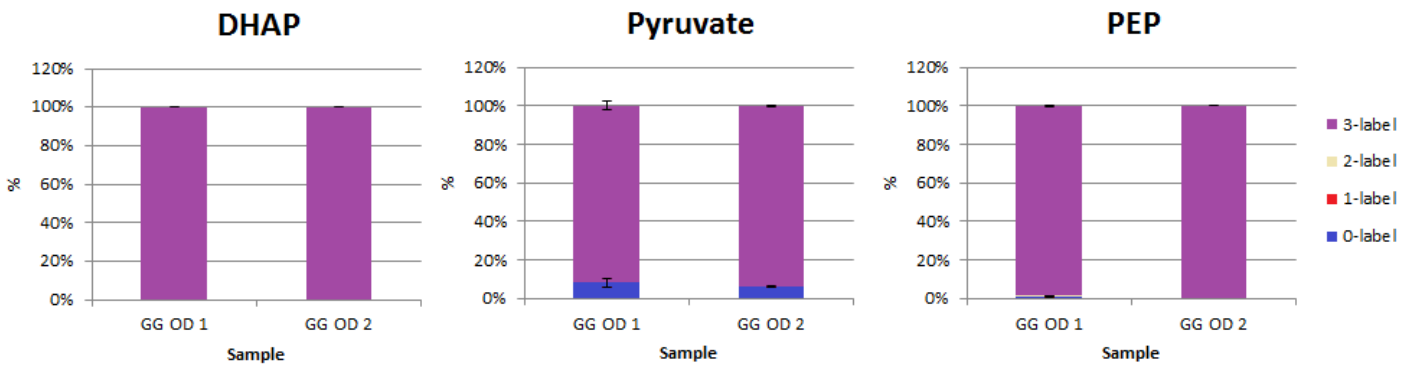

Figure 26. The isotopic labeling fractions, with standard deviations, for three intracellular, lower glycolytic, 3C metabolites when grown on [U-^{13}C]-Gluc and nonlabeled glutamate. The two columns for each metabolite represent the average isotopic labeling distribution at OD 1 (left) and OD 2 (right). Abbreviations used: DHAP, dihydroxy-acetone-phosphate; PEP, phosphoenolpyruvate

Glutamate was incorporated into the metabolic network via αKG (Fig. 27). The metabolite αKG was 97% nonlabeled, which showed a large deviation in isotopic pattern relative to citrate's 6% nonlabeled fraction (Fig. 27). To confirm that glutamate did not enter the metabolic network upstream of αKG, the isotopic pattern of aconitate was examined (Fig. 28). At the first sampling point, aconitate was 50% nonlabeled; this fraction dropped to 15% nonlabeled by the second sampling point (Fig. 28). The isotopic distribution of aconitate at OD_{600} 2 closely resembled that of citrate, although aconitate had a slightly higher proportion of nonlabeled fraction (Fig. 27, 28). This resemblance indicated that aconitate was derived from citrate, which in turn was predominantly derived from Gluc (Fig. 23, 27). In contrast, the large fraction of aconitate that was nonlabeled in the first OD_{600} sampling point seemed to indicate an early reversibility in the TCA cycle, as nonlabeled aconitate could only be derived from glutamate which did not pass through citrate (Fig. 27, 28).

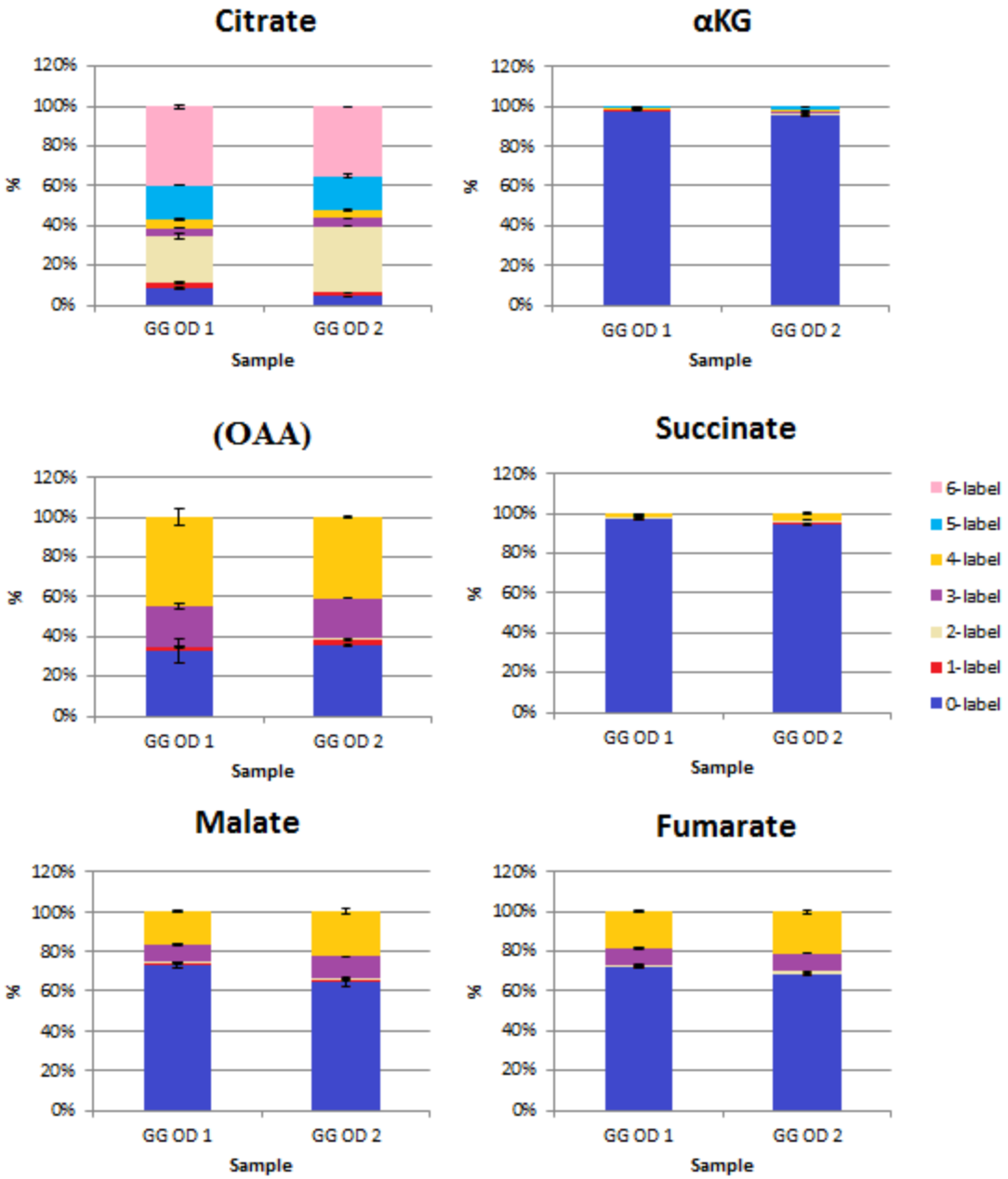

Figure 27. The isotopic labeling fractions, with standard deviations, for six intracellular metabolites in the TCA cycle when grown on [U-^{13}C]-Gluc and nonlabeled glutamate. The two columns for each metabolite represent the average isotopic labeling distribution at OD 1 (left) and OD 2 (right). The abbreviation αKG stands for α-ketoglutarate.

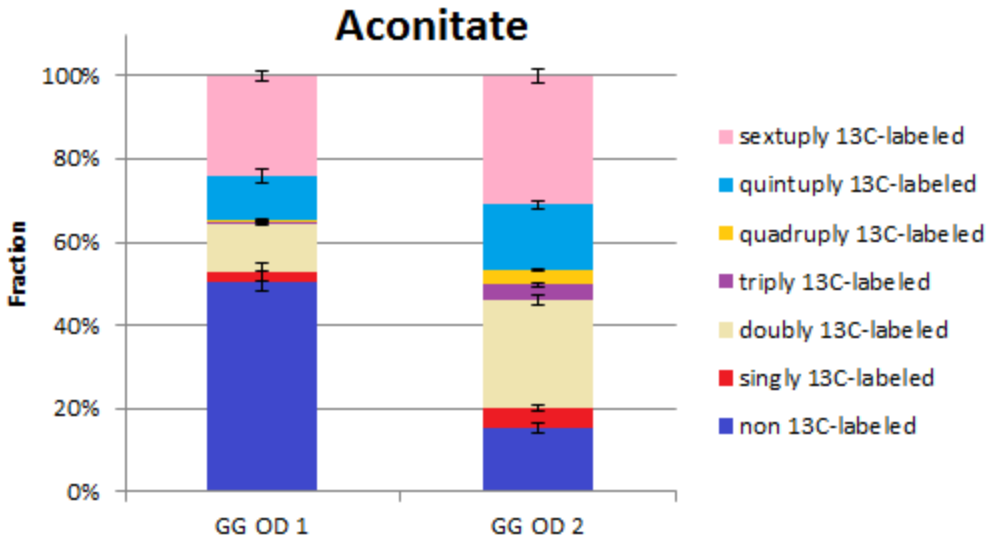

Figure 28. The isotopic labeling fractions, with standard deviations, for the metabolite aconitate when grown on [U-^{13}C]-Gluc and nonlabeled glutamate. The two columns for each metabolite represent the average isotopic labeling distribution at OD 1 (left) and OD 2 (right).

In the previous experiments, the isotopic profile of succinate was clearly derived from both the isotopic labeling of malate and αKG (Fig. 8, 14, 20). By contrast, the contribution from αKG to the succinate metabolite pool was overwhelming in the Gluc:glutamate condition (Fig. 26). This could indicate that the influx of glutamate into the TCA cycle is overwhelming the bacterium, and effectively reprogramming the TCA cycle to capitalize on the abundant resource. We noted that the quadruply ^{13}C-labeled and triply ^{13}C-labeled fractions of malate and fumarate were clearly derived from OAA, and not from αKG; this flux from OAA to malate and fumarate was not as clearly implied in the other experiments (Figures 8, 14, 20). To investigate if the flux bottlenecks observed in the previous conditions persisted in the Gluc:glutamate mixture, key metabolite pools were quantified and compared to the Gluc alone condition (Fig. 29). The αKG pool was larger in the Gluc:glutamate condition than in the Gluc condition, indicating that there was a ready influx of substrate into the TCA cycle (Fig. 29). While both succinate and fumarate were more prevalent in the Gluc:glutamate condition, there was still a dramatic decrease in metabolite quantities between αKG and succinate, which clearly indicates a low flux between

these nodes (Fig. 29). It is also important to note that aspartate and citrate were less prevalent in the Gluc:glutamate condition than the Gluc condition, which supports the hypothesis that glutamate does not completely cycle through the TCA cycle (Fig. 29).

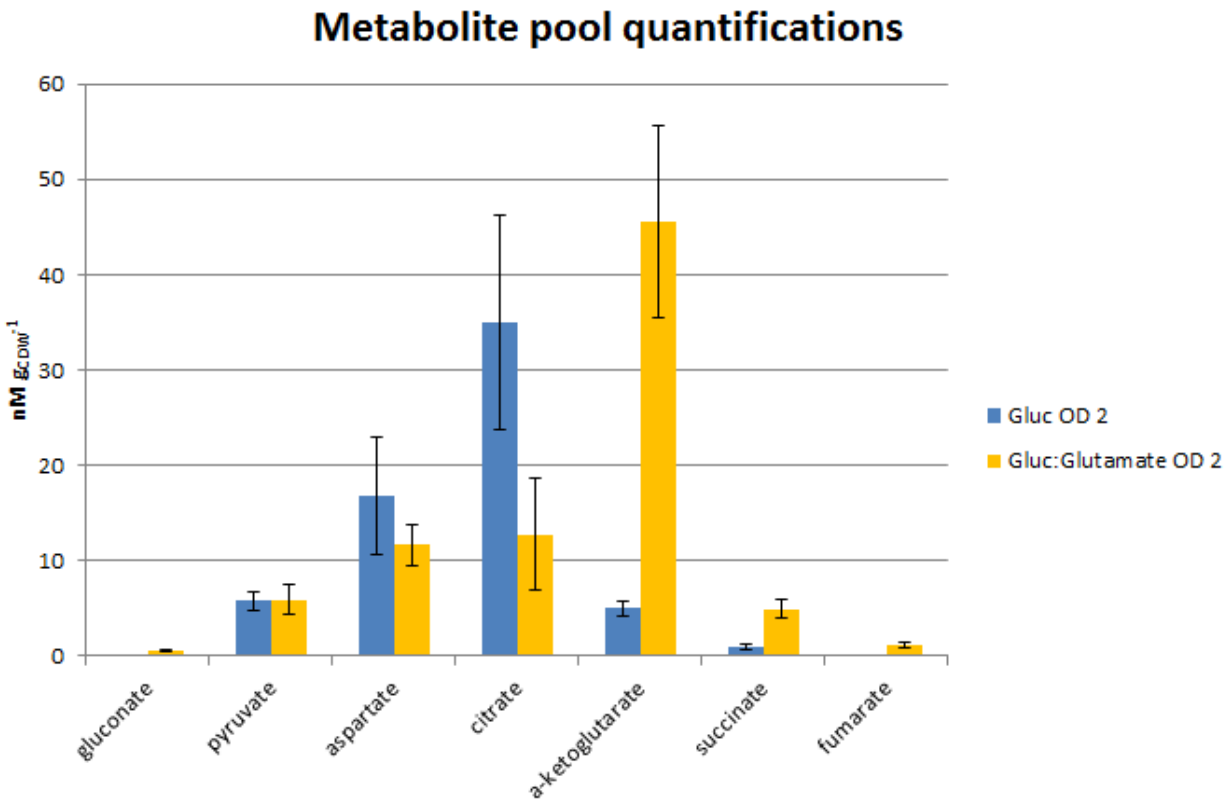

Figure 29. The quantification of several metabolites for the [U-^{13}C]-Gluc condition (blue) and the equimolar [U-^{13}C]-Gluc and unlabeled glutamate condition (yellow). The quantifications shown were averages of the quantifications two bioreplicates at OD_{600} 2.

On the whole, these long-term isotopic enrichment experiments revealed important flux relationships within the *B. megaterium* QM B1551 metabolic network. The oxidative PP pathway was preferentially used over the non-oxidative PP pathway; gluconate could be incorporated into the metabolic network when available; the TCA cycle was incompletely bifurcated; and gluconeogenesis occurred to a certain extent.

III. Hierarchical Sugar Metabolism

Following the confirmation of the metabolic network structure of *Bacillus megaterium* QM B1551, we investigated how the bacterium channels mixed-sugar substrates through its metabolic network. An equimolar carbon ratio of [1,2,3-^{13}C]-Gluc, [1,6-^{13}C]-Fruc, unlabeled Xyl was used to discern how each substrate was incorporated, and if any metabolites were derived preferentially from certain substrates (Fig. 30). These isotopes were chosen to maximize the distinctive isotopic profiles for as many key metabolites as possible. For example, metabolites derived from Gluc would have triply ^{13}C-labeled moieties in the glycolytic pathway, and doubly ^{13}C-labeled moieties in the pentose metabolites of the PP pathway (Fig. 30). Metabolites derived from Fruc would have doubly ^{13}C-labeled moieties in the glycolytic pathway, and singly ^{13}C-labeled moieties in the pentose metabolites of the PP pathway (Fig. 30). Finally, metabolites derived from Xyl would be nonlabeled throughout the entire metabolic network (Fig. 30). This scheme was less effective at distinguishing from which substrate metabolites were derived with smaller metabolites like PYR, which could have nonlabeled isotopes from either [1,2,3-^{13}C]-Gluc or unlabeled Xyl; in cases like this, isotopic profiles of upstream metabolites were used to determine which substrate contributed more to the metabolite in question.

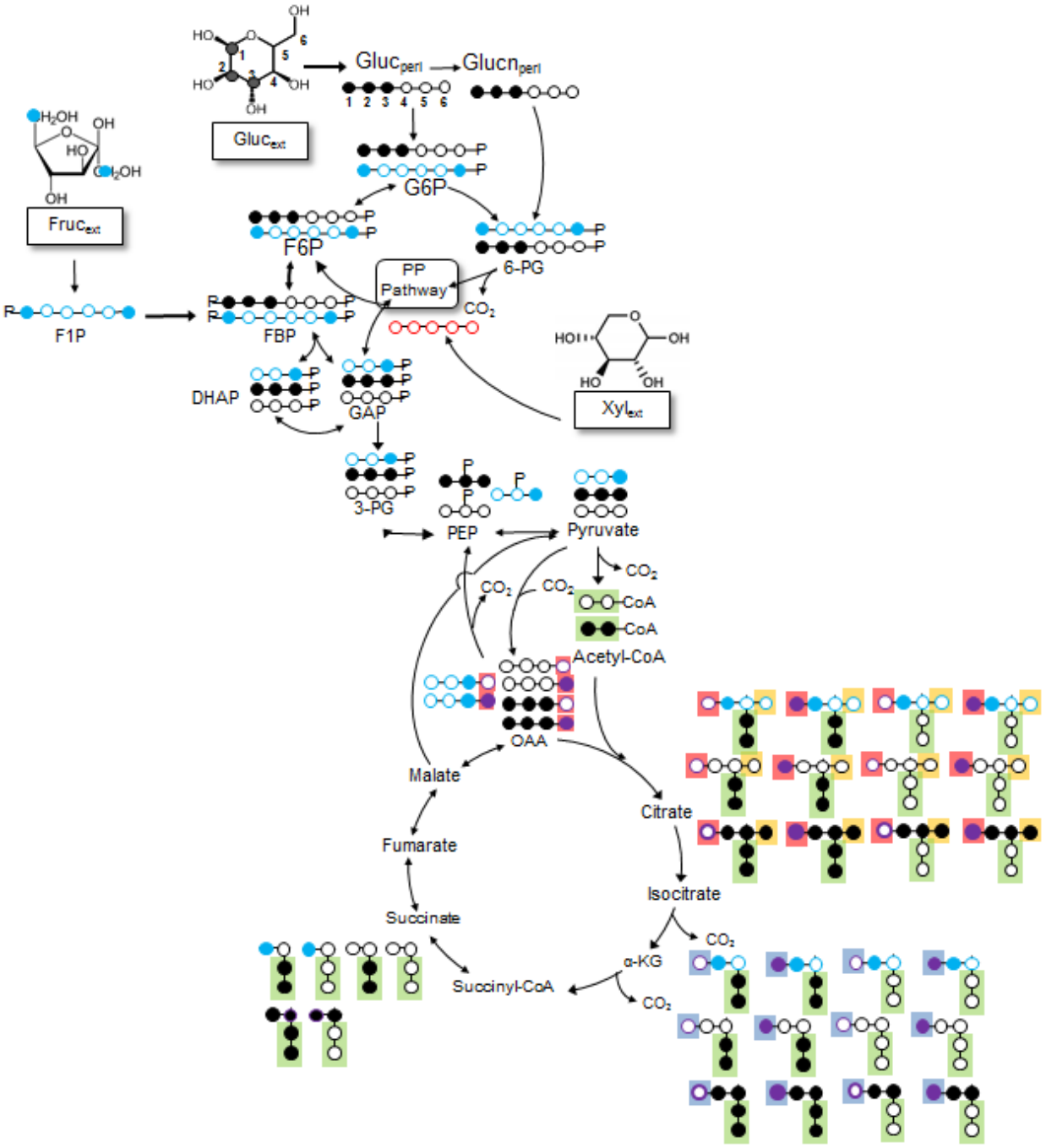

Figure 30. The theoretical isotopic distribution of the metabolic network of *B. megaterium* growing on [1,2,3-^{13}C]-Gluc (black), [1,6-^{13}C]-Fruc (blue), and unlabeled Xyl (red). The purple carbons are incorporated CO_2. The green background shows the fate of the Ac-CoA atoms in the TCA cycle. The yellow background shows the carbons that are canonically cleaved in decarboxylation reaction from citrate to αKG. The blue background shows the carbons that are canonically cleaved in decarboxylation reaction from αKG to succinate. The red background reiterates the position of the added CO_2 when OAA is flipped prior to its acetylation.

Canonical bacterial metabolic databases have established that Gluc is incorporated into the metabolic network as G6P, Fruc is incorporated as FBP, and that Xyl is incorporated as pentose metabolites (Kanehisa and Goto, 2000; Kanehisa et al., 2017). Glycolytic metabolites derived from Gluc should be triply ^{13}C-labeled in this scheme, while metabolites derived from Fruc or Xyl should be doubly ^{13}C-labeled or nonlabeled, respectively. We found that G6P, gluconate, and 6-PG were approximately 70%, 90%, and 85% triply ^{13}C-labeled, respectively (Fig. 30, 31). The next largest isotopic fraction for G6P and 6-PG was the doubly ^{13}C-labeled moieties, at 16% and 10%, respectively (Fig. 31). The isotopic proportions of these metabolites indicated that Gluc was the preferred substrate for the upper glycolytic pathway in this mixed sugar condition, that Fruc was incorporated to some extent, and that Xyl was not used for the upper glycolytic pathway. These isotopic fractions further support the theory that gluconate was synthesized by *B. megaterium* QM B1551, because an 85% triply ^{13}C-labeled 6-PG metabolite pool cannot be derived solely from a 70% triply ^{13}C-labeled G6P metabolite pool (Fig. 31).

Figure 31. The isotopic labeling fractions, with standard deviations, for five metabolites in the glycolytic EMP pathway when grown on [1,2,3-^{13}C]-Gluc, [1,6-^{13}C]-Fruc, and nonlabeled Xyl. The two columns for each metabolite represent the average isotopic labeling distribution at OD 1 (left) and OD 2 (right). Abbreviations used: G6P, glucose-6-phosphate; F6P, fructose-6-phosphate; 6PG, 6-phospho-gluconate; FBP, fructose-bis-phosphate

Based on our findings of the metabolic network of *B. megaterium*, we expected to see a large flux through the oxidative PP pathway; pentose phosphate metabolites derived from Gluc would be largely doubly ^{13}C-labeled if synthesized through the oxidative PP pathway, and

largely triply or doubly ^{13}C-labeled if synthesized through the nonoxidative PP pathway. These same metabolites would be singly 13C-labeled if synthesized through either the oxidative or nonoxidative PP pathway if derived from Fruc. Similarly, all the pentose phosphate metabolites should be primarily nonlabeled if derived from Xyl. We found that R5P and Xu5P were 60% doubly ^{13}C-labeled, 16% triply ^{13}C-labeled, 9% singly ^{13}C-labeled, and 5% nonlabeled (Fig. 32). The highest isotopic fraction of the pentose metabolites was doubly 13C-labeled moieties, which suggests that the oxidative PP pathway was more active than the nonoxidative PP pathway, and that Gluc was the preferred substrate for the PP pathway. The labeling patterns showed minimal incorporation of Xyl, both in the PP pathway and throughout the metabolic network, indicating that in the presence of Gluc and Fruc, *B.* megaterium QM B1551 had minimal uptake of Xyl (Fig. 31, 32). Thus, from this point forward, Xyl will not be considered as a significant carbon source from the mixture unless stated otherwise.

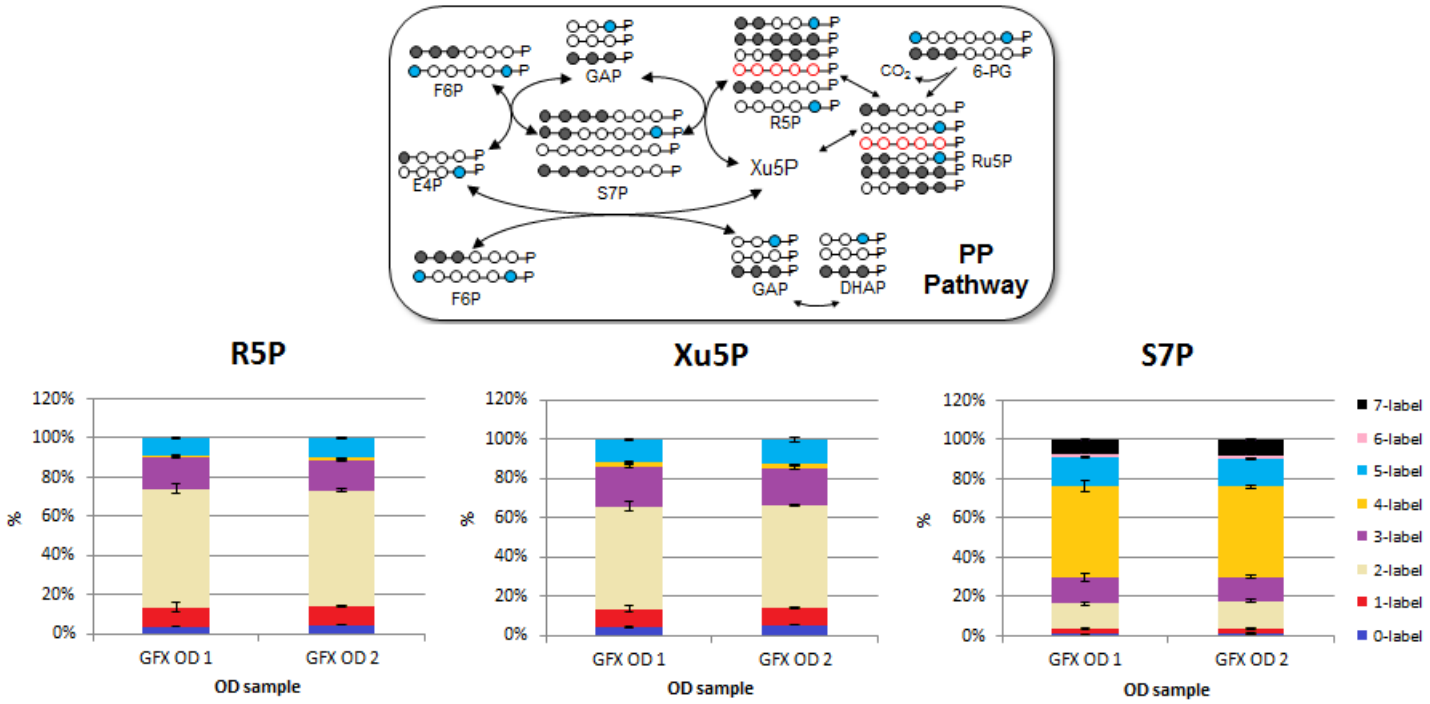

Figure 32. The isotopic labeling fractions, with standard deviations, for three PP pathway metabolites when grown on [1,2,3-^{13}C]-Gluc, [1,6-^{13}C]-Fruc, and nonlabeled Xyl. The two columns for each metabolite represent the average isotopic labeling distribution at OD 1 (left) and OD 2 (right). The theoretical isotopic distribution of the PP pathway of *B. megaterium* growing on Gluc:Fruc:Xyl is shown. The blue carbons were derived from Fruc, the black carbons from Gluc, and the red carbons from Xyl. Abbreviations used: R5P, ribose-5-phosphate; Xu5P, xyulose-5-phosphate; S7P, sedoheptulose-7-phosphate

The other glycolytic metabolites, F6P and FBP, contained ~43% and 32% triply ^{13}C-labeled fractions, respectively (Fig. 31). This indicated that Gluc was incorporated to a significant degree throughout the glycolytic pathway. Similarly, Fruc was incorporated into the metabolic network similarly as Gluc in the metabolites F6P and FBP (~41% and 23% doubly ^{13}C-labeled, respectively) (Fig. 31). A high fraction of doubly ^{13}C-labeled FBP would be expected if Fruc was entering the network through this node, and a high fraction of doubly ^{13}C-labeled F6P could indicate a strong flux from FBP to F6P. Alternatively, doubly ^{13}C-labeled F6P can be derived from a transketolase reaction from the PP pathway, and thus additional metabolite information is needed to elucidate the exact contribution of Fruc and Gluc to these metabolic nodes.

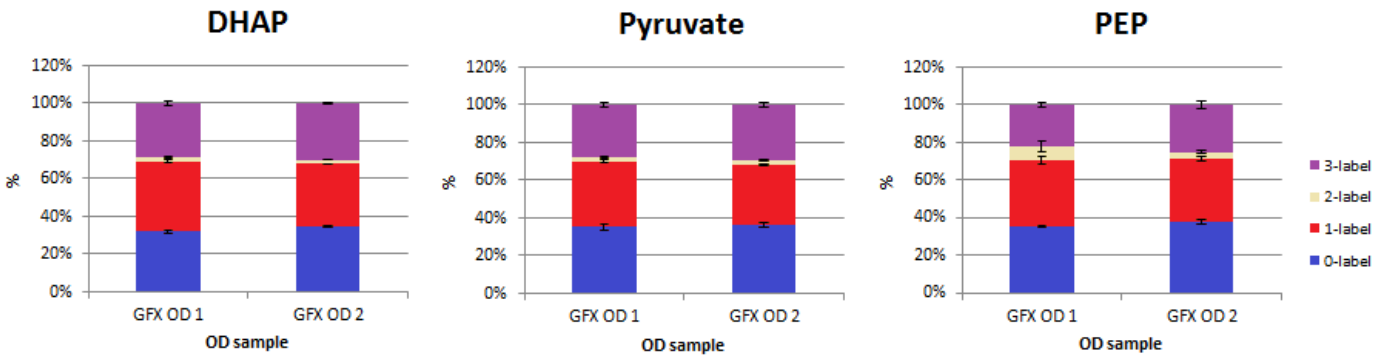

Figure 33. The isotopic labeling fractions, with standard deviations, for three lower glycolytic 3C metabolites when grown on [1,2,3-^{13}C]-Gluc, [1,6-^{13}C]-Fruc, and nonlabeled Xyl. The two columns for each metabolite represent the average isotopic labeling distribution at OD 1 (left) and OD 2 (right). Abbreviations used: DHAP, dihydroxy-acetone-phosphate; PEP, phosphoenolpyruvate

As products of the aforementioned labeling patterns in the glycolytic and PP pathways, the three-carbon metabolites have roughly equal proportions of nonlabeled, singly ^{13}C-labeled, and triply ^{13}C-labeled moieties (Fig. 33). The splitting of triply ^{13}C-labeled FBP (derived from the labeled Gluc substrate) would result in a triply ^{13}C-labeled DHAP and a nonlabeled GAP, which would rapidly exchange (Fig. 30). The splitting of doubly ^{13}C-labeled FBP (derived from the labeled Fruc substrate) would result in a singly ^{13}C-labeled DHAP and a singly ^{13}C-labeled GAP (Fig. 30). The ratio of nonlabeled, singly ^{13}C-labeled, and triply ^{13}C-labeled fractions (36%, 34%, and 29% respectively for DHAP) were similar, thus implying that Gluc contributed twice as much as Fruc to the isotopic profiles of the three-carbon metabolite (Fig. 33). It is also possible that Xyl made a small contribution to these metabolites (Fig. 33). Gluconeogenic flux through the combination of DHAP and GAP to make FBP led to sextuply ^{13}C-labeled (6.5%), quadruply ^{13}C-labeled (15%), singly ^{13}C-labeled (14%), and nonlabeled (6%) FBP moieties (Fig. 31). The gluconeogenic flux did not extend beyond FBP, as F6P and G6P had minimal quantities of these isotopic fractions (Fig. 31).

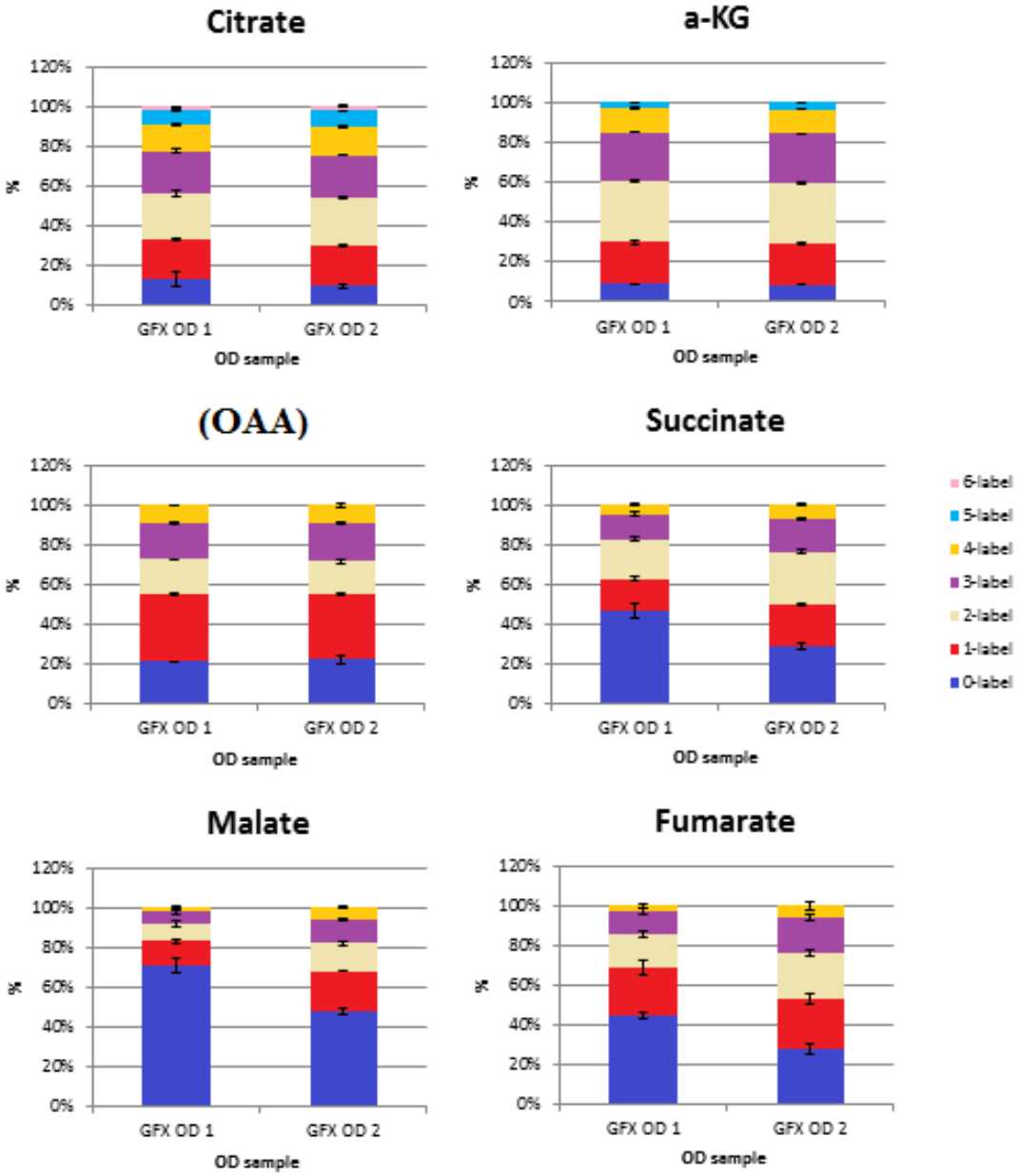

Figure 34. The isotopic labeling fractions, with standard deviations, for six metabolites in the TCA cycle when grown on [1,2,3-^{13}C]-Gluc, [1,6-^{13}C]-Fruc, and nonlabeled Xyl. The two columns for each metabolite represent the average isotopic labeling distribution at OD 1 (left) and OD 2 (right). The abbreviation α-KG stands for α-ketoglutarate.

Proceeding into the TCA cycle, PYR could either combine with CO_2 to produce the isotopic patterns seen in OAA, or undergo a decarboxylation that yielded primarily nonlabeled or doubly ^{13}C-labeled Ac-CoA (Fig. 30, 33). In this sugar mixture condition, the local CO_2 was

~50% nonlabeled (Fig. 7). We therefore predicted OAA would be primarily singly ^{13}C-labeled, followed by roughly equal fractions of nonlabeled, doubly^{13}C-labeled, triply^{13}C-labeled, and quadruply ^{13}C-labeled OAA moieties. The isotopic proportions of the OAA pool were 33% singly ^{13}C-labeled, 21% nonlabeled, 17% doubly ^{13}C-labeled, 18%% triply ^{13}C-labeled, and 9% quadruply ^{13}C-labeled (Fig. 34). These fractions aligned well with our predictions, although the smaller fraction of quadruply ^{13}C-labeled OAA could indicate a slightly higher fraction of nonlabeled CO_2 than predicted (Fig. 7, 34).

Moving forward in the cycle, OAA was combined with Ac-CoA to form citrate, which was then decarboxylated to form α-KG (Fig. 30). The isotopic proportions of OAA, citrate, and α-KG were all relatively similar and followed patterns predicted by the labeling scheme (Fig. 30, 34). Once α-KG had decarboxylated to succinate, however, the predicted patterns were no longer measured (Fig. 30, 34). There was an increase in the nonlabeled fraction of succinate, and the relative isotopic fractions of the succinate pool varied slightly between OD_{600} 1 and 2 (Fig. 34). This increase in nonlabeled moieties was also seen in the malate and fumarate metabolite pools, both of which exhibited instability in isotopic fractions over sampling points (Fig. 34). As discussed before, to ascertain if these metabolites were correctly fractionated by MAVEN, the quantities of several metabolites were found and compared to the Gluc alone condition (Fig. 35). Every metabolite quantified in the mixed sugar condition was either comparable or depleted relative to the Gluc alone condition (Fig. 35). As seen previously, there was a substantial bottleneck between citrate and α-KG, and between α-KG and succinate (Fig. 35). These bottlenecks were less pronounced in the mixed sugar condition (Fig. 35). Fumarate was not significantly produced in this condition, which indicated that the bottleneck from OAA to malate and fumarate was also present (Fig. 34, 35). While we suspect that the increase in nonlabeled

succinate fraction was a result of the bottleneck to this node, there was a source of unlabeled substrate in this sugar mixture. Therefore, more experiments would need to be performed to verify that Xyl was not the source of the nonlabeled TCA cycle metabolites.

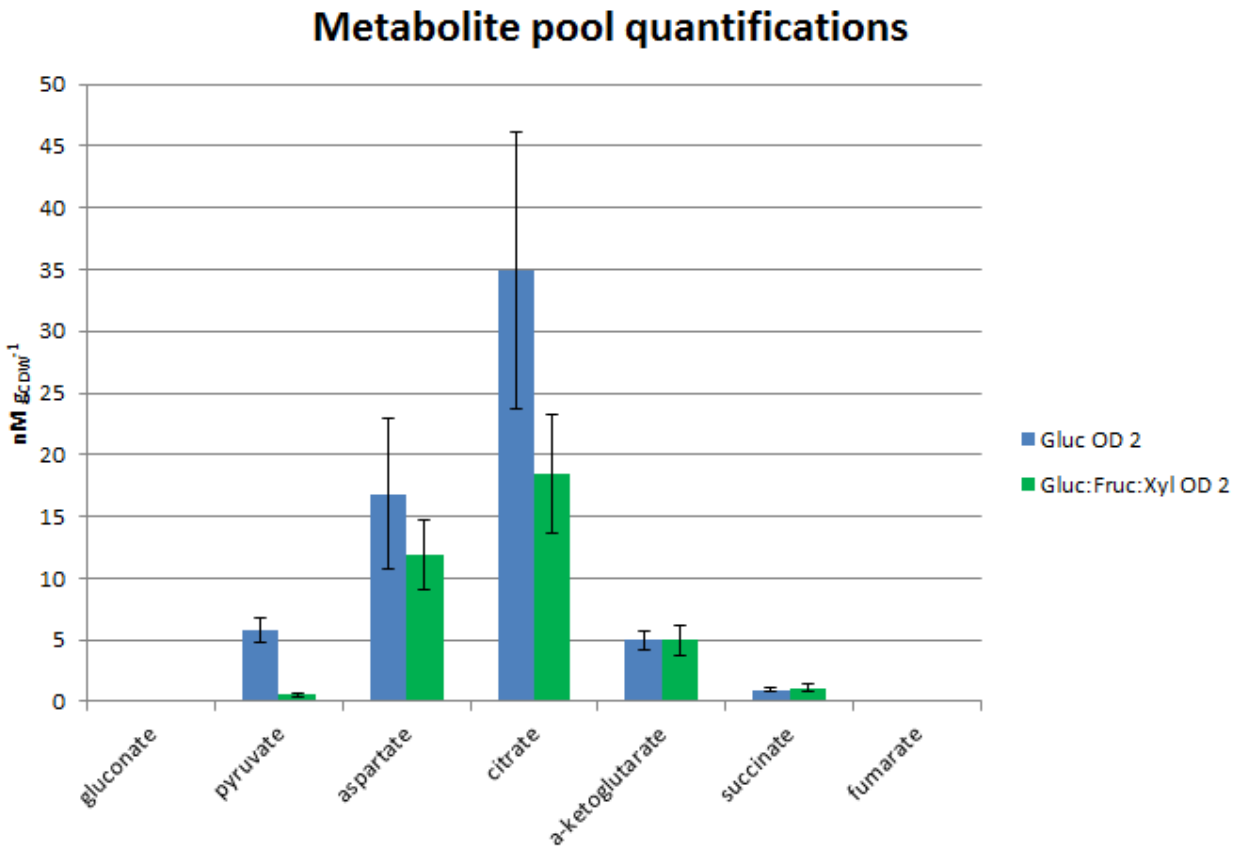

Figure 35. The quantification of several metabolites for the [U-^{13}C]-Gluc condition (blue) and the equimolar [1,2,3-^{13}C]-Gluc, [1,6-^{13}C]-Fruc, and unlabeled Xyl condition (green). The quantifications shown are averages of the quantifications of two bioreplicates at OD_{600} 2.

IV. Metabolic Flux Analysis

The MFA model was based on *B. megaterium* QM B1551 growing on Gluc alone, and was constrained using the Gluc consumption rate, Gluc-specific metabolite secretion rates, Gluc-specific growth rate, and biomass growth. The model served as a diagnostic tool for predicting which reaction pathways were used in the metabolic network.

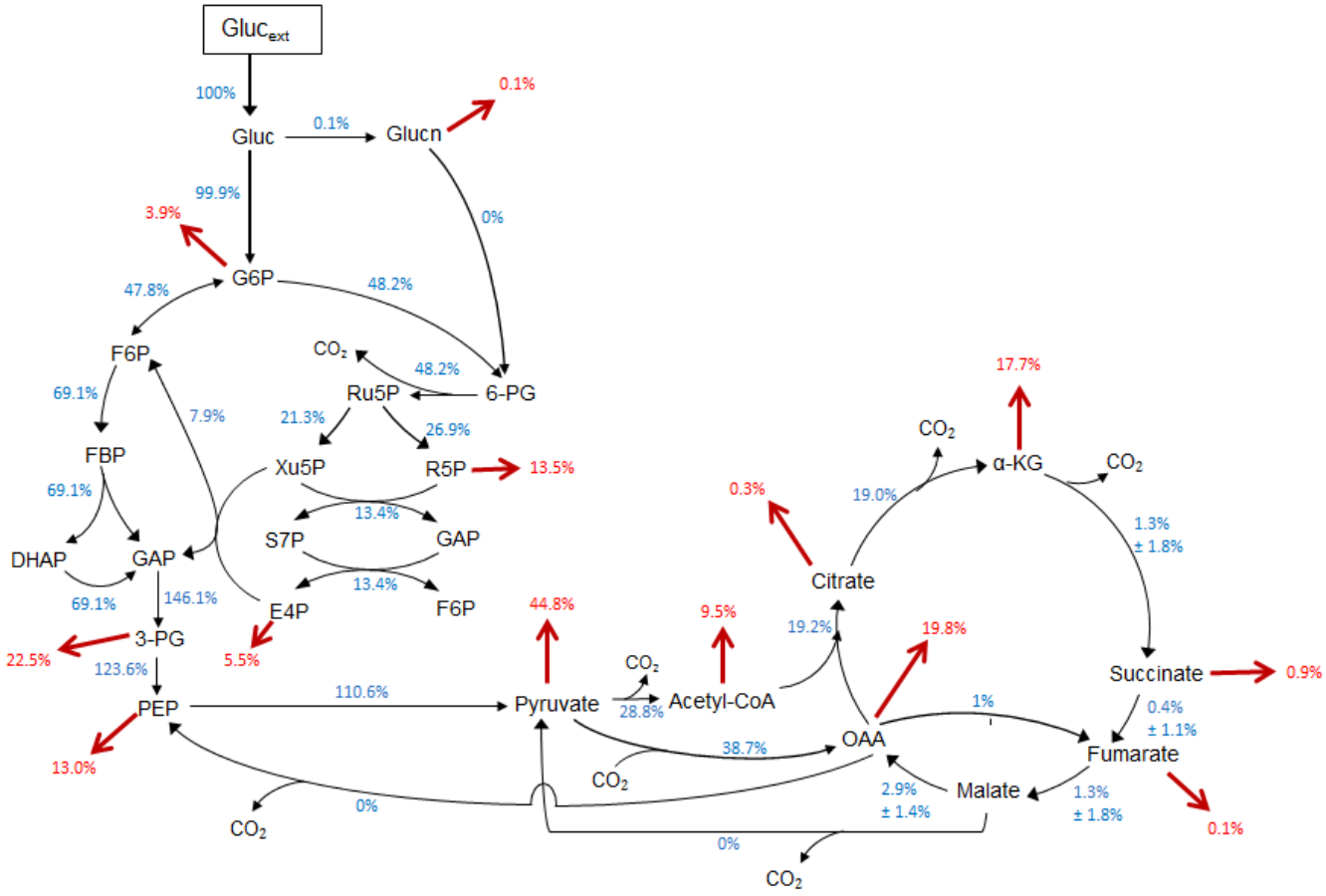

Figure 36. A model of metabolic fluxes in *B. megaterium* QM B1551, normalized to the consumption rate of [1,2-^{13}C]-Gluc. The values listed in blue next to each reaction are the predicted fluxes as a percentage of the influx of Gluc. The red arrows and the values listed in red represent outflows from the metabolic network, and indicate the flux towards excretion and/or biomass. All fluxes were averaged from the optimal fluxes derived from running the model with two biological replicates at OD_{600} 2. The standard deviation for some TCA cycle fluxes were shown to explain that the small fluxes did not add correctly because of their large errors.

The resulting MFA model was compared to a previous model to analyze how the metabolomics approach altered the predicted fluxes from an amino acid-based approach. In particular, the metabolic flux network of *B. megaterium* MS941 from Furch et al. (2007a) was used as a basis of comparison. The calculated fluxes in the upper glycolytic cycle closely matched those previously reported (Furch et al., 2007). In the PP pathway, however, the flux from Xu5P and E4P towards F6P and GAP was found to be about 8% in this model, while it had previously been reported within the range of 32 to 46% (Fig. 36; Furch et al., 2007a). This

dramatic decrease in predicted flux was likely due to the type of experimental data used by both models. Due to the resolution limitations with amino acid labeling, the R5P and Xu5P nodes were treated as a single P5P node in the Furch et al. model (2007a). Consequently, the P5P node had inputs for both R5P and Xu5P, which were balanced by a necessarily large efflux from P5P (Furch et al., 2007a). Thus, the flux from P5P and E4P towards F6P and GAP was bounded by the large influx to both R5P and Xu5P in that model (Furch et al., 2007a). The metabolomics method was able to resolve both Xu5P and R5P, and thus the flux from Xu5P and E4P was constrained by the flux from Ru5P to Xu5P, as well as the other outward fluxes from these nodes (Fig. 36). Since the flux from Ru5P to Xu5P was approximately half of the flux predicted from the Furch et al. (2007a) model, the flux from Xu5P and E4P towards F6P and GAP was forced to be only 8% (Fig. 36). Due to an overestimation of flux into the P5P metabolites, the previous model overestimated the flux out from the PP pathway (Furch et al., 2007a).

This single overestimation from the amino acid method had significant downstream implications in the Furch et al. model (2007a). Our calculated model also predicted that the fluxes into the lower glycolytic pathway would between 110 to 140%, whereas the Furch et al. (2007a) model predicted that these same fluxes would range from 142 to 194%. This increase in predicted fluxes can be traced directly to the overestimation in the PP pathway flux, which contributed to the GAP node (Fig. 36). The incremental decrease in flux between each three-carbon node was a result of large biomass efflux from these metabolites, and was similarly reflected in the Furch et al. (2007a) model (Fig. 36). This similarity was expected, as both the metabolomics model and the amino acid model were constructed using the stoichiometric biomass composition from Dauner et al., 2001b.

The calculated fluxes from PYR towards Ac-CoA and OAA summed to 67.5%, whereas the previous model reported a flux of 184% (Furch et al., 2007a). The difference between these fluxes is over an order of magnitude, and cannot be accounted for solely by the earlier PP pathway flux overestimation. Furch et al. (2007a) reported a 68% flux from malate to PYR, whereas our model predicted this flux would be 0% (Fig. 36). Based on the previous analysis of the long-term isotopic enrichments, it was concluded that malate was not synthesized in large quantities in this bacterial species. A flux of 68% from malate to PYR by Furch et al. (2007a) would require a significant flux into malate from either fumarate or OAA, neither of which was consistent with our metabolomics data nor our MFA analysis. This overestimation in the reported model could again be a result of the resolution in the metabolite labeling patterns in the previous study. The TCA cycle of the Furch et al. (2007a) model consisted of only three nodes: malate, OAA, and a lumped term for organic acids. The organic acids were assumed to encompass citrate, αKG, succinate, and fumarate. We have captured substantial bottlenecks in the fluxes between each of these nodes in our model, but these constricting fluxes were likely masked by the summation across the organic acid nodes in the Furch et al. (2007a) model. In our model, we had a substantial efflux towards biomass and secretion from αKG, which resulted in fluxes smaller than 3% for the rest of the TCA cycle (Fig. 36). While Furch et al. (2007a) also included a substantial efflux from the organic acids in their model, the aforementioned overestimation of fluxes upstream of the TCA cycle resulted in a greater flux into the TCA cycle (Furch et al., 2007a). As such, Furch et al. (2007a) had excess flux in the TCA cycle that was balanced by excess flux from the organic acids towards malate, and then back towards PYR. Given that the long-term isotopic enrichment data did not support these predictions, the previously reported

model was insufficient to accurately predict the balance of fluxes in this section of the *B. megaterium* metabolic network.

V. Kinetics

To observe the *in vivo* incorporation of isotopically ^{13}C-labeled carbon into *B. megaterium* QM B1551, and thus provide an independent experimental comparison for the fluxes predicted by the MFA, kinetic isotopic experiments were performed. The kinetic experiments were performed using [U-^{13}C]-Gluc as a control, and an equimolar mixture of [U-^{13}C]-Gluc and unlabeled glutamate. These experiments allowed us to visualize the *in vivo* changes in metabolic fluxes. Given the previous observations from the long-term isotopic enrichment experiments, we expected to see a faster rate of labeled isotopic incorporation in the glycolytic pathway for the Gluc condition, and a slower rate in the TCA cycle for the Gluc:glutamate condition.

From the experimental setup, glutamate incorporation into the metabolic network would result in stable nonlabeled metabolite fractions. By contrast, Gluc incorporation would result in an increase in ^{13}C-labeled metabolite fractions. According to the long-term enrichment data, glutamate-derived nonlabeled carbons were not incorporated into the glycolytic or PP pathway pathways beyond a fractional contribution to the PYR node (Fig. 26, 37). We examined the *in vivo* kinetic incorporation of both glucose-derived ^{13}C-labeled carbons and glutamate-derived nonlabeled carbons on five glycolytic or pentose metabolites, as well as the TCA cycle metabolites (Fig. 37, 38, 39). The impact of the two conditions on these metabolites were compared based on the initial rate of isotopic incorporation (the initial slope of the kinetics curves), the fraction of isotopic incorporation after 30 minutes (the asymptotic part of the

kinetics curves), and the final fraction of isotopic incorporation (the pseudo-steady state isotopic fractions).

The initial rate of isotopic assimilation appeared to be lower in the mixed condition than in the Gluc alone condition for all glycolytic and PP pathway metabolites except gluconate (Fig. 37). This indicated that the presence of glutamate in the metabolic network dampened the catabolism of Gluc, even in metabolic nodes that were distant from the uptake site of glutamate (Fig. 23, 37). The fraction of fully ^{13}C-labeled isotopes was higher in the Gluc alone condition at all time points tested for G6P, FBP, DHAP, and Xu5P, which indicated that glutamate consistently inhibited the catabolism of Gluc during early exponential growth (Fig. 37). The sharp curvature of the gluconate samples could be a result of MAVEN insensitivity at low metabolite concentrations (Fig. 37). Gluconate is produced in greater quantities in the Gluc and glutamate condition than in the Gluc alone condition (Fig. 29). Thus, the observed rate of isotopic incorporation for gluconate for the Gluc alone condition is likely inaccurate, since it is difficult to measure the rate associated with a very low-level metabolite pool.

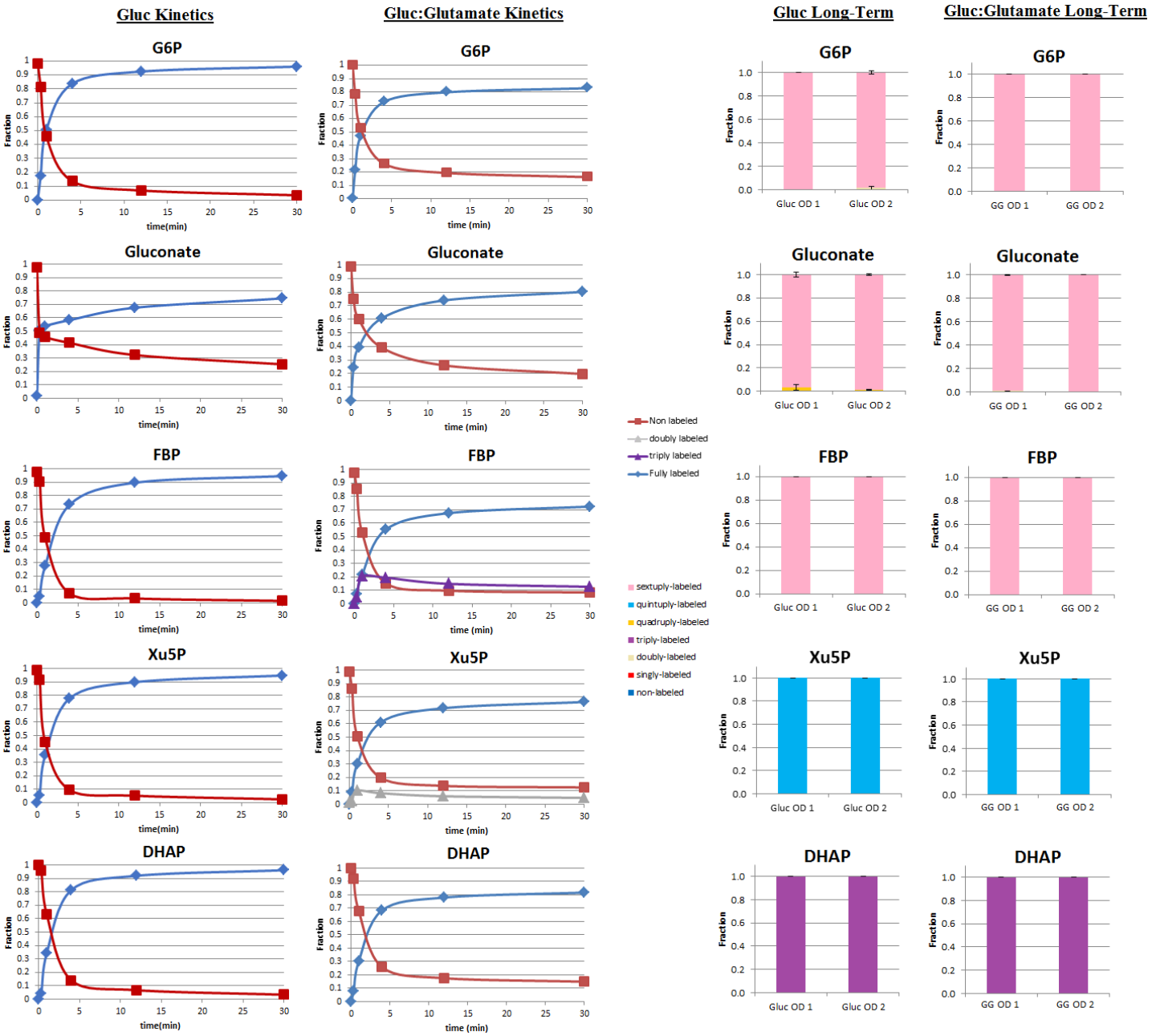

Figure 37. The dynamic changes in the isotopic proportions of G6P, gluconate, FBP, Xu5P, and DHAP for [U-^{13}C]-Gluc (left kinetics) and [U-^{13}C]-Gluc unlabeled Glutamate (right kinetics). Any isotopic fraction that was less than 10% for the entire 30 minutes was omitted for clarity. All standard deviations of both sets of kinetics data were less than 5%. The long-term isotopic enrichments for [U-^{13}C]-Gluc (left long-term) and [U-^{13}C]-Gluc and unlabeled glutamate (right long-term) show the final proportions of the labeled fractions of these metabolites at OD_{600} 1 and 2.

After 30 minutes, the proportion of fully ^{13}C-labeled metabolites was ~20% less for G6P, FBP, Xu5P, and DHAP in the Gluc and glutamate experiment than in the Gluc experiment (Fig.

37). However, the long-term isotopic enrichment of these metabolites in both experimental conditions resulted in nearly 100% fully ^{13}C-labeled metabolic pools (Fig. 37). This observation indicated that the time needed to reach pseudo-steady state for isotopic incorporation in *B. megaterium* QM B1551 was dependent on the nutritional conditions. In our case, the presence of glutamate seemed to slow down the synthesis of glycolytic and pentose phosphate metabolites, thereby preventing them from reaching pseudo-steady state as quickly as in the Gluc alone (Fig. 37).

The final three-carbon metabolite, PYR, displayed similar labeling kinetics as DHAP for the kinetic incorporation of ^{13}C-labeled fractions (Fig. 38). As before, the initial rate of isotopic assimilation appeared to be lower in the mixed condition than in the Gluc alone condition, and the identical isotopic proportions of DHAP and PYR were similar at each time point (Fig. 37, 38). This indicated that PYR was not synthesized as readily from Gluc in the Gluc and glutamate condition as in the Gluc alone condition. This observation, along with those from the glycolytic and PP pathways, implied a transient cellular preference for glutamate during initial growth, followed by a preference for Gluc after ~12 minutes (Fig. 37, 38). The initial preference for glutamate over Gluc was shown by the decreased rate of initial ^{13}C-labeled metabolite assimilation in the early time points in the Gluc and glutamate condition relative to the Gluc alone condition (Fig. 37, 38). The long-term enrichment experiments revealed that a small nonlabeled fraction persisted in the PYR metabolite pool, while none persisted in the DHAP metabolite pool (Fig. 38). Thus, the kinetic labeling data was insufficient to determine which metabolites were populated via gluconeogenic fluxes.

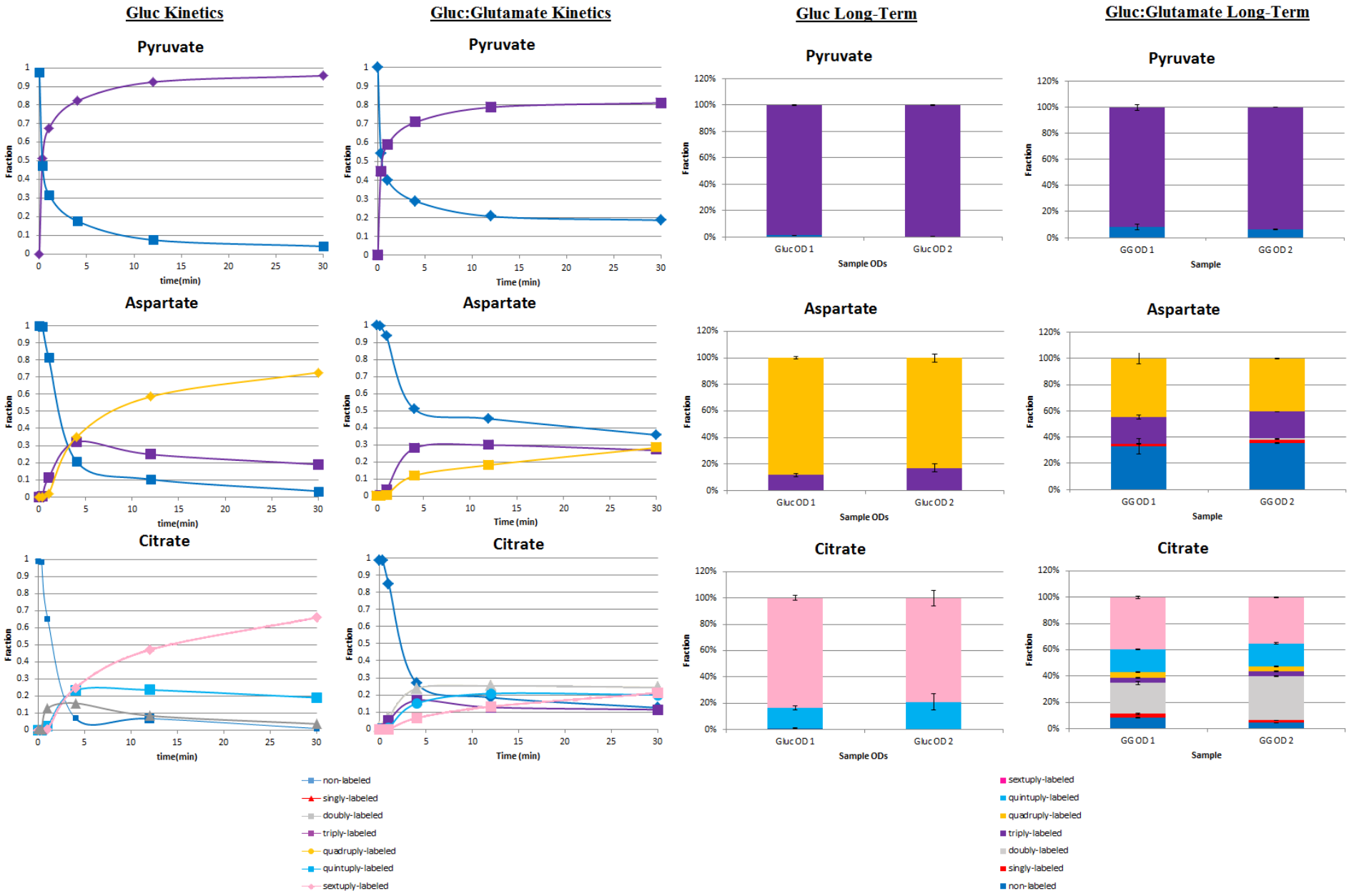
Gluc Kinetics
Gluc:Glutamate Kinetics
Gluc Long-Term
Gluc:Glutamate Long-Term
Pyruvate
Aspartate
Citrate
Fraction
time(min)
Time (min)
Gluc OD 1
Gluc OD 2
GG OD 1
GG OD 2
Sample ODs
Sample
non-labeled
singly-labeled
doubly-labeled
triply-labeled
quadruply-labeled
quintuply-labeled
sextuply-labeled

Figure 38. The time-dependent changes in the proportions of labeled fractions of pyruvate, aspartate, and citrate for [U-^{13}C]-Gluc (left kinetics) and [U-^{13}C]-Gluc: nonlabeled Glutamate (right kinetics). Any labeled fraction that was less than 10% for the entire 30 minutes was omitted from the kinetics graphs for clarity. All standard deviations of both sets of kinetics data were less than 5%. The long-term isotopic enrichments for [U-^{13}C]-Gluc (left long-term) and [U-^{13}C]-Gluc: nonlabeled Glutamate (right long-term) show the final proportions of the labeled fractions of these metabolites at OD_{600} 1 and 2. Note that the colors used for the kinetics legend correspond with every graph, while the shapes of the points may vary.

The most dramatic impacts of glutamate incorporation on metabolic labeling kinetics were seen in the TCA cycle (Fig. 38). It has been observed that OAA (deduced from aspartate labeling) was likely derived from PYR, because the two metabolites typically shared similar isotopic profiles. The initial rate of isotopic incorporation into aspartate was lower in the Gluc and glutamate condition than in the Gluc alone condition (Fig. 38). In the Gluc alone condition, aspartate was populated first by triply ^{13}C-labeled carbons (1 min) before being primarily populated by quadruply ^{13}C-labeled carbons (12 min) (Fig. 38). These isotopes reflected the isotopic profile of PYR combined first with nonlabeled CO_2 and then with fully ^{13}C-labeled CO_2, respectively (Fig. 38). By contrast, the largest fraction of aspartate in the Gluc and glutamate condition was still nonlabeled after 30 minutes (Fig. 38). These two findings implied that aspartate is derived preferentially from glutamate during early stages of growth (Fig. 38). The long-term isotopic enrichment experiment revealed that the pseudo-steady state fraction of nonlabeled aspartate was significantly higher in the mixed condition than the Gluc alone condition, which implied that while the flux of glucose-derived ^{13}C-labeled carbons to OAA did eventually increase, there was a persistently strong flux of glutamate-derived ^{13}C-labeled carbons to OAA (Fig. 38). Thus the TCA cycle was reprogrammed in the presence of glutamate, and the TCA cycle of *B. megaterium* QM B1551 was not completely bifurcated in all substrate conditions.

The citrate labeling kinetics provided further evidence of an initial preferential uptake of glutamate. The initial rate of isotopic incorporation was decreased in for citrate in the mixed condition relative to the Gluc alone condition (Fig. 38). As the fraction of nonlabeled citrate was depleted, the fraction of doubly ^{13}C-labeled citrate remained the highest isotopically labeled fraction throughout the 30 minute time course (Fig. 38). Since OAA was minimally doubly ^{13}C-labeled throughout the growth of the bacterium, doubly ^{13}C-labeled citrate could only be derived from nonlabeled OAA and doubly ^{13}C-labeled Ac-CoA (Fig. 23, 38). Thus, in the first 30 minutes of the mixed condition, citrate was derived from a TCA cycle that was primarily populated with glutamate-derived nonlabeled carbons, as well as from the lower glycolytic pathway which was populated primarily with glucose-derived ^{13}C-labeled carbons. This confirmed that for at least the first 30 minutes of growth, glutamate populated the TCA cycle while Gluc populated the glycolytic and PP pathways. The fraction of sextuply ^{13}C-labeled citrate was ~25% after 30 minutes of growth, but increased to ~40% at pseudo-steady state (Fig. 38). As before, this indicated that there was an early substrate preference for glutamate, followed by a preference for Gluc.

The strongest influx of glutamate into the metabolic network occurred in the αKG node (Fig. 39). Both the initial rate of isotopic incorporation and the fraction of incorporation over the 30 minute time course were lower in the mixed condition than in the Gluc alone condition (Fig. 39). Indeed, the αKG metabolite pool had a greater than 90% nonlabeled fraction over the first 30 minutes of growth in the mixed condition, and the pseudo-steady state isotopic profile of αKG was nearly 100% nonlabeled (Fig. 39). These results implied a minimal influx of glucose-derived ^{13}C-labeled carbons into this metabolite; by extension, the results implied a bifurcation

of the TCA cycle, as the flux from glutamate to αKG overpowered any flux from citrate to αKG (Fig. 23, 39).

Since succinate was immediately downstream from αKG, it received minimal input from Gluc catabolism through the classical clockwise reactions of the TCA cycle (Fig. 23, 39). Fumarate and malate both had significant proportions of quadruply ^{13}C-labeled and triply ^{13}C-labeled fractions during the kinetic labeling experiment, and even greater proportions of these isotopic fractions at pseudo-steady state (Fig. 39). This indicated that fumarate and malate were partly populated by glucose-derived ^{13}C-labeled carbons from OAA (Fig 38, 39). We noted that in contrast to the other metabolites, fumarate had a greater rate of initial isotopic incorporation in the Gluc and glutamate mixture than the Gluc alone condition (Fig. 39). In the Gluc alone labeling kinetics, the fraction of nonlabeled fumarate did not drop below 90% for the first 30 minutes, indicating that there was minimal isotopic incorporation into fumarate and that fumarate was not synthesized (Fig. 39). The larger pool size of fumarate in the Gluc and glutamate condition indicated that fumarate was synthesized in this condition, and thus the increased initial rate of isotopic incorporation for fumarate in the mixed condition was a reflection of the increased presence of this metabolite (Fig. 29, 39). Since succinate did not have significant proportions of glucose-derived ^{13}C-labeled carbons either during the 30 minute kinetic labeling time course or at pseudo-steady state, there was no flux from fumarate to succinate in this condition (Fig. 39). However, the increase in the nonlabeled fraction of the kinetic labeling data of malate in the mixed substrate condition compared to the Gluc alone condition implied that there was a net flux of glutamate-derived nonlabeled carbons from succinate to fumarate, and from fumarate to malate (Fig. 39). Thus, *B. megaterium* QM B1551 can employ the full TCA cycle when necessary (Fig. 29).

The above analysis implied not only reversibility in the TCA cycle from (OAA to malate, and from malate to fumarate), but also a bottleneck in the flux from citrate to αKG, and a bottleneck in the flux from succinate to fumarate. Fumarate was only two nodes distant from αKG in the metabolic network, so it should have experienced the same overwhelming input of glutamate-derived nonlabeled carbon as succinate (Fig. 23). By contrast, fumarate and malate were ~70% nonlabeled at pseudo-steady state, which implied a low flux from succinate to fumarate. This hypothesis was verified by the metabolic pool sizes; even when the size of the αKG and succinate pools were increased drastically relative to the Gluc condition, the increase in the size of the fumarate pool was minimal, and the citrate and aspartate pool sizes were comparable between Gluc and Gluc:glutamate conditions (Fig. 29). Thus, the kinetic data and the metabolite quantifications prove that even with substrate influx directly into the TCA cycle, the fluxes between the TCA cycle metabolites were very low, partially bifurcating the TCA cycle.

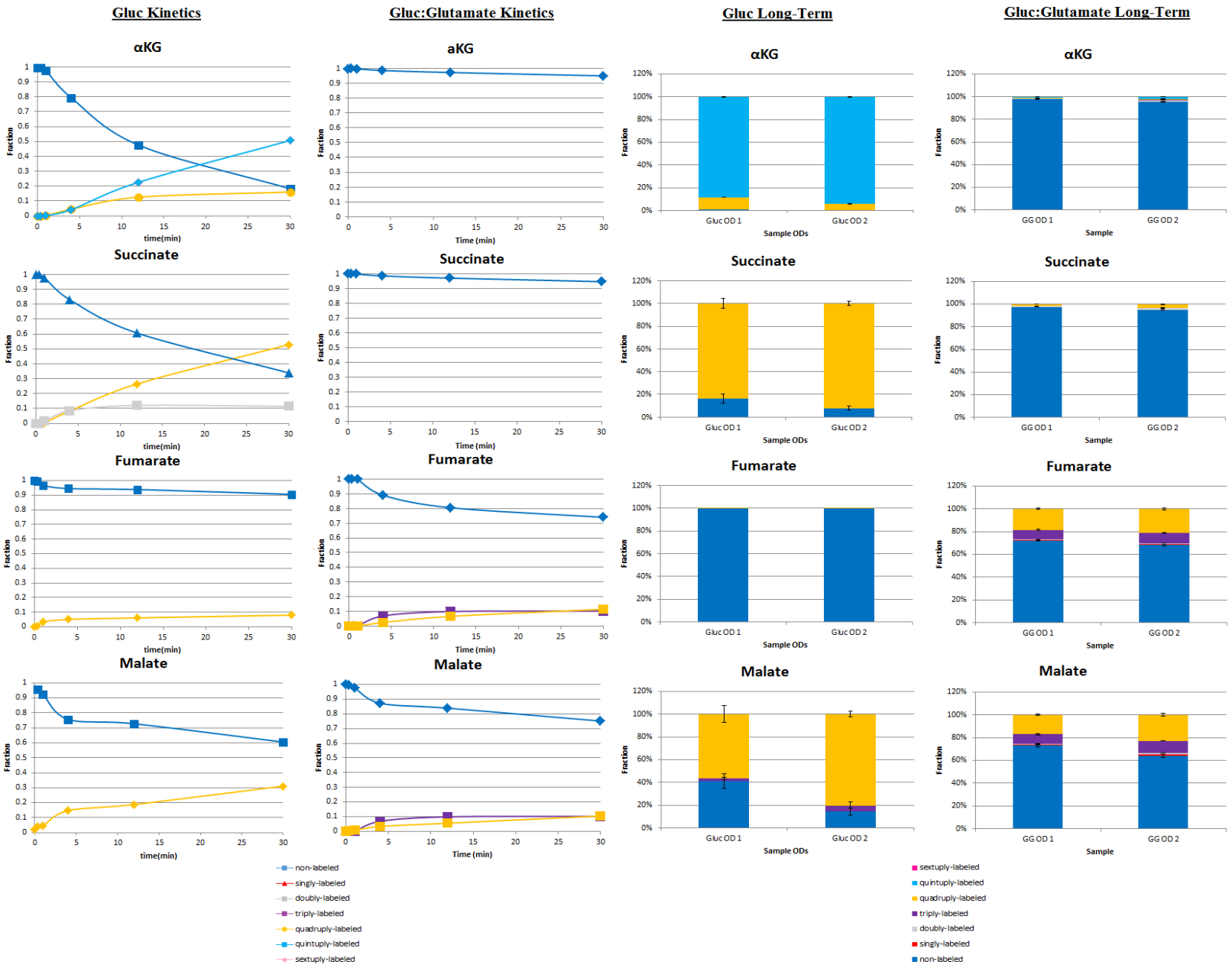
Gluc Kinetics
Gluc:Glutamate Kinetics
Gluc Long-Term
Gluc:Glutamate Long-Term
αKG
aKG
Succinate
Fumarate
Malate
Fraction
time(min)
Time (min)
Gluc OD 1
Gluc OD 2
Sample ODs
GG OD 1
GG OD 2
Sample
non-labeled
singly-labeled
doubly-labeled
triply-labeled
quadruply-labeled
quintuply-labeled
sextuply-labeled

Figure 39. The time-dependent changes in the proportions of labeled fractions of αKG, succinate, fumarate, and malate for [U-^{13}C]-Gluc (left kinetics) and [U-^{13}C]-Gluc: nonlabeled Glutamate (right kinetics). Any labeled fraction that was less than 10% for the entire 30 minutes was omitted from the kinetics graphs for clarity. All standard deviations of both sets of kinetics data were less than 5%. The long-term isotopic enrichments for [U-^{13}C]-Gluc (left long-term) and [U-^{13}C]-Gluc: nonlabeled Glutamate (right long-term) show the final proportions of the labeled fractions of these metabolites at OD_{600} 1 and 2. Note that the colors used for the kinetics legend correspond with every graph, while the shapes of the points may vary. Abbreviation used: αKG, alpha-ketoglutarate

To ascertain that glutamate was truly entering the TCA cycle through αKG and not an upstream metabolite, the kinetic carbon incorporation of aconitate was monitored (Fig. 40). In the Gluc alone condition, the aconitate metabolite pool was rapidly populated with ^{13}C-labeled isotopes (Fig. 40); in the Gluc and glutamate condition, however, the incorporation kinetics resembled those of aspartate, in which the nonlabeled fraction was still dominant at the end of 30 minutes (Fig. 38, 40). Aconitate is an intermediate node between citrate and αKG, and while the decrease in nonlabeled was clearly greater in aconitate than in αKG, the decrease in nonlabeled in citrate was greater than in aconitate (Fig. 38, S4, 40). By minute 4, the fraction of nonlabeled citrate was 30%, but the fraction of nonlabeled aconitate was ~60% (Fig. 38, 40). Since αKG is presumed to have no flux backwards through the TCA cycle, no glutamate-derived nonlabeled carbons can flow to aconitate without passing through citrate. Therefore, the slower incorporation of ^{13}C-labeled carbon in aconitate than in citrate implied a decreased flux from citrate to aconitate, in agreement the previously observed bottleneck of citrate from the long-term enrichment experiments.

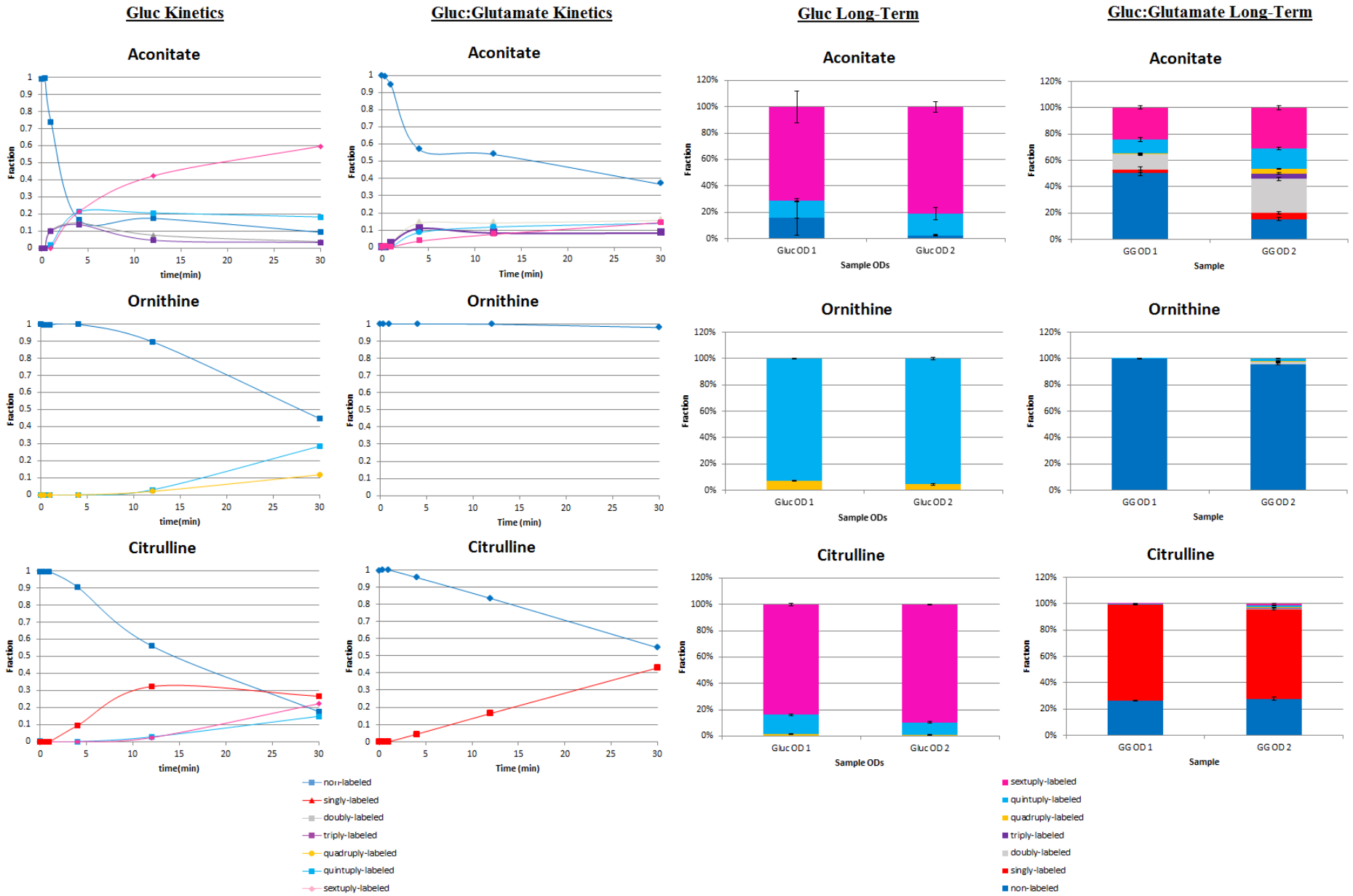
Gluc Kinetics
Gluc:Glutamate Kinetics
Gluc Long-Term
Gluc:Glutamate Long-Term
Aconitate
Ornithine
Citrulline
Fraction
time(min)
Time (min)
Gluc OD 1
Gluc OD 2
GG OD 1
GG OD 2
Sample ODs
Sample
non-labeled
singly-labeled
doubly-labeled
triply-labeled
quadruply-labeled
quintuply-labeled
sextuply-labeled

Figure 40. The time-dependent changes in the proportions of labeled fractions of aconitate, ornithine, and citrulline for [U-^{13}C]-Gluc (left kinetics) and [U-^{13}C]-Gluc: nonlabeled Glutamate (right kinetics). Any labeled fraction that was less than 10% for the entire 30 minutes was omitted from the kinetics graphs for clarity. All standard deviations of both sets of kinetics data were less than 5%. The long-term isotopic enrichments for [U-^{13}C]-Gluc (left long-term) and [U-^{13}C]-Gluc: nonlabeled Glutamate (right long-term) show the final proportions of the labeled fractions of these metabolites at OD_{600} 1 and 2. Note that the colors used for the kinetics legend correspond with every graph, while the shapes of the points may vary.

In conclusion, these experiments have shed light on several aspects of the metabolic network of *B. megaterium* not previously reported. Metabolite quantifications showed that while gluconate was not synthesized in large quantities by this bacterium, gluconate can be incorporated into the metabolic network to a significant extent when present in the environment. This finding holds implications for future modeling efforts, as it lends support to the simplification of the metabolic network via gluconate omission while also cautioning the modelers to be mindful of the environmental conditions. It was evident in every long-term isotopic enrichment experiment that the TCA cycle is bifurcated, although the Gluc and glutamate trial proved that the TCA cycle can still function in its entirety when provided a direct influx of substrate. The MFA model supported the conclusion that the TCA cycle of *B. megaterium* QM B1551 was incompletely bifurcated. The kinetic experiments independently supported the TCA cycle bifurcation conclusion as well as the MFA model, as the dynamic incorporation of carbon into the TCA cycle metabolites succinate, fumarate, and malate was very low, even in the presence of glutamate. These same experiments demonstrated that *B. megaterium* can have temporal and sectional preferences for substrates; glutamate was incorporated into the TCA cycle extensively early in the exponential growth phase, while Gluc was preferentially incorporated into the glycolytic and PP pathways independent of time. Finally, long-term isotopic enrichment using a mixture of Gluc, Fruc, and Xyl revealed hierarchical sugar

preferences of *B. megaterium* QM B1551; the bacterium consumed Gluc and Fruc more or less equally, and Xyl was minimally incorporated when these hexose sugars were present.

For the future direction of this project, additional MFA models for each mixed substrate condition would further elucidate how the metabolic network changes in response to different carbon sources. Similarly, additional kinetic experiments on mixed substrate conditions would provide essential evidence and verification for the MFA models. These two efforts will help direct this research towards a better understanding of how *B. megaterium* regulates its metabolic network, which will in turn allow for optimized industrial use of this bacterium.

BIBLIOGRAPHY

Amador-Noguez, D., Feng, X. J., Fan, J., Roquet, N., Rabitz, H., and Rabinowitz, J. D. 2010. Systems-level metabolic flux profiling elucidates a complete, bifurcated tricarboxylic acid cycle in *Clostridium acetobutylicum*. *Bacteriology*. 192 (17): 4452-4461.

Aristilde, L., Lewis, I. A., Park, J. O., and Rabinowitz, J. D. 2015. Hierarchy in pentose sugar metabolism in *Clostridium acetobutylicum*. *Applied and Environmental Microbiology*. 81(4): 1452-1462.

Biedendieck, R., Bunk, B., Furch, T., Franco-Lara, E., Jahn, M., et al. 2010. Systems biology of recombinant protein production in *Bacillus megaterium*. In Wittmann, C., and Krull, R. 2010. *Biosystems engineering I*. 133-162

Clasquin, M. F., Melamud, E., and Rabinowtiz, J. D. 2012. LC-MS data processing with MAVEN: a metabolomic analysis and visualization engine. Current Protocols in Bioinformatics. 37: 14.11.1-14.11.23

Dauner, M., Bailey, J. E., and Sauer, U. 2001a. Metabolic flux analysis with a comprehensive isotopomer model in *Bacillus subtilis*. *Biotechnology and Bioengineering*. 76(2): 144-156.

Dauner, M., and Sauer, U. 2001b. Stoichiometric growth model for riboflavin-producing *Bacillus subtilis*. *Biotechnology and Bioengineering.* 76(2): 132-143.

Eppinger, M., Bunk, B., Johns, M. A., Edirisinghe, J. N., Kutumbaka, K. K., et al. 2011. Genome sequences of the biotechnologically important *Bacillus megaterium* strains QM B1551 and DSM319. *Journal of Bacteriology*. 193(16): 4199-4213.

Furch, T., Hollmann, R., Wittmann, C., Wang, W., and Deckewr, W. D. 2007a. Comparative study on central carbon metabolic fluxes of *Bacillus megaterium* strains in continuous culture using ^{13}C labeled substrates. *Bioprocess Biosystems Eng*. 30: 47-59.

Furch, T., Wittmann, C., Wang, W., Granco-Lara, E., Jahn, D., et al. 2007b. Effect of different carbon sources on central metabolic fluxes and the recombinant production of a hydrolase from *Thermobifida fusca* in *Bacillus megaterium. Journal of Biotechnology*. 132: 385-394.

Issaly, I. M., and Issaly, A. S. 1974. Control of ornithine carbamoyltransferase activity by arginase in *Bacillus subtilis.* European Journal of Biochemistry. 49: 485-495.

Kanehisa, M., Furumichi, M., Tanabe, M., Sato, Y., and Morishima, K. 2017. KEGG: new perspectives on genomes, pathways, diseases and drugs. Nucleic Acids Res. 45: D353-D361.

Kanehisa, M., and Goto, S. 2000. KEGG: Kyoto Encyclopedia of Genes and Genomes. Nucleic Acids Res. 28: 27-30.

KoÈgel-Knabner, I. 2002. The macromolecular organic composition of plant and microbial residues as inputs to soil organic matter. *Soil Biology and Biochemistry*. 34(2): 139-162.

Korneli, C., Bolten, C. J., Godard, T., Franco-Lara, E., and Wittmann, C. 2012. Debottlenecking recombinant protein production in *Bacillus megaterium* under large-scale conditions – targeted precursor feeding designed from metabolomics. *Biotechnology and Bioengineering*. 109(6): 1538-1550.

Kukurugya, M. A. 2017. Quantifying the intracellular metabolic network that establishes the simultaneous utilization of sugars and aromatic substrates in *Psuedomonas putida* KT 2440 (Unpublished master's thesis). Cornell University, Ithaca, NY.

Legrain, C., Stalon, V., Noullez, J.P., Mercenier, A., Simon, J.p., et. al. 1977. Structure and r\function of ornithine carbamoyltransferases. European Journal of Biochemistry. 80: 401-409.

Liu, X., Zhao, H. and Chen, S. 2006. Colonization of maize and rice plants by strain Bacillus *megaterium* C4. *Current microbiology*. 52(3):186-190.

Marchland, N., and Collins, C. H. 2016. Synthetic quorum sensing and cell-cell communication in Gram-positive *Bacillus megaterium*. *ACS Synthetic Biology*. 5: 597-606.

Melamud, E., Vastag, L., and Rabinowitz, J. D. 2010. Metabolomic analysis and visualization engine for LC-MS data. Analytical Chemistry. 82(23): 9818-9826.

Quinn, P. J., Peden, J. M. M., and Dick R. E. 1989. Carbon-phosphorus bond cleavage by gram-positive and gram-negative soil bacteria. *Applied Microbiology & Biotechnology*. 31: 283-287.

Sano, K., Otani, M., & Umezawa, C. 1988. Glucose metabolism via the Embden-Meyerhof pathway is not involved in ATP production during spore germination of *Bacillus megaterium QM B1551*: A study with a mutant lacking hexokinase. Biochemical and biophysical research communications, 151(1), 48-52.

Santos, S., Neto, I. F. F., Machado, M. D., Soares, H. M. V. M., and Soares, E. V. 2014. Siderophore production by *Bacillus megaterium*: Effect of growth phase and cultural conditions. *Applied Microbiology & Biotechnology*. 172: 549-560.

Sasnow, S. S. 2016. Effects of iron limitation and carbon source on extracellular excretions and intracellular carbon metabolism in *Pseudomonas putida*. Retrieved from eCommons Cornell University. http://hdl.handle.net/1813/39471

Sasnow, S. S., Wei, H., and Aristilde, L. 2016. Bypasses in intracellular glucose metabolism in iron-limited *Pseudomonas putida*. *MicrobiologyOpen*. 5(1): 3-20.

Sauer, U., Hatzimanikatis, V., Bailey, J. E., Hochull, M., Szypersky, T., et al. 1997. Metabolic fluxes in riboflavin-producing *Bacillus subtilis. Nature Biotech*. 15: 448-452.

Tannler, S., Decasper, S., and Sauer, U. 2008. Maintenance metabolism and carbon fluxes in *Bacillus* species. *Microbial Cell Factories*. 7:19.

Weitzel, M., Nöh, K., Dalman, T., Niedenführ, S., Stute, B., and Wiechert, W. 2012. 13CFLUX2 - High-Performance Software Suite for 13C-Metabolic Flux Analysis. Bioinformatics. doi: 10.1093/bioinformatics/bts646

Werra, P., Pechy-Tarr, M., Keel, C., and Maurhofer, M. 2009. Role of gluconic acid production in the regulation of biocontrol traits of *Pseudomonas fluorescens* CHA0. *Applied and Environmental Microbiology*. 75(12): 4162-4174.

Vary, P. S. 1994. Prime time for *Bacillus megaterium*. Microbiology. 140: 1001-1013.

Vary, P. S., Biedendieck, R., Fuerch, T., Meinhardt, F., Rodhe, M., et al. 2007. *Bacillus megaterium* – from simple soil bacterium to industrial protein production host. *Applied Microbiology & Biotechnology*. 76: 957-967.

Appendix

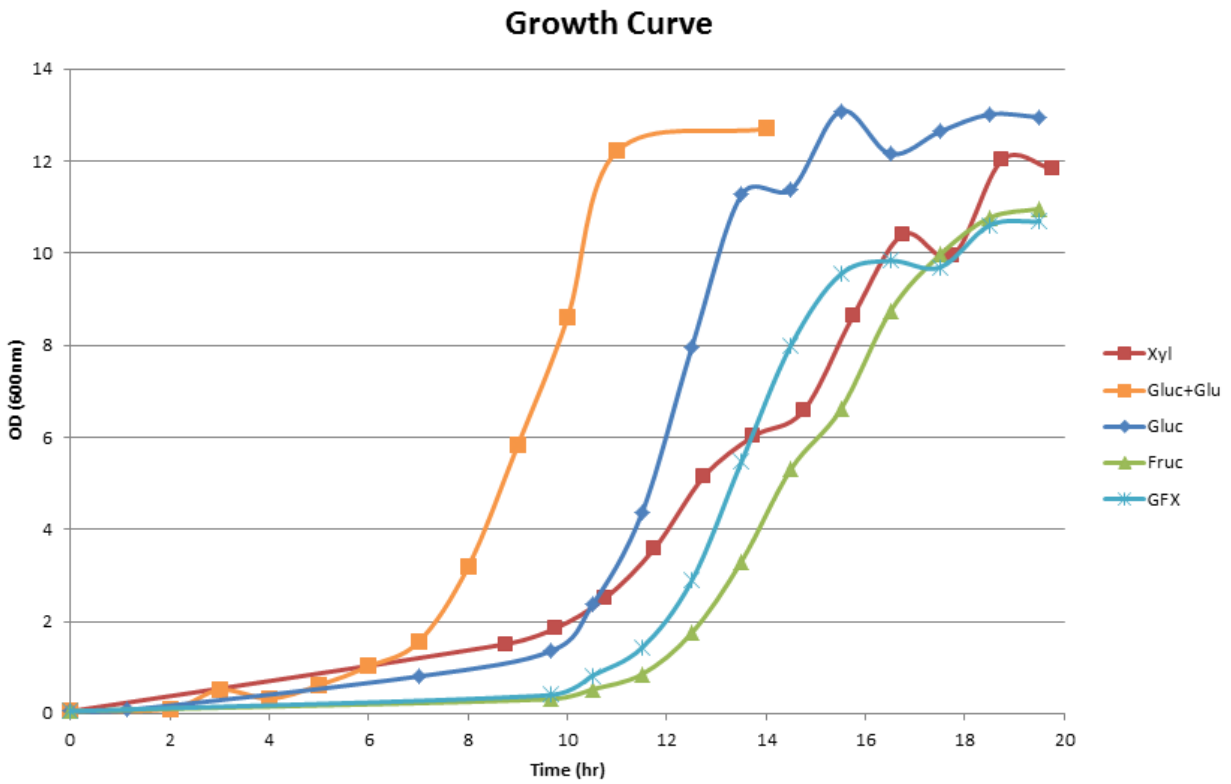

Figure S1. The individual growth curves for each experimental condition; Gluc (blue), Fruc (green), Xyl (red), Gluc:Fruc:Xyl (light blue), and Gluc:Glutamate (orange). These curves were used to plan subsequent experiments which required timing of bacterial growth. The growth rates were obtained during the g_{CDW} experiments.

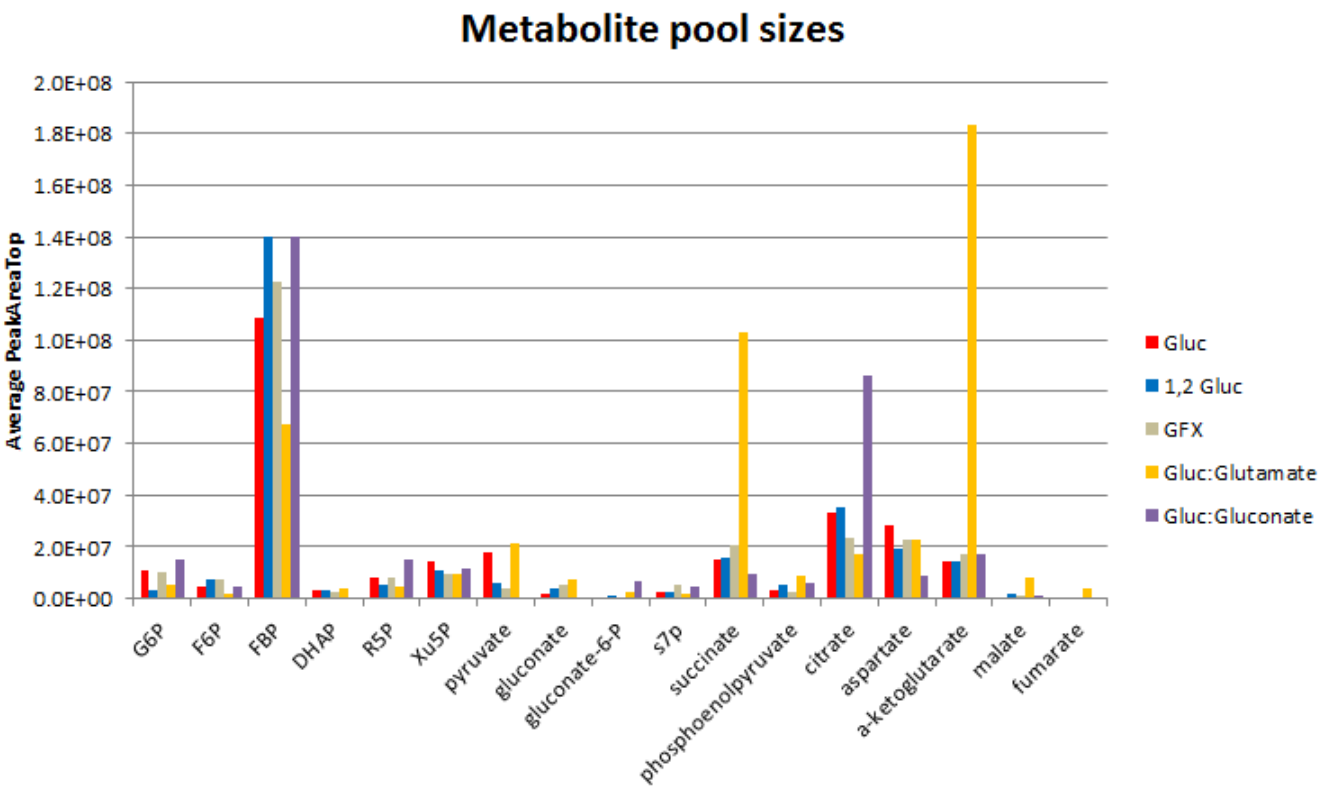

Figure S2. The average Peak Area Top of each metabolite and each experimental condition. The pool size for gluconate in the Gluc:Gluconate experiment ($2.05*10^9$) was omitted for scaling purposes. Abbreviations used: G6P, glucose-6-phosphate; F6P, fructose-6-phosphate; FBP, fructose-bis-phosphate; R5P, ribose-5-phosphate; Xu5P, xyulose-5-phosphate; S7P, sedoheptulose-7-phosphate

Table S1. The MFA output of each metabolic reaction, the flux value, and the standard deviation of the flux value normalized to the Gluc consumption rate. The reactions and fluxes shown in red are either secretions or biomass effluxes from the identified node. The values in blue represent the values seen in Fig. 36.

Reaction	Flux Value (%)	Standard Dev (%)
BM_AKG	17.7017	4.3E-05
BM_E4P	5.45478	1.2288
BM_OAA	19.7679	6.7E-05
BM_PEP	12.9945	1.02541
BM_PG3	22.477	0.51813
BM_PYR	43.2077	0.03195
BM_R5P	13.5387	4.9E-05
BM_AcCoA	9.54686	0.00092
Ex_Fum	0.0613	0.04144
Ex_Cit	0.24509	6.6E-05
BM_G6P	3.88292	0.00026
Ex_Glucn	0.11924	0.00023
Ex_Succ	0.87513	0.4325
OAA -> Fum	0.96412	1.36339
Mal -> Pyr + CO2	0.00012	6.7E-05
G6P -> 6PG	48.2079	0.00017
G6P -> F6P	47.7893	1.74685
FBP -> DHAP + GAP	69.0843	1.33706
GAP -> PG3	146.089	1.85482
PG3 -> PEP	123.612	2.37294
PEP -> Pyr	110.617	1.3476
DHAP -> GAP	69.0843	1.33706
$Gluc_{peri}$ -> Glucn	0.1198	0.0004
F6P -> FBP	69.0843	1.33706
6PG →Ru5P	48.2085	0.00034
Ru5P -> R5P	26.9135	0.40945
Ru5P -> X5P	21.295	0.40979
X5P + R5P -> GAP + S7P	13.3749	0.4095
GAP + S7P -> E4P + F6P	13.3749	0.4095
E4P + X5P -> F6P + GAP	7.92009	0.8193
Pyr -> AcCoA + CO2	28.7584	1.78936
Pyr + CO2 -> OAA	38.6514	0.47364
OAA -> PEP + CO2	0.0002	6.7E-05
OAA + AcCoA -> Cit	19.2115	1.78843
Cit -> αKG	18.9664	1.78837

αKG -> Succ + CO2	1.26473	1.78833
Succ -> Fum	0.3896	1.11042
Fum -> Mal	1.3377	1.78082
Mal -> OAA	2.89212	1.36312
Gluc -> $Gluc_{peri}$	100	1.74602
$Gluc_{peri}$ -> G6P	99.8802	1.74642
$Glucn_{peri}$ -> 6PG	0.00056	0.00017

Table S2. The absolute optimal flux values from the MFA for Gluc metabolism average over two bioreplicates. The units for the Average value and the Standard deviation (std dev) were (mmol metabolite g_{CDW}^{-1} h^{-1}) / (mmol Gluc g_{CDW}^{-1} h^{-1}).

Reaction	Average Value	std dev
BM_AKG	0.1836	4.3E-07
BM_E4P	0.05658	0.01229
BM_OAA	0.20503	6.7E-07
BM_PEP	0.13478	0.01025
BM_PG3	0.23313	0.00518
BM_PYR	0.44814	0.00032
BM_R5P (really BM_P5P)	0.14042	4.9E-07
BM_AcCoA	0.09902	9.2E-06
Ex_Fum	0.00064	0.00041
Ex_Cit	0.00254	6.6E-07
BM_G6P	0.04027	2.6E-06
Ex_Glucn	0.00124	2.3E-06
Ex_Succ	0.00908	0.00433
OAA -> Fum	0.01	0.01363
Mal -> Pyr + CO2	1.3E-06	6.7E-07
G6P -> 6PG	0.50001	1.7E-06
G6P -> F6P	0.49566	0.01747
FBP -> DHAP + GAP	0.71653	0.01337
GAP -> PG3	1.51521	0.01855
PG3 -> PEP	1.28208	0.02373
PEP -> Pyr	1.14731	0.01348
DHAP -> GAP	0.71653	0.01337
$Gluc_{peri}$ -> Glucn	0.00124	4E-06
F6P -> FBP	0.71653	0.01337
6PG →Ru5P	0.50001	3.4E-06
Ru5P -> R5P	0.27914	0.00409
Ru5P -> X5P	0.22087	0.0041

X5P + R5P -> GAP + S7P	0.13872	0.0041
GAP + S7P -> E4P + F6P	0.13872	0.0041
E4P + X5P -> F6P + GAP	0.08215	0.00819
Pyr -> AcCoA + CO2	0.29828	0.01789
Pyr + CO2 -> OAA	0.40089	0.00474
OAA -> PEP + CO2	2.1E-06	6.7E-07
OAA + AcCoA -> Cit	0.19926	0.01788
Cit -> αKG	0.19672	0.01788
αKG -> Succ + CO2	0.01312	0.01788
Succ -> Fum	0.00404	0.02221
Fum -> Mal	0.01387	0.03562
Mal -> OAA	0.03	0.01363
Gluc -> $Gluc_{peri}$	1.03719	0.01746
$Gluc_{peri}$ -> G6P	1.03594	0.01746
$Glucn_{peri}$ -> 6PG	5.8E-06	1.7E-06